Engineered Cardiac Troponin C

Structure-Function Studies: Designing Proteins for Treatment of Cardiomyopathies

Dan Wang

A dissertation
submitted in partial fulfillment of the
requirements for the degree of

Doctor of Philosophy

University of Washington

2012

Reading Committee:

Dr. Michael Regnier, Chair

Dr. Valerie Daggett

Dr. Donald Martyn

Dr. Yanfeng (Mei) Speer

Program Authorized to Offer Degree:

Department of Bioengineering

University of Washington

ABSTRACT

Engineered Cardiac Troponin C Structure-Function Studies:
Designing Proteins for Treatment of Cardiomyopathies

Dan Wang

Chair of the Supervisory Committee:
Professor Michael Regnier
Department of Bioengineering

The functional effects of mutations associated with cardiomyopathies generally suggest that the Ca^{2+} responsiveness of the myofilament was affected. This functional change appears to be independent of which protein contains the mutation and therefore indicates that the altered Ca^{2+} sensitivity could be a critical or causative component of disease expression and progression. However, the correlation underlying this functional change with the disease phenotype is still unclear. Thus, in this work a series of single amino acid-substituted cardiac troponin C (cTnC) variants with altered Ca^{2+} binding affinities were studied to determine how they influence the Ca^{2+} activation pathway in myofilament contraction and whether this change in Ca^{2+} binding will result in adaptive changes in intact cardiomyocytes. These variants have not been identified as associated with any cardiomyopathies and therefore may eventually provide clues as to whether altered Ca^{2+} signaling of myofilament contraction is causal or an adaptive response in diseased hearts.

Firstly, we sought structural and mechanistic explanations for the increased/decreased Ca^{2+} sensitivity of contraction for the cTnC variants using an array of biophysical techniques. The properties of these cTnC variants were characterized by determining their effects on Ca^{2+} binding ability, cTnC-cTnI interaction and their modulation by PKA phosphorylation in solution, and their structural alterations using molecular dynamic simulations. We found that cTnC variants have different effects on both binding of Ca^{2+} and cTnI to cTnC, and they also respond differently upon PKA phosphorylation. MD simulations show, for the first time, that cTnC variants could

disrupt crucial hydrophobic interactions so that the closed form of cTnC or the Ca^{2+} binding loop is destabilized. The findings emphasize the importance of the regulatory domain of cTnC's conformation in the regulation of contraction and suggest that mutations in cTnC that alter myofilament Ca^{2+} sensitivity can do so by modulating Ca^{2+} and cTnI binding. Secondly, the functional capacity of the Ca^{2+} desensitizing variants was characterized by expressing them in cardiomyocytes using adenovirus. Additionally, we demonstrate that engineered cTnC variants can correct the disease-induced abnormal Ca^{2+} binding sensitivity. Our study provides insights for the development of novel therapeutic strategies for the treatment of cardiomyopathies.

Dedicated to my family

ACKNOWLEDGEMENT

TABLE OF CONTENTS

LIST OF FIGURES

LIST OF TABLES

LIST OF ABBREVIATIONS

ATMdist	distances between the center of mass of two atoms
Ca^{2+}	element calcium
cTn	cardiac whole troponin
cTnC	intact cardiac troponin C
cNTnC	N-domain of cTnC
cTnI	cardiac troponin I
$cTnI_{147-163}$	cTnI peptide corresponding to residues 147-163
$C\alpha$-RMSD	root-mean-square deviation of $C\alpha$ atom coordinates from the starting structure
COMdist	distances between the center of mass of two objects
DTT	dithiothreitol
EDTA	ethylene diamine tetraacetic acid
EGTA	ethylene glycol tetraacetic acid
IANBD	N-(2-(iodoacetoxy)ethyl)-N-methyl)amino-7-nitrobenz-2-oxa-1,3-diozole
MD	molecular dynamics
n_H	Parameter of Hill fit to IANBD-pCa data, slope of IANBD-pCa at pCa_{50} of IANBD fluorescence
K_D	dissociation constant
K_{off}	dissociation rate
MOPS	3-(N-morpholino) propanesulfonic acid
pCa	$-lg[Ca^{2+}]_{free}$
pCa_{50}	Parameter of Hill fit to IANBD fluorescence-pCa data; pCa at half-maximal IANBD fluorescence increase
PDB	Protein Data Bank
PKA	Protein Kinase A
SASA	solvent accessible surface area
Quin-2	2-{[2-bis(carboxymethyl)amino-5-methylphenoxy]methyl}-6-methoxy-8-bis(carboxymethyl)aminoquinoline

| WT | wild-type |
| ITC | Isothermal Titration Calorimetry |

List of amino acids:

A	Ala	Alanine
N	Asn	Asparagine
D	Asp	Aspartic acid
R	Arg	Arginine
C	Cys	Cysteine
Q	Gln	Glutamine
G	Gly	Glycine
E	Glu	Glutamic acid
H	His	Histidine
I	Ile	Isoleucine
K	Lys	Lysine
L	Leu	Leucine
F	Phe	Phenylalanine
M	Met	Methionine
S	Ser	Serine

Chapter 1

Introduction

1.1. Significance

Cardiomyopathy is disease of the heart muscle that results in a weakening of cardiac muscle or a change in cardiac muscle structure, and it is the leading cause of heart failure (*1*). In the United States, 3 million people are currently living with cardiomyopathy, and another 400,000 people are diagnosed each year. The number of people affected and the economic impact of heart disease on the economy have made cardiomyopathy a public health problem. Current therapies that exist to treat patients with heart disease merely address symptoms and slow the progression of disease. In order to develop therapies to truly treat patients with cardiomyopathy, more research must be done to understand the underlying cause for this disease.

1.2. Cardiac muscle contraction and thin filament activation

Cardiac muscles are composed of tubular myofibrils (Figure1.1.A), which are packed with repeating structural units known as sarcomeres. The sarcomere is the smallest contractile unit of muscle and is composed of thick and thin filaments (Figure1.1.B and C). The thick filaments are made of myosin, the heads of which are called cross-bridges when myosin is bound to actin (CB). The thin filament proteins include three components (Figure 1.1.D): a double helix of actin monomers, coiled-coil dimers of tropomyosin (Tm) and cardiac troponin (cTn) complex that has three subunits,

the Ca^{2+} binding subunit (cardiac Troponin C, cTnC), the inhibitory subunit (cardiac Troponin I, cTnI) which binds to actin and inhibits the exposure of CB binding sties on actin during low intracellular Ca^{2+} concentration, and Troponin T (cTnT) that stabilizes the Tn complex in the thin filament through its interaction with Tm(*2*).

In each sarcomere, the thick and thin filaments overlap each other, such that a change in the length of the sarcomere alters the number of myosin heads that are able to interact with actin. This is the basis for the sliding of thick and thin filaments model of muscle contraction, which involves the force generating interactions between myosin cross-bridges and actin (Figure1.1.C). The force generation resulting from myosin binding to actin is the basis of muscle contraction, and requires the coordination of multiple myosin heads and the activation of the thin filament.

Calcium entry to the cell (as a result of an action potential) results in Ca^{2+} binding to the cTnC, which triggers thin filament activation and thus initiates cardiac muscle contraction. Each single cTn complex is associated with seven actin monomers and one Tm dimer (Figure 1.1.D). This cTn/Tm/7actins complex constitutes the structural regulatory unit of thin filament, and in each half-sarcomere there are about 26 such units along each actin strand that are connected by head-to tail Tm overlap. The position of Tm and Tn on the thin filament determines the exposure of the myosin binding sites on actin. These binding sites are considered as blocked, closed, or open. When intracellular Ca^{2+} concentration is low, Tm, together with the C-terminus of cTnI, on the actin helix blocks the myosin binding sites on actin, which is referred as the blocked state (unable to bind CB). When intracellular Ca^{2+} concentration rises, Ca^{2+} binds to the regulatory domain of cTnC. This enhances the cTnC-cTnI interaction and weakens the inhibitory

interaction of cTnI with actin (*3*). Next, the Ca^{2+} activation signal is translated through the cTnT interaction with Tm that allows the movement of Tm on actin to positions such that the myosin binding sites are exposed and ready for weak myosin binding. This thin filament state is closed (able to weakly bind CB). Force is generated during the subsequent transition of the myosin-actin interaction from weakly to strongly bound, which moves Tm further along actin and increases the availability myosin binding sites on the actin filament. At this stage, the thin filament is activated and turned into an open state (able to strongly bind multiple CBs). This dynamic three state model of thin filament activation is supported by extensive biochemical and structural studies (*4-6*). Although some details about the regulation of the processare still under investigation, it is known that thin filament activation is regulated by both Ca^{2+} binding to cTnC and strong cross-bridge binding to actin. Thus, if either the Ca^{2+} binding (to cTn) or CB binding (to thin filaments) is changed (for example by altering the Ca^{2+} binding to cTnC), there could be profound effects on the regulation of cardiac muscle contraction, and potentially even further alterations to whole heart function. This has been reported in many functional studies of cardiomyopathy-related mutations in the cTn proteins, where in many cases, mutations that alter the dynamics of the troponin complex result in alterations to the Ca^{2+} sensitivity of contraction. However, it is still unclear whether this altered Ca^{2+} signaling in the thin filament activation is a causal or an adaptive response in diseased hearts. Before further discussing the studies of current cardiomyopathy related mutations in the cTn complex, since knowledge of the structures and functions of the cTn complex and its subunits is crucial for the understanding of the cardiac disease development and the mechanism that underlie the functional changes, a review of the cTn subunits follows.

1.3. Structure and function of the cTn complex and its subunit proteins

The structure of the core domain of human cTn complex in the Ca^{2+} saturated state was solved using X-ray crystallography(*7*), and (Figure 1.2) contains the full length of cTnC, residues 41-136 and 147-191 of cTnI(missing the N-extension region (residues 1-33), the inhibitory region (residues 134-146) and the last 18 residues in the C-terminus (residues 192-209)), as well as and truncated cTnT (residues 183-288) missing the Tm binding region (residues 1-182). More detailed structure information of each subunit is discussed below.

1.3.1. cTnC

Cardiac troponin C (~18kDa), the Ca^{2+}- binding subunit of the troponin (Tn) complex, consists of N-terminal and C-terminal EF-hand motifs connected by a long central helix (Figure 1.3)(*8-10*). The two globular domains each contain two helix-loop-helix motifs that bind divalent metal ions (site I and site II). The N domain of cTnC (cNTnC) differs from the N domain of skeletal TnC (sTnC) in that Site I in cTnC is does not bind Ca^{2+} due to several loop residue substitutions (*11*) and thus has only one lower affinity ($\sim10^5 M^{-1}$) Ca^{2+} binding site (site II) responsible for initiating thin filament activation and the subsequent force generation and contraction of cardiac muscle (*12*). Studies using skinned muscle preparation show that elimination of Ca^{2+} binding of site II of cTnC renders cardiac muscle force generation insensitive to Ca^{2+} (*13*). Furthermore, using cTnC with dysfunctional site II but repairing its Ca^{2+} binding property at site I, does not restore Ca^{2+} sensitivity (*14*). Thus, Ca^{2+} binding to cTnC at site II is critical for cardiac muscle activation.

The C domain (cCTnC) contains metal binding sites III and IV which have higher binding affinity, $\sim10^7M^{-1}$ for Ca^{2+} and 10^4M^{-1} for Mg^{2+}. Although sites III and IV are known to primarily play a structural role in anchoring the proteins within the Tn complex, it is thought that they may also be involved in the Ca^{2+} signaling pathway for contractile activation (*15*).

The structure of cTnC has been solved in various Ca^{2+} bound states during the past decades (for reviews, see (*9, 16*)), though there are not yet high resolution structures of the whole cTn complex in different Ca^{2+} bound states. Knowledge of different structural states is critical to understand function since Ca^{2+} binding to cTnC activates conformational changes within the N domain of the cTn complex that lead to thin filament activation and force generation (the structures of the C-domain of sTnC and cTnC, in the Ca^{2+} or Mg^{2+} saturated state, are very similar whether free or bound to TnI (*17-21*)). In the apo states, the regulatory domain of cTnC stays in a closed conformation with most of its hydrophobic residues not exposed. Interestingly, solution structures of the N domain of cTnC and sTnC reveal the most important difference between cardiac and skeletal TnC in response to Ca^{2+} binding. Following Ca^{2+} activation, structural studies demonstrated that Ca^{2+} binding to the regulatory domain of skeletal TnC induces opening of the hydrophobic patch in the N domain, which in turn facilitates cTnI binding and muscle activation (*22*). However, Ca^{2+} binding to cNTnC does not cause similar structural alteration and the hydrophobic patch remains largely un-exposed even in the presence of calcium (*23*). Subsequent studies showed that both the binding of Ca^{2+} and the interaction with the switch region of cTnI are needed for cNTnC to maintain stable in the open state (*24, 25*), which is discussed in more detail in the following sections. .

Cardiac TnI (~24kDa) is the inhibitory subunit of the Tn complex, distinguished from skeletal TnI by an N-extension region (~27-33 residues). Figure1.4 is a cartoon picture illustrating how cTnI interacts with other cTn components, Tm and Actin. As a highly flexible protein that is able to adapt favorable conformations for binding to cTnC, cTnT, actin and Tm (*26*), cTnI can be divided into several distinct structural segments (for reviews, see (*27, 28*)) as shown in Figure 1.2 and 1.4: (1) the N-termianl cardiac-specific extension region (cTnI$_{1-30}$) that contains two protein kinase A (PKA)-dependent phosphorylation sites, a praline helix linker and an acidic region; (2) an IT-arm region (cTnI$_{34-136}$), which consists of two α-helices that interact with the C-lobe of cTnC and the α-helix of the C-termianl domain of TnT; (3) the inhibitory region (cTnI$_{128-147}$) which binds both TnC and actin-Tm; (4) the switch region (cTnI$_{147-163}$) that binds the N-domain of TnC in response to Ca^{2+}; (5) the C-terminal mobile domain (cTnI$_{164-210}$), a second actin-Tm binding site on cTnI. The full structure of cTnI in the cTn complex, regardless of Ca^{2+} binding has not been solved, though solution or x-ray structures of cTnI fragments are available for all of the individual functional cTnI regions.

<u>N-extension region:</u>

NMR studies show that in the absence of phosphorylation, the N-extension region (cTnI$_{1-30}$) is less structured, most likely weakly interacting with the N-domain of cTnC (*29*). PKA phosphorylation of cTnI at S23/S24 causes a structural extension of cTnI$_{1-30}$ at the C-terminus (residues 21-30), which further weakens the interaction between cTnI$_{1-30}$ and cNTnC. This repositioning of cTnI$_{1-30}$ makes subsequent interaction inhibitory region

of cTnI more favorable, and as a result decreases the calcium sensitivity of muscle contraction (*29*).

<u>IT-arm region:</u>

cTnI $_{34-80}$, the first half part of the IT-arm region, has been shown to bind to the hydrophobic cleft in the C-domain of cTnC (*18*). The adjacent region, or second half of the IT-arm, cTnI$_{80-136,}$ forms a helical coiled-coil with a portion of cTnT, which was also predicted previously as playing a more structural role of anchoring the whole cTn complex in the thin filament (*30*).

<u>Inhibitory Region:</u>

The inhibitory region, cTnI$_{128-147}$, is missing in the core domain structure, but it has long been considered as the crucial region as it inhibits the actin-crossbridge binding through its interaction with actin (*31, 32*). Moreover, when this region is not bound to actin, tropomyosin moves, and myosin binding sites are exposed. While this section of TnI is bound to actin, on the other hand, no myosin binding sites are available and force generation will not occur. Despite the agreement on function, the studies that address the structure of this region are not in very good agreement. No structures exist to describe the structure of the inhibitory region when bound to actin, but there are various structures that propose conformation of the inhibitory region TnI in isolation. In cardiac muscle, Tung *et al* proposed this region to be a β-hairpin-dominant by using cross-linking and fluorescence-detected resonance energy transfer (FRET) (*33*). Conversely, the recent NMR structure of cTnI$_{128-147}$ shows a helix structure formed by residues 134-139, while residues 140-147 adopt an extended conformation, potentially interacting with the C domain of cTnC (*20*). A site-directed spin labeling technique demonstrated that residues

130-135 interacts with a region of cTnT and the 129-137 region forms a regular 3.6 residue turn α-helix, while residues 139-145 display no secondary structure characteristics (*34*).

Switch Region:

Next to the inhibitory region, the switch region of cTnI (from residue 147-163), has been described in the cNTnC●Ca^{2+}●cTnI$_{147-163}$ complex using NMR (*25*). In this structure, the N-terminus of cTnI$_{147-163}$ binds to the hydrophobic patch within cNTnC, stabilizing the 'open' conformation of cNTnC˙Ca^{2+}, while the C-terminus of this switch region is unstructured. Though the relative position of this switch region in this binary complex is different from that in the ternary complex (cTn x-ray structure) (*7*), the conformation and orientation of the switch region of cTnI with the cNTnC are in good agreement. The C-terminal region of cTnI (cTnI$_{164-210}$) forms an α-helix structure and is free of contact with actin, Tm or cNTnC.

C-terminal Region:

The C-terminal region is known as a mobile domain of cTnI (from residue 164-209) that binds actin-tropomyosin. The core domain x-ray structure of the whole cTn complex shows that the C-terminal region of cTnI has a α-helical structure and is free of contact with either cTnC or cTnT.

1.3.3. cTnT

TnT exists multiple isoforms both in skeletal and cardiac muscles. In human heart, cardiac TnT is spliced from a single gene to yield four isoforms (cTnT1,cTnT2,

cTnT3 and cTnT4). cTnT is the Tm binding subunit in the cTnC complex, molecular weight of which ranges from ~31kDa to ~36kDa, with 250-300 amino acids.

cTnT is regarded as a highly asymmetric elongated protein, and can be divided into two functionally distinct regions: the N-terminal T1 region ($cTnT_{1-181}$) that interacts with Tm; and the C-terminal T2 region ($cTnT_{181-288}$) that is integrated into cTn complex, and interacts with both cTnC and cTnI. There is no solved structure and limited structural data available for the T1 region of cTnT. Ertz-Berger and Tardiff *et al* were able to computationally build α-helix structure for residues 70-170 (*35*), part of the T1 region, and later docked this model to the known Tm structure to perform larger scale computational studies (*36*). High resolution structure of the T2 region is available through the cTn complex structure, which shows two α-helices that are considered as the most conserved structure among different isoforms of TnT (*30*). The T2 region both interacts with the IT-arm of cTnI and the C-domain of cTnC, anchoring the cTn complex in the thin filament (shown in orange in Figure 1.2 and Figure1.4).

1.3.4. cTn complex

The overall structure of the cTn complex can be divided into two subdomains (Figure 1.2), the regulatory domain and the IT domain, which are connected by flexible linkers (*9*). The regulatory domain mainly includes the N-domain of cTnC (cNTnC) and the switch region of cTnI, and the IT domain contains the C-domain of cTnC (cCTnC), the IT arm region of cTnI and cTnT. The linker of cTnC (between D and E helices) and the inhibitory region of cTnI (missing in the core structure) form a region like a'flexible joint' of the two subdomains, not only connecting two subdomains together but also allowing further adjustment of their relative orientations during muscle contraction and

relaxation. The structure of the core domain of the cTn complex fits quite well with the commonly accepted mechanism of thin filament activation. Ca^{2+} binding to the regulatory domain (N-domain) of cTnC triggers the interaction between cTnC and cTnI, which is followed by the binding of the switch region of cTnI to the hydrophobic patch of cTnC$\bullet$Ca^{2+}. The binding of the switch region of cTnI to cTnC$\bullet$Ca^{2+} drags the inhibitory region of cTnI off of Tm, allowing Tm to move along actin. This in turn further releases the C-terminal of cTnI from its interaction with actin (*9*). Despite some knowledge of the cTn switch mechanism during thin filament activation, the lack of high resolution structures of the cTn complex in the apo state (absence of Ca^{2+}) hinders a more complete understanding of the cTn switch mechanism.

1.3.5. cTnC-cTnI interaction

From both the structural and functional biology of the troponin complex, it has been shown that the interaction between cTnC and cTnI plays a critical role in transferring the Ca^{2+}-signal to the other myofilament proteins in heart muscle contraction and relaxation (*37*). As discussed earlier, the solution structures of the N domain of cTnC and sTnC reveal the most important difference between cardiac and skeletal TnC in response to Ca^{2+} binding. When Ca^{2+} binds to sNTnC (*22*), it results in an exposure of the hydrophobic patch within sNTnC that enables interaction with the switch region of sTnI, a transition from 'closed' to 'open' state. However, Ca^{2+} binding to cNTnC does not cause similar structural alteration, so full exposure of and stabilization of the hydrophobic patch on cTnC requires further interaction with the switch region of cTnI.(*23*). Not only do studies of cTnC-cTnI provide insight into the differences in the mechanism of muscle activation between skeletal and cardiac muscle, but it also offers insight into potential

targets for therapeutic agents that could mediate the Ca^{2+} sensitivity of the myofilaments in diseased hearts (*37*).

Levosimendan is an example of a novel Ca^{2+}-sensitizer that has been shown to be well-tolerated and an effective treatment for patients with severe heart failure (for review (*38*)), though there is a debate about how this molecule binds to the cTnC-cTnI complex (*39, 40*). From therapeutic point of view, targeting cTnC or the cTnC-cTnI interface, rather than altering calcium levels *per se*, is considered more beneficial as it does not affect the overall intracellular Ca^{2+}, which could disrupt the regulation of other Ca^{2+} signaling pathways and result in various undesirable side effects and heart dysfunction. Determination of how altered Ca^{2+} binding influences cTn subunit interactions, therefore, is critical to understand the signaling of thin filament activation.

1.3.6. PKA phosphorylation of cTnI

The molecular switch mechanism of cTn is regulated not only by Ca^{2+}, but also by the phosphorylation of cTnI and cTnT (*41, 42*). PKA phosphorylation of cTnI during β-adrenergic stimulation has been found to decrease the interaction between N-extension of cTnI-cNTnC (*29*) and reduce the affinity of cTnI for actin (*43*), which results in reduced myofilament Ca^{2+}-sensitivity, and an increase in relaxation rate and cross bridge cycle kinetics(*44-47*). Since PKA phosphorylation of cTnI is diminished in the failing heart (due to down-regulation of the β-adrenergic sytem), understanding of the mechanism by which PKA phosphorylation affects heart function is critical in order to understand failure and to develop targeted therapies.

1.4. Cardiomyopathies related mutations in cTn subunit proteins

Increasing numbers of mutations in the cTn subunits related with cardiomyopathies have been found recently. Hypertrophic cardiomyopathy (HCM), characterized by ventricular hypertrophy, is one of the most common inherited cardiac disorders. HCM affects one in five hundred people in the general population, and the most common cause of sudden death from cardiac diseases in young people (*48*). Dilated cardiomyopathy (DCM) is another cardiomyopathy subtype and features ventricular dilation (enlarged ventricle) and systolic dysfunction. Thus far 69 HCM-related and 18 DCM-related mutations have been found in cTn component proteins (for reviews, see (*49, 50*)), among which 8 mutations occur in cTnC (*51*), 32 mutations occur in cTnI, and 47 mutations occur in cTnT (shown in Figure 1.5). These mutations were identified in different functional regions of the proteins. Although the regions where the HCM/DCM mutations occur in the C-terminus of cTnI (residues 192-209) and cTnT1 (residues 1-188) are missing from the crystal structures available, the atomic high resolution cTn structure (Figure 1.2) does contain the regions where there exist HCM/DCM mutations. Thus, analysis of these structures and their dynamics allows us to evaluate the potential structural effects caused by these disease-causing mutations and the possible disruption of key protein–protein interactions within the cTn, e.g cTnC-cTnI interaction that may occur in disease states.

The effects of the cardiomyopathy-related mutations on cardiac muscle function have been extensively studied using biochemical and physiological methods. Ca^{2+} binding affinity of cTnC has been examined intensively for the disease-related mutations using fluorescence based spectroscopy (*51-53*); studies have demonstrated that the mutation-induced alterations in Ca^{2+} binding affinity parallel the mutation-related

alterations to Ca^{2+} sensitivity of myofilament contraction (*54, 55*). In order to investigate the effect of mutations on protein-protein interaction and ATPase activity *in vitro*, many mutations have been incorporated into physiologically relevant solutions and reconstituted thin filaments. (*52, 53, 56-58*). Effects of some mutations on contractile mechanic properties such as force generation have been studied using skinned muscle tissue exchanged with recombinant exogenous cTn contacting disease related mutations (*49, 56, 57, 59*). Furthermore, adenovirus containing genes of disease mutations have been used to transduce isolated cardiomyocytes to examine the intact cell shortening and intracellular Ca^{2+} handling (*60*). Several transgenic animal models have also been developed to study the disease progression (*61-67*).

In general, functional studies of HCM-related mutants have shown that the Ca^{2+} sensitivity of contractile regulation is increased compared with wild type. In strong contrast, studies of DCM mutations in thin filament regulatory proteins have shown that these cause the opposite effect, a decrease in Ca^{2+} sensitivity, which suggests a fundamentally different effect of these mutations at the level of the sarcomere (*49*). However, it is still unknown how, and to what extent, these alterations of Ca^{2+} sensitivity are involved in the progression of HCM or DCM. Knowledge of both the molecular and clinical pathogenesis for cardiomyopathies is necessary to achieve the ultimate goal of using genotype information to help diseased patients.

Besides studying the clinically observed disease-related mutations, a series of non-disease related, engineered cTnC variants have been developed in order to better understand the effects of altered calcium binding affinity of cTnC since these mutations have shown that the Ca^{2+} binding affinity of cTnC could be tuned progressively (*68, 69*).

1.5. Engineered cTnC with altered Ca^{2+} binding affinities

cTnC plays a central role in the cardiac muscle contraction as a Ca^{2+} sensor that involves in regulation of the thin filament activation. Generally, alterations in Ca^{2+} binding affinity directly correlate to Ca^{2+} sensitivity of contraction, although this is not always the case (*54, 55*). One of the limitations of many currently available drugs is that they do not directly target cTnC (*70*).

It is known that solvent accessibility of hydrophobic residues (due to exposure of the hydrophobic patch of cTnC) is increased by either Ca^{2+} binding to the N-domain of sTnC, or switch region of cTnI binding to the regulatory domain of cTnC. According to this theory, Pearlstone *et al*. reasoned that the replacement of hydrophobic residues in the N-domain of TnC with more polar residues should increase the N-domain Ca^{2+} affinity by reducing the energy needed to drive the transition between different Ca^{2+} binding states (*71*). They mutated several hydrophobic residues to polar residues (A, T and Q), which indeed showed an increase in Ca^{2+} binding affinities (*71*). Inspired by this work, Davis *et al.* systematically studied the effects of all hydrophobic residue substitutions with Q on Ca^{2+} binding in sNTnC (*72*), and published a list of these sNTnC variants and characteristics such as Ca^{2+} binding affinities and dissociation rates (*73*), e.g. I62Q sTnC severely lost Ca^{2+} binding ability compared to the control. Several cardiac TnC variants have been further selected and characterized (*68, 69, 74*) based on the information and key findings from the skeletal muscle system.

All engineered cTnC variants that have been reported to date that have altered Ca^{2+} binding affinities are substitutions of residues in the N-domain of cTnC. Figure 1.6 illustrates the residue sequence of the cNTnC. Residues that have been mutated to a Q

residue in previous studies are highlighted such that those that resulted in increased Ca^{2+} binding affinity are blue circles and those that resulted in decreased calcium binding affinity are red (for cardiac muscle only). Experimental results from studies of F20Q, V44Q, M45Q, L48Q and M81Q indicated that substitution of hydrophobic residues in these positions with Q changed the Ca^{2+} binding affinities to the thin filament with myosin S1 up to ~2.4-fold higher and ~4.4 fold lower, compared to the control protein (Ca^{2+} affinity : L48Q > V44Q > M45Q ≥ control >M81Q>F20Q). Our lab recently demonstrated that rat L48Q or I61Q cTnC has greatly increased or decreased (respectively) Ca^{2+} sensitivity of contraction in rat trabeculae and myofibrils (*75*), results that have been supported by other recent work as well (*76*), consistent with the results from other muscle species studied previously (*68, 73*). Furthermore, studies of A23Q and S37Q showed an increase in Ca^{2+} binding to isolated cTnC, an increase in Ca^{2+} sensitivity of skinned myocardial contraction, and an increase in ATPase sensitivity. Similar work on two other variants, E40A and V79Q, showed that these variants resulted in decreased calcium binding affinity, calcium sensitivity, and ATPase compared to the control cTnC (*76*).

As discussed above, even though biochemical and cellular mechanical properties of cTnC variants with altered Ca^{2+} binding affinities have well-studied, the molecular mechanisms of how these single residue substitutions alter cTn protein-protein interaction and lead to the changes in function are not well-understood. Furthermore, the lack of information about structural alterations caused by these single amino acid substitutions in cTnC at the atomic level hinders the understanding of the inter- and intra- molecular interactions within the cTn complex. Further investigation of these structural details will

not only offer insight into the design of new variants, but also will provide crucial clues for understanding how related changes in cTnC structure result in distinct functional changes. Lastly, the effects of these variants on responsiveness to PKA phosphorylation and the contractile function in intact cardiomyocytes also await further investigation-both *in vitro* and *in silico*.

1.6. Computational Structural studies for contractile proteins and disease related mutants

Structure relevance to function has long been a central topic of biochemistry and biophysics in the study of biomolecules. The link between specific alterations in thin filament protein structure by single point mutations that result in complex functional phenotypes remains unknown. The available high resolution structures of cTn complex and its subunits proteins not only illuminate details of the molecular switch mechanism in thin filament regulation, but also allow for the visualization of the amino acid residues and domains of troponin that are sensitive to modifications.

Molecular dynamics (MD) simulations have been widely used in the past 25 years as an important tool for understanding the physical basis of the structure and function of biological molecules (*77, 78*). It provides great insights into complex dynamic processes that occur in these biological systems; it enables in depth analysis of parameters such as protein stability, conformational changes and folding/unfolding/misfolding (*79, 80*), interactions between protein-protein (*81*) or protein and small molecules (*82*), ion transportation (*83*), protein-ligand binding free energies (*84*), computer-aided drug design (*85, 86*) and modeling of biological catalysis such as enzyme mechanisms (*87*). Also, many disease-related missense mutants have been studied using MD in order to better

understand their role in the disease development. For example, using extensive MD simulations Van der Kamp and Daggett found that five pathogenic mutations of prion protein (PrP) have significant effects on the dynamics and stability of PrP (including the propensity to misfold), which may contribute to the pathogenic process of PrP-related disease (*88*).

The use of MD has been a component of an interdisciplinary approach to study the precise influences of disease-related thin filament mutations on protein structure that may lead to the cardiac dysfunction. As one example, our lab has been using MD simulations to study the structural characteristics of myosin and how cardiomyopathy related mutations in myosin alter the structure (paper in preparation). In another, Ertz-Berger *et al* performed MD simulations on a murine cTnT fragment (from residue 70 to 170) for FHC-related R92W and R92L mutants of cTnT, and found that both mutant peptides show a pronounced hinge motion near the region of residue 104 compared with little motion in the WT peptide simulation (*35, 89*). These simulations predicted alterations in protein dynamics of cTnT that are hypothesized to be associated with a change in myocellular growth and ultimately pathogenic cardiovascular remodeling that have been characterized using transgenic mouse model studies (*62, 90*). Lim *et al* reported computational analysis for DCM-related D75Y cTnC mutation that suggested that the concerted motions of Ca^{2+} binding pocket were markedly decreased by D75Y mutation (*91*). However, the simulations in this study were only carried out for <6 ns (a time before which equilibrium may not have been obtained), and thus sufficient information about cTnC protein dynamics has not yet been obtained.

Recently, Lindert *et al.* studied the dynamics and Ca^{2+} association to wild type

cNTnC using both conventional MD and accelerated MD (*92, 93*). They performed 100ns conventional and 50ns accelerated simulations on the structures of three different states of cNTnC: apo, Ca^{2+} bound, and Ca^{2+}-cTnI-bound. No obvious structure alterations were observed between the two types of MD simulations, but the accelerated MD did reveal some differences in the dynamics of the three states structures of cNTnC. Our lab was the first to perform MD simulation studies on cTnC variants with altered Ca^{2+} binding affinities, the results of which are later described in Chapter 3, 4 and 7.

1.7. Project motivation and overview

In this study, a series of single amino acid substituted cTnC variants with increased/decreased Ca^{2+} binding affinities have been chosen and developed to determine how they influence the Ca^{2+} activation pathway in cardiac myofilaments. These variants have not been clinically identified (to date) as associated with HCM or DCM, and thus may eventually provide clues as to whether altered Ca^{2+} signaling in myofilament contraction is casual or an adaptive response in diseased hearts. Additionally, it is also possible that 'corrective' manipulation of myofilament Ca^{2+} sensitivity could arrest or even reverse development of HCM or DCM, thus these cTnC variants could potentially be used as therapeutic gene therapy to treat heart disease. In order to accomplish this long-term goal, the biochemical and functional effects of these variants must be studied in order to predict the physiological consequences of these variants. This objective has been achieved by completing the following three major components of this project:

A. Determine the Ca^{2+} binding properties of cTnC variants and their influences on cTnI-cTnC interactions.

18

B. Determine the structural alterations of cTnC variants using Molecular Dynamic (MD) simulations.

C. Determine the influences of cTnC variants on intact cardiomyocyte contraction/relaxation.

1.7.1. Rationale of the cTnC variants selection

It is generally found that there is a correlation between the Ca^{2+} affinity of cTnC and the Ca^{2+} sensitivity of contraction in skinned fibers, although a few exceptions have been observed (*94*). In this study, a series cTnC variants were selected and designed based on previous reports of their effects on calcium binding affinity and myofilament calcium sensitivity of contraction (reviewed earlier in section 1.5) as well as computational studies (in chapter 2 and 3). L48Q and L48A were selected and designed since the unique position of residue 48 at the interface of cTnI binding region has the potential to influence its interaction with cTnI. I61Q/A/H were selected and designed to disrupt the Ca^{2+} binding loop. Residue V64 has been previously shown by nuclear magnetic resonance (NMR) studies to undergo significant chemical shift changes upon Ca^{2+} binding to cTnC (*95*) and thus V64Q is included. L57Q, which is located on the C helix away from the regulatory Ca^{2+} binding site and closer to the interface of cTnI binding pocket was also selected. To note, all of these single amino acid substitutions (L48Q, L48A, L57Q, I61Q, I61A, I61H and V64Q) that have been studied in this project are located in the N-domain of cTnC, which interacts directly with the switch region of cTnI (residue 147-163) upon Ca^{2+} binding and partially with the cardiac specific N-extension region of cTnI (residue 1-30) upon PKA phosphorylation.

1.7.2. In solution studies of the cTnC variants

The overall goal of the solution studies is to characterize and determine the effects of cTnC variants on the Ca^{2+} binding affinity, cTnC-cTnI interaction and its modulation by PKA phosphorylation in solution (Chapter 3, 4 and 5). An important question for therapeutic consideration is whether modified Ca^{2+} binding and/or TnC-TnI interactions can manipulate cooperative interactions to compensate for impaired contractile performance in diseases. Thus, these solution studies were carried out in parallel with *in vitro* cultured adult cardiomyocytes (Chapter 6) studies, which are a necessary precursor to our long-term goal of producing modifications of thin filament regulatory proteins to treat cardiomyopathies. The Ca^{2+} binding affinity of isolated cTnC, cTnC-cTnI complex, or whole cTn-complex and differences between PKA phosphorylated and non-phosphorylated cTnI binding affinities to cTnC were examined using steady-state fluorescence spectroscopy. The Ca^{2+} dissociation rates were determined by stopped-flow measurements. Isothermal Titration Calorimetry (ITC) was used to monitor the complete thermodynamics of interactions between cTnI and cTnC variants. The variants have been divided into two categories and discussed in Chapter 2 (for increased Ca^{2+} binding affinity variants) and Chapter 3 (for decreased Ca^{2+} binding affinity variants). In Chapter 4, the PKA phosphorylation effects on the cTnI-cTnC interactions and Ca^{2+} binding affinities of all studied cTnC variants are discussed.

1.7.3. in silico studies of the cTnC variants

Although the basic functional and structural roles of cTnC in modulating muscle contraction are relatively well studied, the underlying mechanism is not well understood. We hypothesize that structural alterations caused by single amino acid substitutions may lead to the development of observed functional changes. The goal of this *in silico* studies

using computational method of MD Simulation is to investigate the effects of these single amino acid substitutions on the structure and function of TnC and how it interacts with TnI. These structures and simulations enable better understanding of the biochemistry of the Troponin complex and to better interpret the data from the solution (Chapter 3, 4 and 5) and single intact cell (Chapter 6) studies.

The structure of the TnC-TnI complex has important implications for understanding the regulation of muscle contraction. However, to date there is no full publicly available structure for cTnI-cTnC complex. Besides the inhibitory region (cTnI $_{137-142}$) and C-terminal mobile domain (cTnI$_{164-210}$), which are known bind to actin-tropomyosin, the main regions of cTnI that interact with cTnC include (Figure1.2 and 1.4): (1) the cardiac specific N-extention region (cTnI$_{1-33}$), which contacts the regulatory domain of cTnC (cNTnC), and is further weakened by PKA phosphorylation at S23/S24 of cTnI; (2) IT-arm region (cTnI$_{34-136}$), which binds to the C-domain of cTnC (cCTnC); (3) switch region (residues147-163), which binds to cNTnC regulated by Ca^{2+} binding at site II; and (4) inhibitory region (residues 128-146), which likely releases its inhibition from actin and is repositioned to interact with the beginning (E-helix) of cCTnC in the Ca^{2+} saturated state. While these regions of interaction have been identified, the dynamics of the interaction of cTnI and cTnC are yet unknown. The IT-arm region of cTnI is thought to be structural rather than functional (though there is still a debate), and the interaction between cTnI$_{1-33}$-cNTnC is relatively weak and unclear. Therefore, detailed information about the interaction between cTnI$_{147-163}$ region and cNTnC could help to unambiguously trace the overall interaction between cTnC-cTnI. Since all of our cTnC variants (L48Q/A, L57Q and I61Q) are in the N-domain of cTnC, it enables us to

examine how changes to the sequence of the cTnC N-region may affect the interaction between cTnC and cTnI, and ultimately how these changes may result in functional alterations at the myofilament level. The NMR structure of cNTnC$\bullet$Ca^{2+} $\bullet$cTnI$_{34\text{-}136}$ complex has been selected to perform MD simulations. Additionally, simulations of cNTnC alone, both apo-cNTnC and Ca^{2+} saturated cNTnC, were also studied to further determine if the structural change is dependent on Ca^{2+} or cTnI$_{147\text{-}163}$ binding. The MD simulation results, together with those from the solutions studies, for L48Q cTnC are discussed in Chapter 3, while L57Q and I61Q are included in Chapter 4.

1.7.4. Intact cell studies of the cTnC variants

The goal of the intact cell studies is to determine the influences of cTnC variants with altered Ca^{2+} binding affinities on intact cardiomyocyte contraction. The cultured adult cardiomyocyte provides a useful platform on which to make a variety of measurements, including contractility, intracellular Ca^{2+} transients and metabolism, and protein isoform content. Experiments with L48Q have been conduction by a post-doctoral fellow in our research group (with a manuscript in review). Thus, the work presented here focuses on cultured cardiomyocytes infected with viral constructs containing DNA for the L57Q and I61Q cTnC variants. These *in vitro* experiments allow us to first characterize effects of the L57Q and I61Q cTnC variants at the cellular level in the absence of neuro-hormonal signaling and systemic viral-mediated responses (such as immune response and inflammation) *in situ*. Knowledge of how adult rat cardiomyocytes respond to incorporation of these cTnC variants into myofilaments is also a necessary precursor for us before moving to animal models. The results of this work are discussed in Chapter 6.

Lastly, in Chapter 7, the idea of using engineered cTnC variants to correct the disease phenotype was tested. A mutation known to be implicated in HCM pathogenesis, R145G cTnI was characterized. Data related to this study is presented and discussed in Chapter 7.
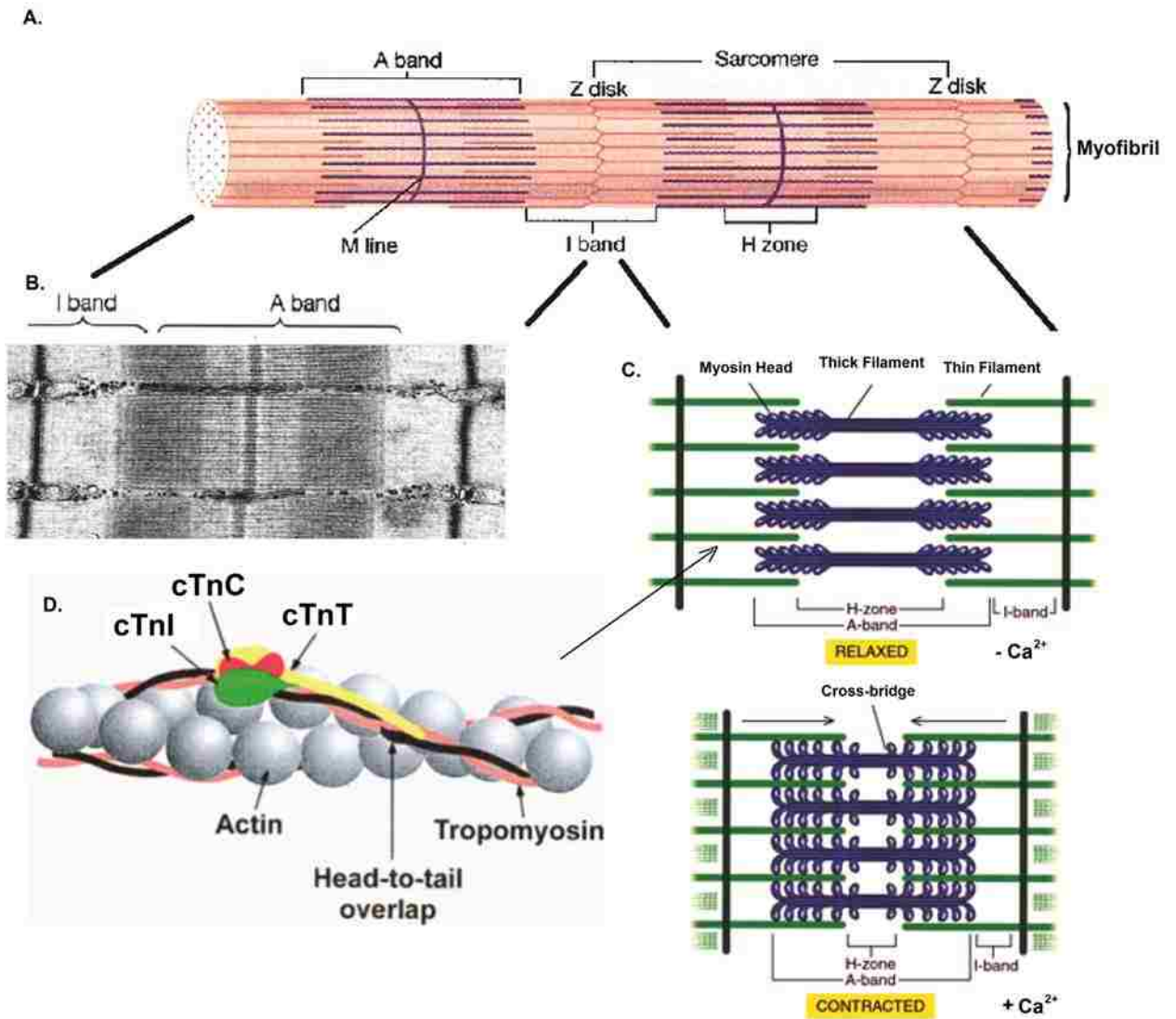
Figure 1.1. The contractile apparatus of cardiac muscle. A: Myofibril that is composed of repeating sections of sarcomeres. B: An electron micrograph image of muscle sarcomere (courtesy R. Craig, University of Massachusetts, USA). C: The Ca^{2+} dependent muscle contraction-relative sliding of the thin (green) and thick (blue) filaments within a sarcomere. D. Molecular components of thin filament proteins(*2*): Actin (gray), α-(black) and β-(orange) tropomosion, troponin C (red), troponin I (green), troponin T (yellow).
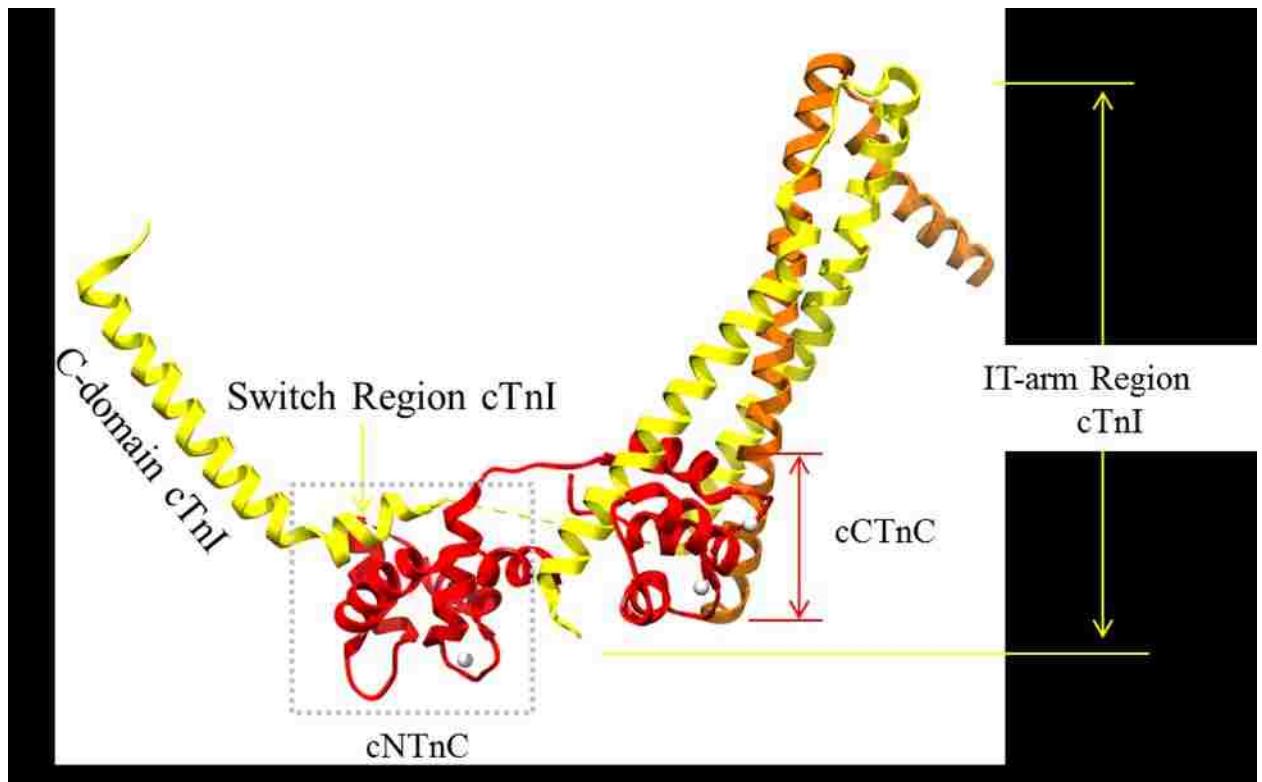
Figure 1.2. The x-ray crystal structure of the cTn complex (PDB:1J1E (*7*)) : cTnC (full length, red), cTnI (residues 40-133 and residues 147-191, yellow), cTnT (the T2 region: residues 183-288, orange) and Calcium (light gray), figure generated by Chimera (*96*).
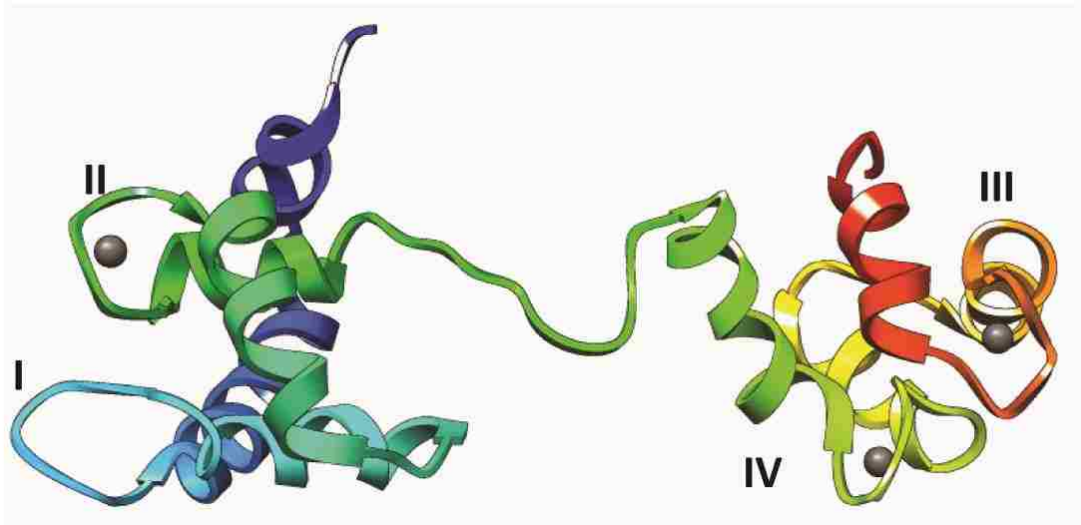
Figure 1.3. NMR structure of Ca^{2+} saturated cTnC (PDB:1LA0(*10*)): Ca^{2+} shown as gray spheres, figure generated by Chimera(*96*).
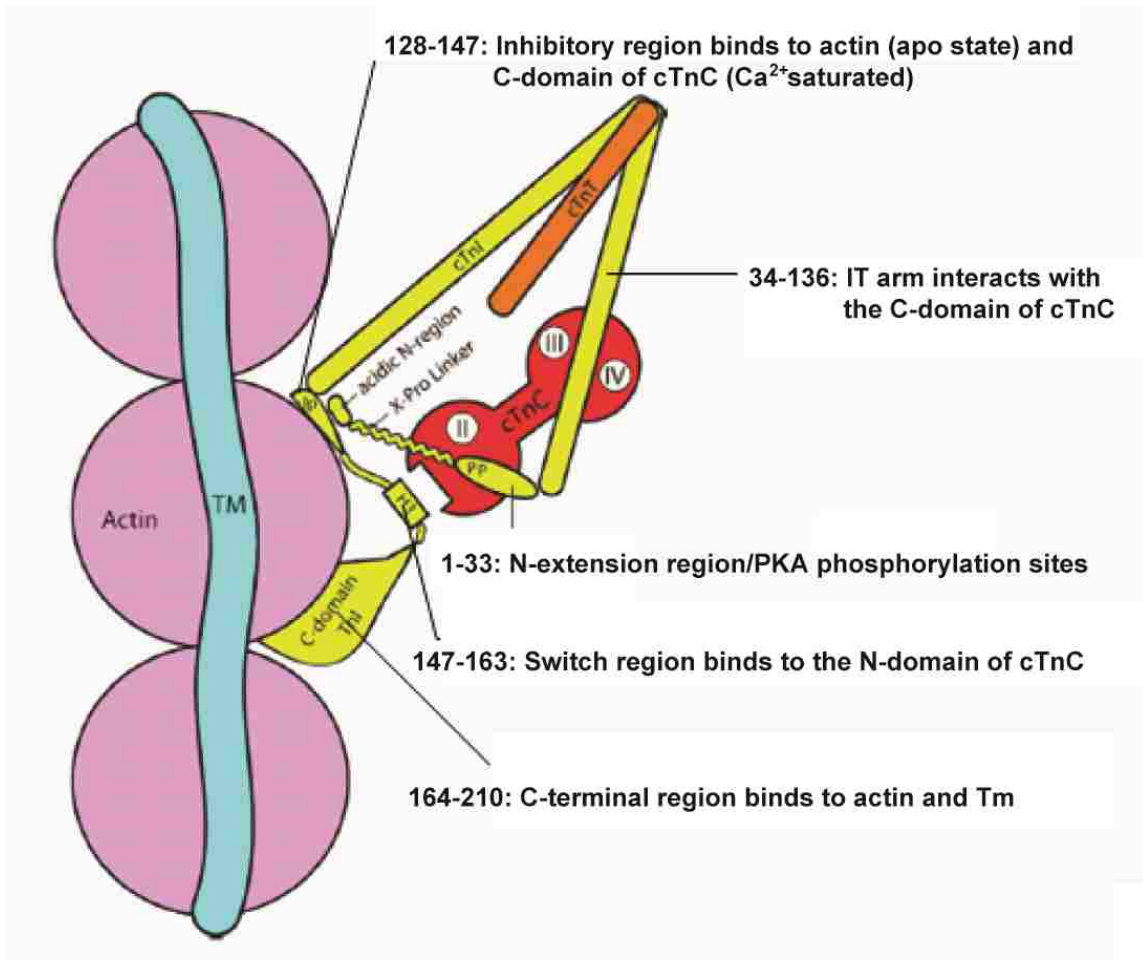
Figure 1.4. Cartoon illustrating the interactions of cTnI with other cTn subunits and thin filament proteins: cTnC (red), cTnI (yellow), cTnT (orange), Actin (pink), Tm (blue). Modified from (*28*).
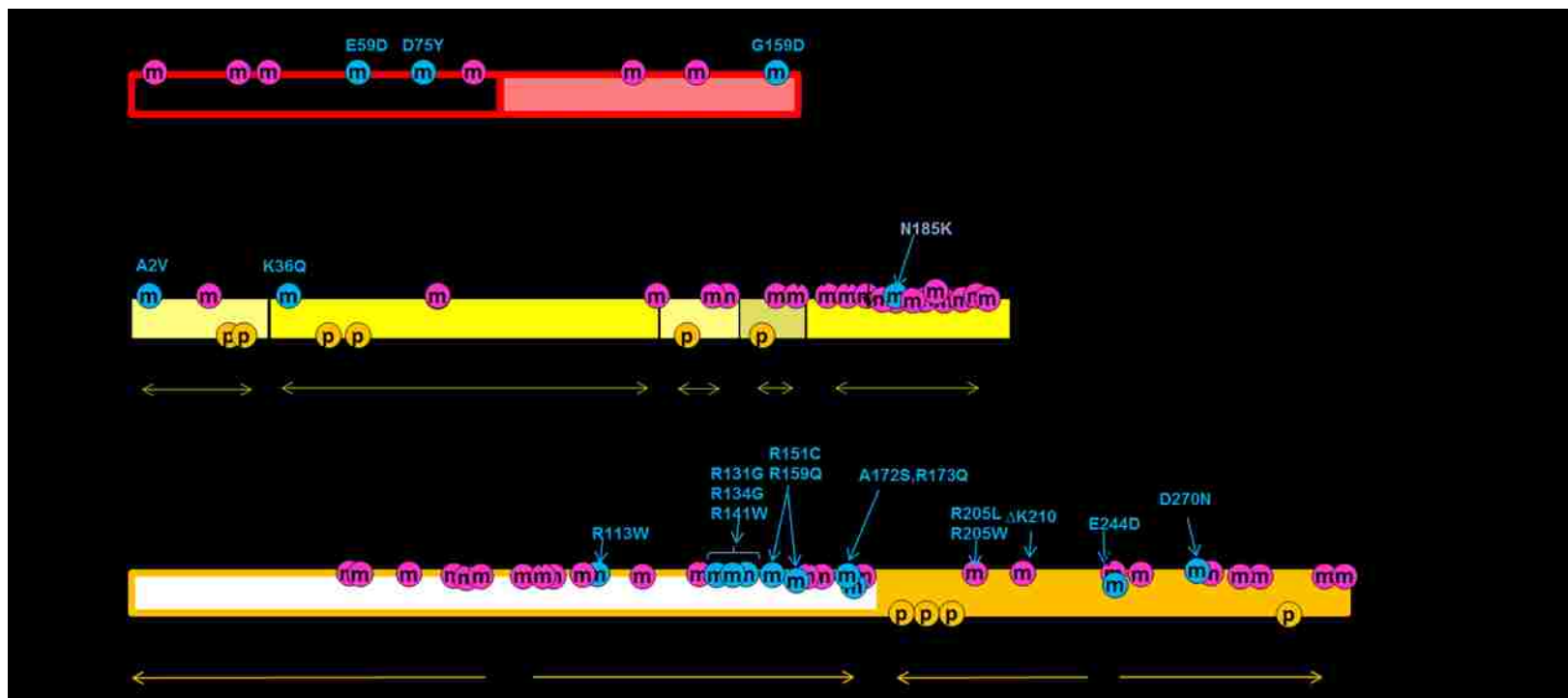
Figure 1.5. HCM and DCM related mutations and phosphorylation sites as identified on the primary sequences of human cTnC, cTnI, and cTnT: HCM associated mutations shown in pink, DCM shown in blue, phosphorylation sites labeled in gold.

Figure 1.6. Residue sequence in the regulatory domain of cTnC including Ca^{2+} binding site I (defunct) and site II, and and the helices N,A,B,C and D. Hydrophobic residues that were individually mutated to Q showing increased (blue circles) or decreased (red circles) of Ca^{2+} sensitivity. Modified from (*68*).

Chapter 2

Materials and Methods

2.1. Biochemical studies in solution

2.1.1. Protein Mutagenesis and Purification

Construction and expression of wild-type rat cTnC, cTnI and cTnT in pET24a vector has been described in a previous publication(*97*). cTnC^{C35S}, cTnC(L48Q)^{C35S}, cTnC(L48A)^{C35S}, cTnC(L57Q)^{C35S}, cTnC(I61Q)^{C35S}, cTnC(I61A)^{C35S}, cTnC(I61H)^{C35S}, cTnC(V64Q)^{C35S} were constructed from the rat wild-type cTnC plasmid by a primer based site-directed mutagenesis kit and confirmed by DNA sequence analysis. The plasmids for cTnC variants were then transformed into *Escherichia Coli* BL21 cells and expressed and purified. The DNA encoding cNTnC (residues 1-89) was inserted into pET3a expression vector as previously described (*98*). The L48Q mutation was engineered using a quikchange site-directed mutagenesis kit from stratagene (using paired 30-mer oligonucleotides, 5'-AAG GTG ATG AGA ATG CAA GGC CAG AAC CCC-3' and 5'-GGG GTT CTG GCC TTG CAT TCT CAT CAC CTT-3'). The construct of cNTnC(L48Q) was transformed into *Escherichia Coli* BL21 cells, expressed, and purified. ^{15}N-labeled cNTnC(L48Q) protein was expressed in minimal media enriched with (^{15}NH$_4$)$_2$SO$_4$ (*99*).

2.1.2. Fluorescent Labeling of Protein

The labeling procedure used here was as previous described(*100*). The C35S mutation was introduced to allow site-specific attachment of a fluorescent probe at C84. Briefly, cTnC^{C35S} and all other variants, respectively, were first dialyzed against 1mM DTT in a buffer containing 6M urea, 25mM TRIS, 1mM ethylenediamine-N,N,N9,N9-tetraacetic acid (EDTA) at pH8.0. 5mM DTT was added and the proteins were then dialyzed against the same buffer but without DTT for at least 12h with 3 buffer changes. 100mM IANBD (N-(2-(iodoacetoxy)ethyl)-N-methyl)amino-7-nitrobenz-2-oxa-1,3-diozole Mw=406.14) (in dimethylformamide) was added in 3-fold molar excess over TnC^{C35S} or cTnC(L48Q)^{C35S} and the protein solutions were gently shaken in the dark for >4hr at 4 °C. The labeling reaction was terminated by addition of 10mM DTT and the labeled protein solution was dialyzed against buffer containing 20mM MOPS,150mM KCl,3mM MgCl$_2$,2mM EGTA,1mM DTT, pH7.0 to remove unreacted IANBD (3 times for at least 12h). Finally, cTnC^{C35S} and cTnC(L48Q)^{C35S} were labeled at C84 of cTnC with IANBD. We have demonstrated that the fluorescence probe at this position monitors cTnC N-terminal Ca^{2+} binding (*100*). Labeling efficiency was calculated by determination of the IANBD fluorophore to protein molar concentration ratio. The IANBD concentration in the labeled protein was determined by dividing the absorbance of the labeled protein at the maximum absorbance for the fuorophore by the extinction coefficient of IANBD (21000M^{-1}cm^{-1}) at 481nm wavelength. All protein concentrations were determined using Bio-Rad protein assay. The final labeling efficiency was then determined as 90%.

2.1.3. PKA phosphorylation of cTnI

The protocol for PKA phosphorylation of cTnI is provided by Dr.Wenji Dong (Washington State University, Department of Bioengineering). Briefly, cTnI was phosphorylated by the catalytic subunit of PKA, using a cTnC affinity column. A sample of purified cTnI was loaded on a cTnC affinity column equilibrated in 50mM KH_2PH_4 at pH 7.0, 500mM KCl, 10mM $MgCl_2$ and 0.5 mM DTT, and 125 U PKA/mg. cTnI was added directly to the column and followed by adding ATP to the column to initiate the reaction. The column was incubated in water bath at 30°C for 30 min. Then the column was washed with a buffer containing 50mM MOPS at pH7.0, 500mM KCl, 2mM $CaCl_2$ and 0.5 mM DTT. Phosphorylated cTnI was eluted with a buffer containing 6 M urea, 10mM EDTA, 0.5 mM DTT and 50 mM MOPS at pH 7.0. Previously, it has been shown that phosphorylation by this protocol yields nearly 90% phosphorylation of PKA sites in cTnI (*101*). We further verify the phosphorylation by western blot using antibodies of rabbit polyclonal to Cardiac Troponin I (phospho S22 + S23) (from Abcam, ab58545) and goat anti-rabbit IgG-HRP (Santa Cruz Biotechnology, Inc., sc2004).

2.1.4. Reconstitution of Tn Complexes

The Tn subunits cTnI, and cTnT were first dialyzed separately against 6M urea, 25mM TRIS, 1mM EDTA at pH8. After dialysis, IANBD-cTnC^{C35S}, or other variants /cTnI/cTnT were mixed at the molar ratio of 1:1:1. After incubating at room temperature for 30 min, the protein solution was dialyzed through a series of steps against (1) 2M urea, 0.75M KCl, 20mM MOPS, 3mM $MgCl_2$, 1mM $CaCl_2$, pH 7.0 (2) 1M urea, 0.75M KCl, 20mM MOPS, 3mM $MgCl_2$, 2mM EGTA, pH 7.0 (3) 0.75M KCl, 20mM MOPS, 3mM $MgCl_2$, 2mM EGTA, pH 7.0 (4) 0.5M KCl, 20mM MOPS, 3mM $MgCl_2$, 2mM EGTA, pH 7.0 (5) 0.25M KCl, 20mM MOPS, 3mM $MgCl_2$, 2mM EGTA, pH 7.0 (6) Finally,

150mM KCl, 20mM MOPS, 3mM $MgCl_2$, 2mM EGTA, ,1mM DTT, pH 7.0. All dialysis was done in the dark (without stirring) at 4 ℃. Proteins that precipitated during the dialysis with decreasing KCl concentration were removed by centrifugation (*102*).

2.1.5. Determination of the effects of cTnC variants on Ca^{2+} binding affinity of WT and cTnC variants in isolation, cTnC-cTnI complexes and in the whole cTn complex

All steady-state fluorescence measurements were performed using a Perkin Elmer Luminescence Spectrometer LS50B at 15 ℃. IANBD fluorescence will be excited at 490nm and monitored the emission spectrum at ~530nm (both bandwidths set at ~8nm). Protein buffer solutions contain 20mM MOPS,150mM KCl, 3mM MgCl2, 2mM EGTA, and 1mM DTT (pH7.0). Fluorescence signal of 2mL IANBD-cTnC^{C35S}, cTnC^{C35S}-cTnI complex and IANBD-Tn^{C35S} (0.6μM) were monitored with titration of microliter amounts of Ca^{2+} in the presence (100μM) or absence of Ca^{2+}. The free Ca^{2+} concentration was calculated using the Maxchelator program (http://maxchelator.stanford.edu) (*103*). Ca^{2+} dependence of conformational changes (pCa value at half maximal fluorescence signal change) and dissociation constant K_D of cTnI for cTnC were obtained by fitting the binding curve with the sigmoid Hill equation as previously described (*104*). The reported values are the mean of three to five successive titrations. Data were presented as mean ± S.E.M. Statistical significance was determined by Student's t-test using SigmaPlot Software (Systat SoftwareInc.). $p < 0.05$ was considered as statistical significance.

2.1.6. Determination of the effects of cTnC mutants on Ca^{2+} dissociation rates (k_{off}) of WT and cTnC variants in the whole cTn complex

The Applied Photophysics Ltd. (Leatherhead, U.K.) model SX.18 MV stopped-flow instrument was used to measure the Ca^{2+} dissociation rates (koff) from whole Tn

complexes (no fluorescence labeling). This method uses Quin-2 (Calbiochem) as a fluorescent chelator. Whole Tn (WT and mutants) was dialyzed into: 250mM KCl, 20mM MOPS, 5mM MgCl2, 1mM DTT, pH 7.0. Each complex (6 μM) with 30 μM CaCl$_2$ was rapidly mixed with an equal volume of Quin-2 (150 μM) at 15ºC. Quin-2 reports the dissociation of Ca^{2+} from both the N and C terminus as a series of reactions with different time durations (50ms to 20 sec). These were then fitted with either single or double exponentials as appropriate. The k$_{off}$ values presented for the N-terminus of each protein was calculated by summing and fitting the data from three reactions and then repeating this at least 4 more times. The rate presented for the C-terminus represents the second rate from a double exponential fit of data collected over a 20s period.

2.1.7. Determination of the effects of cTnC variants on cTnC-TnI interaction in the presence and absence of Ca^{2+} upon PKA phosphorylation of TnI

IANBD fluorescence was monitored similarly to Ca^{2+} binding affinity measurements as described above. Wild type or PKA phosphorylated TnI was titrated in microliter amounts to 2ml of each cTnC variant (0.6μM) both with and without Ca^{2+}(100 μM) with constant stirring.

2.1.8. Determination of the effects of cTnC variants on the thermodynamics of cTnC-cTnI interaction by ITC

All experiments were performed using a Microcal, Inc isothermal titration microcalorimeter (ITC-200) in the Analytical Biopharmacy Core at the University of Washington. Experimental conditions were 30 °C, 20 mM MOPS, pH 7.0, 150mM KCl, 3 mM MgCl$_2$, 2 mM EGTA, 1mM CaCl$_2$. The sample cell was filled with 200 μl 3 μM

cTnI (with 1mM Ca^{2+}) and titrated with 2 µl per injection of 50-70 µM cTnC (WT or L48Q, Ca^{2+} saturated). Control titration of cTnC (WT or L48Q) to buffer was performed for each independent experiment. Binding parameters were calculated by the Origin-ITC data analysis software package using single set of sites mode. All data is shown as a mean value ±S.E.M.

2.2. Computational studies using molecular dynamic (MD) simulations

2.2.1. Basic MD simulation parameters

The starting structure of the N-terminus of cTnC (cNTnC, from residue 1 to 89) and cTnI$_{147-163}$ complex (cNTnC•Ca^{2+}•cTnI$_{147-163}$)was taken from model 18 of the NMR structure (PDB entry 1mxl) (25). The starting structure of cNTnC in the Ca^{2+} saturated (cNTnC•Ca^{2+}) form was from model 14 of the NMR structure (PDB entry 1ap4) (23). Model 13 of the NMR structure (PDB entry 1spy) (23) was used for the apo state (cNTnC alone). Figure 2.1.A,B,and C illustrate these the starting structures. cNTnC The L48Q, L48A, L57Q and I61Q mutations, individually was created *in silico* using UCSF Chimera (96) in all three structures. First, the side chain atoms of the substituted residue will be deleted. Second, different rotamers of the target residue type will be added based on the dynameomics rotamer library to generate multiple structures; the structure with the smallest interaction energy between the side chain of the substituted residue and the surrounding residues will be selected as the starting structure.

All-atom, explicit solvent MD simulations were performed at 15 °C (to match solution measurements in this study and previous mechanical measurements in cardiac muscle and myofibrils (17)) in the microcanonical (NVE, constant number of particles, volume, and total energy) ensemble using the *in lucem* molecular mechanics (*il*mm)

program (*105*) and the Levitt *et al.* force field (*106*). Starting structures, minimized for 1000 steps of steepest descent minimization, were solvated in a rectangular box of flexible three-center (F3C) water (*107*) with walls located at least 10 Å from any protein atom. The solvent density of the box was adjusted to 0.999129 g/mL, the experimental density for the simulation temperature of 15 °C (*108*). A 2 fs time step was used, and structures were saved every 1 ps for analysis. Multiple (n≥3) simulations for the $cTnI_{147-163}$·$cNTnC$·Ca^{2+} complexes (L48Q/A, L57Q, I61Q and WT), apo cNTnC (L48Q and WT) and Ca^{2+} saturated cNTnC (L48Q and WT), respectively, were performed of up to 70ns each. All protein images will be generated using UCSF Chimera (*96*). Analysis of MD trajectories was performed with *il*mm (*105*) .

2.2.2. Analysis of simulations to address general stability of the systems.

The root-mean-square deviations (RMSD) of the Cα atoms to the starting structure were calculated to measure the degree of change from the starting conformation.

2.2.3. Analysis of simulations to address the contacts between $cTnI_{147-163}$ and cNTnC.

Contacts between residues were defined as having a distance between two carbon atoms of ≤ 5.4 Å or any other non-carbon atoms of ≤ 4.6 Å. These contacts could be further classified as intra and inter molecular hydrogen bonds, hydrophobic contacts and other non-specific interactions. A hydrogen bond was defined if the distance between H-acceptor is ≤ 2.6 Å and angle of donor-H-acceptor is ≥ 135º. Hydrophobic contacts were identified if the carbon-carbon distance between CH groups is ≤ 5.4 Å. Any two non-carbon (and non-hydrogen) atoms were considered in non-specific interaction when ≤ 4.6 apart.

2.2.4. Analysis of simulations to address the structural alterations relevant to the hydrophobic patch

Figure 2.1 D, E and F show the hydrophobicity surfaces of the starting structures of different cNTnC states. It is clear that upon the binding of cTnI $_{147-163}$, the hydrophobic core within cNTnC becomes more exposed. We selected hydrophobic residues F20, A23, F24, I26, F27, I36, L41, V44, L48, L57, M60, F77, M80, and M81 as hydrophobic patch residues. The sum of the solvent surface area (SASA) of these residues were calculated and used to evaluate the exposure of the hydrophobic patch. Distances were measured between specific atom pairs or between the centers of mass of groups of atoms (e.g. two helices). The RMSD of the Cα atoms of either two helices (A/B, B/C etc.) of the structure to the starting structure were monitored over time to detect any major structural alterations. Interhelical angles were calculated using the program interhlx (K. Yap, University of Toronto). The SASA was calculated using Lee and Richards (*109*) algorithm. For all WT and variants cNTnC·Ca^{2+}·cTnI$_{147-163}$ simulations, cTnI$_{147-163}$ was removed from the MD trajectories so that the SASA of the hydrophobic patch residues in cNTnC could be then calculated. All error bars for results from the WT and variants MD simulation are based on the standard deviation in the average values of the multiple runs of simulations.

2.2.5. Analysis of simulations to address the structural alterations at Ca^{2+} binding site II

D65, D67, S69, T71, D73, and E76 are considered to be the Ca^{2+} binding coordinating residues, and are located in the regulatory domain of cTnC (*8, 110*) (Figure 2.2 A), and D65, D67, S69 & E76 (residues shown in sticks, Figure 2.2.B) have been

further investigated and have been shown to largely contribute to Ca^{2+} binding of cTnC . Since the interaction of these residues with each other and the calcium-binding pocket itself are critical regulators of the contractile process, the distances between Ca^{2+} and these Ca^{2+}-coordinating residues were calculated and averaged over time to evaluate the overall stability of the Ca^{2+} binding site. Distance between Ca^{2+} and Ca^{2+}-binding atoms (atmdist) were calculated as respect to binding affinity. Residue 61 is located very close to the Ca^{2+} pocket, and thus contacts formed between residue 61 and residues in the Ca^{2+} binding loop were probed to address any disruption at this site due to I61Q. **2.3.**

Physiological studies using cultured cardiomyocytes *2.3.1. Mutagenesis and generation of recombinant adenovirus*

The AdEasy™ system will be used as described previously (*111*) to generate recombinant adenoviral vectors to express either L57Q, I61Q or WT cTnC (poly-Histidine tagged) from the cytomegalovirus (CMV) promotor. The genes were first cloned into the shuttle vector pAdTrack-CMV. Green fluorescent protein (GFP) were cloned in as an indictor to identify transduced cells via fluorescence microscopy, and a GFP-only vector were produced as a viral control. The resultant plasmid were linearized by digesting with restriction endonuclease PmeI, and subsequently co-transformed into *E. coli.* BJ5183 cells with an adenoviral backbone plasmid pAdEasy-1. Recombinants were selected for kanamycin resistance, and recombination were confirmed using restriction endonuclease analysis. Linearized recombinant plasmid were transduced into adenovirus packaging 293 cell lines to produce high titer adenoviral preparations. In preliminary studies done in the Regnier lab, high titer levels of vector and incorporation into cardiomyocytes was achieved for L48Q cTnC (*Korte et al, paper in preparation*).

2.3.2. Cardiomyocyte isolation and culture

Adult rat cardiomyocytes (ARCs) were isolated and enzymatically digested from hearts from 6-8 week old female Fischer 344 rats using previously described methods(*112*). The harvested cells were plated on to 25mm^2 glass coverslips (1.0 thickness) pre-coated with laminin (in PBS). After settled for 2-4 hours, plating media was removed and cells will be transfected with plating media containing adenovirus (~250 viral particles per cardiomyocyte) overnight.

2.3.3. Cell viability and morphology

Microscopic examination of cell cultures were performed frequently (twice a day). Quantitatively, the % of surviving cells were determined by Trypan Blue exclusion and Live/Dead staining kits (Molecular Probes). In addition to cytologic evaluations, cardiomyocyte width, length and sarcomere length were also determined. Viability were assessed as responsiveness to stimulation during contraction measurements.

2.3.4. Cardiomyocytes contractile assessments

For all cardiomyocytes, video microscopy was performed using a 40x objective (Olympus UWD 40) and 25x intermediate lenses. Contractile assessments were performed at room temperature in buffer containing 1.8 mmol/L CaCl$_2$, 1.0 mmol/L MgCl$_2$, 5.4 mmol/L KCl, 140 mmol/L NaCl, 10 mmol/L HEPES, 0.33 mmol/L NaH$_2$PO$_4$, 5 mmol/L glucose; pH 7.4. Contractile properties were compared between different groups of cardiomyocytes (Non-treated/WT/GFP-only/L57Q/I61Q):

1) Intact cardiomyocyte magnitude and rate of shortening re-lengthening (relaxation) were monitored and recorded using IonOptix SarcLen system video microscopy (IonOptix, Milton, MA, USA). Cells will be paced at 0.5HZ, 1HZ and 2HZ

to determine if infection strategies influence contraction/relaxation differentially at higher heart rates. At each frequency a minimum of 10 contractions were used for the myocyte to achieve a steady state and no less than 8 subsequent contractions will be used for analysis(*113*).

2) Calcium transients induced by the electrical stimulation were measured in Fura2 AM (Molecular Probes) loaded cardiomyocytes using the IonOptix equipment as described previously (*114*). The kinetics of Ca^{2+} transients were analyzed in conjunction with myocyte mechanical measurements. Altered contraction properties of infected cardiomyocytes could result from cTnC variants directly affecting cross-bridge binding and cycling or indirectly via alterations in Ca^{2+} signaling that result in increased Ca^{2+} transients during excitation-contraction coupling. Experiments were looked at the amplitude and kinetics of Ca^{2+} transients in field-stimulated control and transduced cells.

2.3.5. Protein expression

To investigate whether there are changes in sarcomeric protein isoform expression in transduced cTnC variant cells, cardiomyocytes ($\sim$1-2x10^5) were harvested from individual wells from a 6-well tissue culture dish by mild (0.05%) trypsin treatment. For characterization of total cellular sarcomeric protein isoform content, we used SDS-PAGE and Ruby stain. Intact cardiomyocytes were made into samples immediately after collecting from culture. Proteins were separated on a 12% SDS-Page gel.

2.3.6. Sarcomere and SR protein phosphorylation levels

Phosphorylation levels of myofibrillar proteins (cTnI, cTnT, myosin binding protein-C, myosin light chain) by either PKA or PKC (or both) were determined with

Pro-Q Diamond assays and Western Blot analysis, using phosphorylation specific antibodies.

2.3.7. Data & statistical analysis

Shortening amplitude and the velocity of shortening and calcium transient decay were examined by non-linear regression analysis. The data was fitted to a single three parameter decaying exponential ($y=y_0+ae^{-bx}$). Relaxation and calcium transient decay will be evaluated by determining the time to 10%, 50%, and 90% relaxation (RT_{10}, RT_{50}, and RT_{90}, respectively). Contractile relaxation and calcium transient rise were fitted to the data with a single three parameter rising exponential ($y=y_0+ a (1-e^{-bx})$). Values were calculated and shown as mean $\pm$ S.E.M., unless indicated otherwise. An ANOVA test was used on each measurement for all groups to determine significant differences, with unpaired two-tailed t-tests performed between each study group (SigmaStat). Differences at the p-value < 0.05 were considered statistically significant.
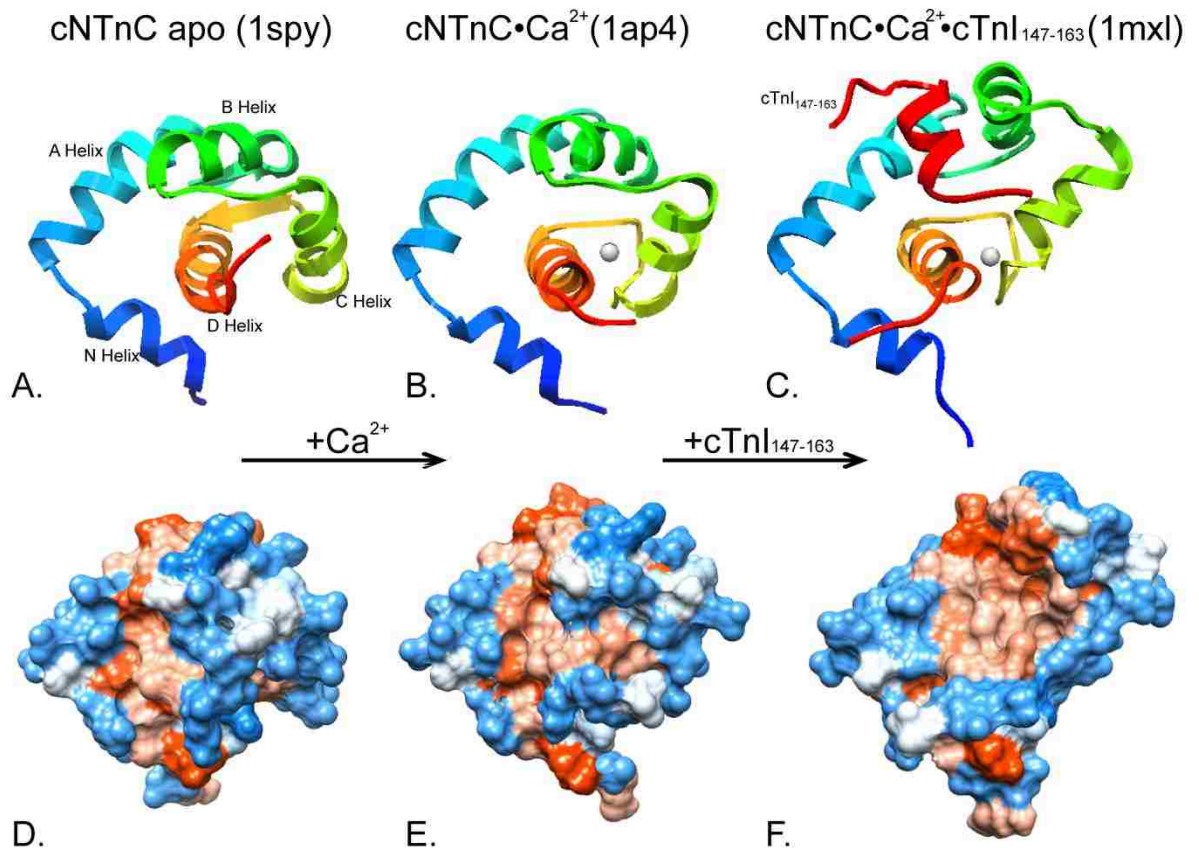
Figure 2.1. MD simulation starting structures. A-C: NMR structures of cNTnC apo

(1spy), cNTnC•Ca^{2+}(1ap4), and cNTnC•Ca^{2+}•cTnI$_{147-163}$(1mxl), Ca^{2+} shown in gray

sphere. D-F: structures from panel A, B, and C surface color-coded by amino acid

hydrophobicity, from dodger blue for the most polar residues, to white, to orange red for

the most hydrophobic residues. Generated by Chimera (*96*).
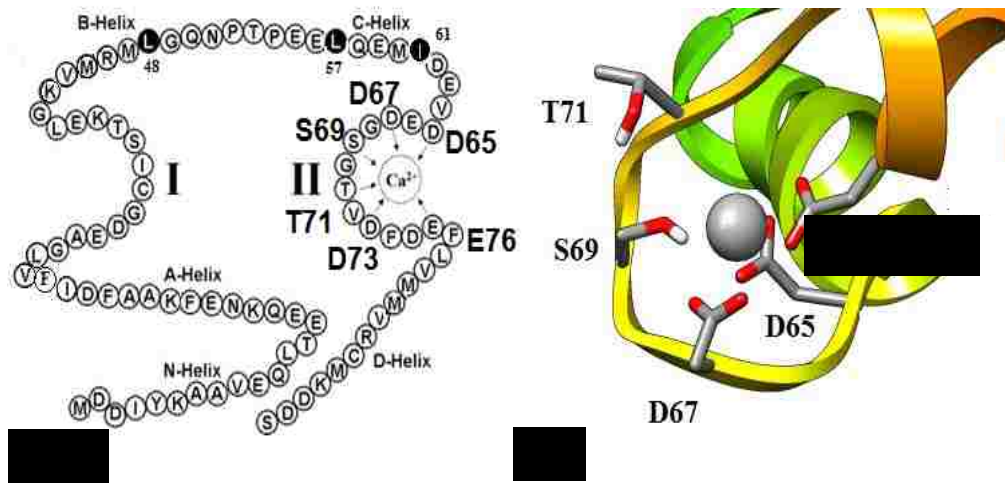
Figure.2.2. Ca^{2+} binding site II in cNTnC. A, schematic representation of the regulatory domain of cTnC, black circles represent the residues at 48, 57 and 61, modified from(*68*); B, illustration of Ca^{2+} binding site II in cNTnC, created from cNTnC•Ca^{2+}•$cTnI_{147-163}$NMR structure(*25*).

Table 2.1 Protein samples.

Method	cTnC	cTnI	cTnC-cTnI Complexes	cTn Complexes
PELS5 Spectro-fluorimeter	$cTnC_{IANBD}^{C35S}$ (variants*); $cTnC_{IANBD}^{C35S}$; $cTnC$(wt)	$cTnI$(wt); phos-$cTnI^{\#}$	$cTnC_{IANBD}^{C35S}$+cTnI(wt); $cTnC_{IANBD}^{C35S}$(variants) +cTnI(wt); $cTnC_{IANBD}^{C35S}$+cTnI(phos); $cTnC_{IANBD}^{C35S}$(variants)+cTnI(phos)	$cTnC_{IANBD}^{C35S}$+cTnT(wt)+cTnI; $cTnC_{IANBD}^{C35S}$(variants)+cTnT(wt)+cTnI; $cTnC_{IANBD}^{C35S}$+cTnT(wt)+cTnI(phos-); $cTnC_{IANBD}^{C35S}$(variants)+cTnT(wt)+cTnI(phos-)
ITC	cTnC(wt); cTnC(L48Q)	cTnI(wt)		

variants: L48Q, L48A, L57Q, I61Q, I61A, I61H or V64Q

 # PKA Phosphorylated cTnI at S23S24

Chapter 3

Structural and Functional Consequences of the Cardiac Troponin C L48Q Ca^{2+-}Sensitizing Variant

3.1. Introduction

Striated muscle contraction is triggered by a transient increase in intracellular Ca^{2+}, which binds to troponin C (TnC), the Ca^{2+}-binding subunit of the cardiac troponin (cTn) complex on thin filaments. TnC is a dumbbell shaped protein that consists of N-terminal and C-terminal EF-hand motifs connected by a long flexible linker (*17*). There are two isoforms of TnC in striated muscle: skeletal (sTnC) and cardiac (cTnC). The regulatory lobe of sTnC (sNTnC) undergoes a large structural "opening" when it binds two Ca^{2+} ions(*115*). The structural change is much smaller in cNTnC upon binding Ca^{2+} and it remains essentially "closed" (*23*). This difference may be the result of cNTnC having only one functional Ca^{2+} binding site (site II) (*116*). The C-terminus of cTnC (cCTnC) contains high affinity Ca^{2+} binding sites, III and IV. Although these sites are thought to play primarily a structural role by anchoring the Tn complex to the thin filament, they may also be involved in the Ca^{2+} signaling pathway, since disease-related mutations in this region of cTnC affect cardiac muscle function (*15, 117, 118*). cTnC interacts with the other two components of cTn: cardiac troponin I (cTnI) and cardiac troponin T (cTnT). Following Ca^{2+} binding to site II of cNTnC, the "switch" region of cTnI (residues 147-163, cTnI$_{147-163}$) binds to cNTnC and consequently the "inhibitory" region of cTnI (residues 112-146) dissociates from actin. The detachment of cTnI$_{112-146}$

from actin permits increased mobility of tropomyosin over the surface of the thin filament, providing exposure of the myosin binding sites on actin and subsequently actomyosin cross-bridge formation that results in contractile force generation and cell shortening (*2, 119*).

A growing number of genetically identified variants (mutations) in cTn subunits associated with cardiomyopathies have been shown to alter protein-protein interactions involved in thin filament activation (*49*). Thus far, at least 84 mutations in cTn proteins have been identified in patients with hypertrophic, restrictive, and dilated cardiomyopathy (HCM, RCM, and DCM, respectively) (*120, 121*). Functional studies of HCM-associated mutations, in most cases, result in increased Ca^{2+} sensitivity of contraction of skinned myocardium, and at least three variants are located in cTnC (A8V, C84Y and D145E). While the increase in Ca^{2+}-sensitivity may not cause HCM, it is possible the augmented contractility is associated with the progression and severity of HCM over time (*58*). Thus, understanding how altered Ca^{2+} binding influences cTn subunit interactions and signaling of thin filament activation could have considerable clinical relevance.

In this chapter we have focused on a cTnC variant, cTnC(L48Q), which was engineered by site-directed mutagenesis to enhance the Ca^{2+}-sensitivity of cTnC (it has not been identified in HCM patients to date). Previously, Davis and Tikunova showed that human cTnC(L48Q) increased the Ca^{2+} affinity of the Tn complex and thin filaments (*68, 74*). Parvatiyar *et al.* (*76*) showed it increased both Ca^{2+} sensitivity of skinned porcine papillary contraction and ATPase sensitivity. Recently, Kreutziger *et al.* (*75*) reported that the rat L48Q variant of cTnC had similar effects in solution and increased

Ca^{2+} sensitivity of contraction in rat trabeculae and myofibrils. Despite the wealth of functional data, the molecular mechanism for the effect of this mutation on cTnC has yet to be elucidated.

Leu48 makes a number of crucial hydrophobic contacts that contribute to stabilizing a closed form of cNTnC (*17*) – in both the apo and Ca^{2+}-saturated states (*23*). We have employed an integrative approach to understand how cTnC(L48Q) results in increased myofilament Ca^{2+} sensitivity. We used fluorescence spectroscopy and isothermal titration calorimetry (ITC) to confirm that an increase in both Ca^{2+} and cTnI affinity occurs by mutating L48 to glutamine. Molecular dynamics (MD) simulations have been employed to probe the detailed relationship between structure, dynamics and function. In particular multiple 70 ns simulations of cNTnC in the apo, Ca^{2+} saturated and $cTnI_{147\text{-}163}$ bound states were performed. The MD results suggest that L48Q increases the binding affinity of $cTnI_{147\text{-}163}$ for cNTnC by stabilizing its open conformation. Overall, the various results described here are consistent with L48Q stabilizing a more open conformation of cNTnC, which in turn enhances the Ca^{2+} and cTnI binding to cNTnC.

3.2. Results

3.2.1. Effects of cTnC(L48Q) on Ca^{2+} binding to isolated cTnC and cTn complex monitored by fluorescence

To assess the Ca^{2+} binding affinity of the L48Q variant, we attached the fluoroprobe IANBD at C84 of $cTnC_{IANBD}^{C35S}$. IANBD is an environment-sensitive and sulfhydryl-reactive extrinsic fluorophore that has been widely used to label biological molecules for studies of intra molecule interactions with minimal effect on binding properties (*122, 123*). Fluorescence labeling at C84 reports on conformational changes in

cNTnC due to both Ca^{2+} and cross-bridge binding (*124*). We found that Ca^{2+} caused a dose-dependent increase in fluorescence from the IANBD-labeled cTnC, suggesting Ca^{2+} promotes a conformational change in the cTnC that leads to a decrease in the polarity of the environment around IANBD-labeled cysteine.

We compared the Ca^{2+}-dependent conformational changes of $cTnC(L48Q)_{IANBD}^{C35S}$ and $cTnC_{IANBD}^{C35S}$. As shown in the inset graph of Figure 3.1, $cTnC(L48Q)_{IANBD}^{C35S}$ underwent ~1.33 fold maximal increase in IANBD fluorescence when saturated with Ca^{2+} versus a ~1.25 fold increase for $cTnC_{IANBD}^{C35S}$. The enhanced magnitude of total fluorescence change for $cTnC(L48Q)_{IANBD}^{C35S}$ implies a larger structural change of the regulatory domain of $cTnC(L48Q)_{IANBD}^{C35S}$ upon Ca^{2+} binding. We next added $cTnC(L48Q)_{IANBD}^{C35S}$ or $cTnC_{IANBD}^{C35S}$ to wild type cTnI and cTnT to form whole cTn complexes. Consistent with a previous report using recombinant human cTnC variants, the L48Q variant had an enhanced Ca^{2+} binding affinity (*68*). Ca^{2+} sensitivity of the fluorescence signal (reported as pCa at half-fluorescence increase) was shifted +0.32 pCa units, from 6.99±0.03 (cTn_{IANBD}^{C35S}) to 7.31±0.03 ($cTn(L48Q)_{IANBD}^{C35S}$) (curves in Figure 3.1). This matches well the 0.38 pCa unit increase in Ca^{2+} sensitivity of contraction we recently reported upon exchanging $cTn(L48Q)^{C35S}$ into skinned rat trabeculae (*75*).

3.2.2. Effects of cTnC(L48Q) on the cTnC-cTnI interaction in the apo and Ca^{2+} saturated states

Interactions between cTnC and cTnI play a critical role in transferring the Ca^{2+}-signal to other myofilament proteins to initiate cardiac muscle contraction. Thus, in addition to examining Ca^{2+} affinity, we tested whether the L48Q variant also altered cTnI

binding affinity. Binding of cTnI to cTnC was measured by titrating labeled $cTnC_{IANBD}^{C35S}$ with cTnI in the presence or absence of Ca^{2+}. cTnI binding to $cTnC_{IANBD}^{C35S}$ (control) and $cTnC(L48Q)_{IANBD}^{C35S}$, in the apo (panel A) and Ca^{2+} saturated (panel B) states increased IANBD fluorescence (Figure 3.2). For both control and $cTnC(L48Q)_{IANBD}^{C35S}$, the magnitude of maximal IANBD fluorescence change was greater for the Ca^{2+} saturated states than the apo state, indicating a larger conformational change. The amplitude of the fluorescence signal change is a rough indicator of the magnitude of conformational change. This magnitude increase was compared for $cTnC(L48Q)_{IANBD}^{C35S}$ versus control in the apo and Ca^{2+} saturated states. Maximal fluorescence increase did not differ for the apo state, but was significantly increased for $cTnC(L48Q)_{IANBD}^{C35S}$ (3.73 ± 0.18 fold) compared with control (3.29 ± 0.11 fold), suggesting the regulatory domain of cTnC(L48Q) is more open when bound to cTnI. cTnI appeared to bind to $cTnC(L48Q)_{IANBD}^{C35S} \bullet 3Ca^{2+}$ more tightly than to $cTnC_{IANBD}^{C35S} \bullet 3Ca^{2+}$, with dissociation constants of 174 ± 8 nM and 198 ± 5 nM, respectively, but these values did not differ statistically.

3.2.3. Binding of cTnI to cTnC in the presence of Ca^{2+} by ITC

Isothermal titration calorimetry (ITC) was used to obtain a more comprehensive picture of cTnI binding to cTnC. ITC permits monitoring of protein-protein interactions without the need for chemical modifications that may modify the interaction surface. Representative ITC data from the titration of cTnI with Ca^{2+} saturated cTnC(L48Q) are shown in Figure 3.3. For each titration point, the quantity of heat released (as indicated by the negative deflection) is directly proportional to the amount of binding between the

two proteins. The complete binding isotherm was obtained by plotting the integrated heat against the molar ratio of cTnC added to cTnI in the reaction cell. The stoichiometry (n), dissociation constant (K_D) and enthalpy (ΔH) of binding were obtained by fitting these data using the Origin-ITC package. The results from a minimum of three independent ITC binding experiments for cTnC or cTnC(L48Q) binding to cTnI, in the presence of Ca^{2+}, suggested the binding stoichiometry was approximately 1:1 for both WT and cTnC(L48Q). Consistent with the fluorescence data, the affinity of cTnC (L48Q) for cTnI was higher than cTnC, K_D 132 $\pm$ 59 nM for cTnC(L48Q) and K_D 159 $\pm$ 91 nM for cTnC. Furthermore, the total heat released upon binding to cTnI (ΔH) for cTnC(L48Q) was -22.1 $\pm$ 1.5 kJ·mol^{-1}, and -16.1 $\pm$ 3.9 kJ·mol^{-1} for cTnC.

3.2.4. The importance of residue 48 in cNTnC for cNTnC and cTnI$_{147-163}$ interaction

We also used MD simulations to investigate structural changes with the L48Q variant that may explain the experimentally observed increase in cTnI binding to cTnC. Simulations were performed for both cNTnC(WT)•Ca^{2+} and cNTnC(L48Q)•Ca^{2+} complexed with cTnI$_{147-163}$ (1mxl) at neutral pH and 15 ℃. We first investigated the residue contacts between cNTnC and cTnI$_{147-163}$. L48 is located at the end of helix B of cNTnC and makes multiple contacts with cTnI$_{147-163}$ peptide (Figure 3.4 A). Contacts information was sampled over the entire 70ns for multiple simulations ($\geq$5). Residues from cNTnC and cTnI$_{147-163}$ with more than 20% time in contact over entire simulations were chosen and counted as contact pairs between the two proteins. We plotted the number of contact pairs between cNTnC and cTnI$_{147-163}$ for each residue position of cNTnC to determine the overall contact map for cNTnC interaction with cTnI$_{147-163}$. Results are shown for WT in Figure 3.4.B and L48Q in Figure 3.4.C. The general pattern

is similar for both cNTnC structures. The data show that residue 48 contacts the greatest number of residues in cTnI$_{147-163}$ for both proteins, suggesting this position of helix B in cNTnC is important for cNTnC interaction with the switch region of cTnI. However, some cNTnC residues have increased or decreased number of contact pairs for L48Q compared to WT, which may significantly alter the interactions between cNTnC and cTnI switch peptide. While this merits further investigation, detailed analysis is beyond the scope of this study.

We analyzed the detailed contact information between residue 48 and the switch region of cTnI, as demonstrated in Figures 3.4 C and D. Interestingly, the mutation to glutamine at residue 48 increased interactions with several residues in the switch region of cTnI: S149, M153, M154, L157, L158 and G159. According to the NMR structure, these residues all point towards the hydrophobic core in cNTnC (Figure 3.4.D). The increased contact time during simulations of these residues with L48Q might be due to hydrogen bond formation with the side group of Gln (Q) at 48. For example, hydrogen bond was found between Q48 and L157 in cTnI$_{147-163}$ during ~5% of total simulation time. In contrast, residues in cTnI$_{147-163}$ had longer time in contact with L48 (WT) than Q48 (L48Q) located at either the opposite side of the hydrophobic patch of cNTnC or near the ends of cTnI$_{147-163}$ peptide. These residues are less relevant to the binding interface between cTnI$_{147-143}$ and the hydrophobic patch in cNTnC as labeled and shown in Figure 3.4.D.

3.2.5. Effects of L48Q substitution on the mobility of the helix B in cNTnC

A structural deviation in cNTnC·Ca^{2+} associated with binding of the cTnI$_{147-163}$ peptide is the movement of the helix B away from the helix A (*25*). The simulations of

the cNTnC(L48Q)•Ca^{2+}•cTnI$_{147-163}$ complex demonstrated that helix B moved, as shown in Figure 3.5.A by the snapshots from L48Q simulations at 0 and 60ns. (The MD movies are available in the supporting information.) This movement of B helix occurred in all of the cNTnC(L48Q)•Ca^{2+}•cTnI$_{147-163}$ simulations but it was not observed for any of the 5 WT cNTnC•Ca^{2+}•cTnI$_{147-163}$ simulations. To investigate further, we analyzed the distances and interhelical angles between helices A and B. The distances between the centers of mass of helices A and B (COMdist AB), averaged over the last 25 ns of multiple simulations, were 17.7 ± 0.7 Å for L48Q and 16.5 ± 0.7 Å for WT. The differences in COMdist AB (ΔCOMdist AB) at the end (from 45-70ns) compared with the beginning of the simulations (10-25ns) show that helices A and B moved ~0.4 Å further apart from each other for L48Q compared to WT, but the change is subtle, particularly given the dynamic nature of these helices.

To further validate the conformational change in cNTnC by the L48Q mutation, we performed MD simulations of apo and Ca^{2+}-saturated cNTnC structures (PDB entries: 1spy and 1ap4, respectively) for both WT and L48Q. In Figures 3.5.B and C, the starting structures are compared with the structures at 60 ns for cNTnC(L48Q) and cNTnC. For both apo and Ca^{2+}-saturated simulations, the B-helix of cNTnC(L48Q) underwent a large movement away from the core of the domain. For WT cNTnC, no movement of the helix was observed. Figure 3.5.D compares for A and B helices only, for all simulation structures at 60 ns versus the starting structures (90 °counter clockwise rotation from y-axis of the structure shown in panels A, B and C). From this view, it is clear that the AB helices are generally more open for L48Q. This movement of the helix B was not dependent on the binding of Ca^{2+} or cTnI$_{147-163}$ in the Ca^{2+} saturated state. Generally,

cNTnC(L48Q) had greater values of Cα-RMSD of helices A and B relative to the original

NMR structure from all states populated in the simulations (Figure 3.5.E), illustrating the

dynamic character and increased mobility of these helices. The difference in the motion

of the B-helix between cNTnC(L48Q) and cNTnC is presumably due to Gln 48 at the end

of the B-helix in the variant, which disrupts key contacts L48 makes with residues on the

A-helix, such as F20, A23, and F27. This has been proved by our simulations that the

distances between Q48 with F20 or A23 indicate that L48Q are ~2.0 Å and ~0.5 Å away

from F20 and A23, respectively, while L48Q and F27 moved closer to each other for

~1.8 Å compared to WT.

The interhelical angle between A and B helices (Figure 3.5.D) was used to

quantify the degree of opening conformation incNTnC. The A/B interhelical angles

averaged from multiple simulations were ~87 °for L48Q and ~107 °for WT, suggesting a

more open conformation for L48Q cNTnC in the Ca^{2+} and$cTnI_{147\text{-}163}$ bound state. Similar

results were found for both apo and Ca^{2+} saturated simulations, helices A/B were

generally more open for L48Q than WT structures (Table 3.1). In particular, our

simulations suggest there is a decrease of about 10 °in the AB interhelical angle of L48Q

compared to WT in the Ca^{2+} saturated state. This magnitude of change is consistent with

the prediction from ORBplus that the A/B interhelical angle of cNTnC(L48Q)•Ca^{2+} is

~10 °more open than cNTnC•Ca^{2+} (~120 °*versus* ~130 °) (*125*).

To quantify the exposure of the hydrophobic surface in cNTnC that associates

with the binding with the switch region of cTnI, we selected hydrophobic residues F20,

A23, F24, I26, F27, I36, L41, V44, L48, L57, M60, F77, M80, M81 as hydrophobic

patch residues. In simulations these cNTnC residues made contacts for more than 40% of

time with the switch region of cTnI in cNTnC•Ca^{2+}•$cTnI_{147-163}$ (both WT and L48Q). The total SASA of the hydrophobic patch residues was greater in $cNTnC^{.}Ca^{2+.}cTnI_{147-163}$ simulations than in cNTnC.Ca^{2+} or Apo cNTnC in both WT and L48Q simulations (Table 3.2), indicating the hydrophobic patch was more exposed in the presence of $cTnI_{147-163}$. This is consistent with an NMR and X-ray studies showing that binding of the switch region of cTnI induces opening of cNTnC (*7, 25*). In addition, L48Q had greater SASA of the hydrophobic patch area in all structures from the simulations compared to WT (Table 3.2), again showing the larger hydrophobic surface area in cNTnC (L48Q). Figure 3.5.F shows the surface rendering of structures from cNTnC•Ca^{2+} (0 ns and 60 ns) and L48Q cNTnC•Ca^{2+} (60 ns) simulations. The selected hydrophobic patch residues are colored red in all structures with the rest of the protein colored in white.

The distance between the backbone α-carbons of M81 (on helix D) and N50 (B-C loop) was used to quantify the opening of cNTnC (Figure 3.6), as was previously done to monitor the opening of cNTnC when $cTnI_{147-163}$ bound or when Ca^{2+} bound to sNTnC (*25*). M81-D50 distances were generally larger in the cNTnC (L48Q) compared to cNTnC, as calculated from all state simulations (apo, Ca^{2+}saturated and $cTnI_{147-163}$ bound) (Table 3.3). The increase in distance between M81-D50 of L48Q is consistent with the results from the interhelical angle and the distances between helices A/B, which all indicate that the L48Q variant induced a more open state of cNTnC.

Overall, the increased mobility of helix B facilitated the exposure of the hydrophobic patch in cNTnC(L48Q) and disrupted the closed structure of cNTnC, which supports the idea of an increase in the binding affinity of the switch region of cTnI to cNTnC.

3.2.6. Effect of L48Q substitution on the Ca^{2+} coordinating residues at Ca^{2+} binding site II

Independent of the differences in the global structure of cTnC, the EF-hand is a very conserved helix-loop-helix motif, with Ca^{2+}-binding loops containing 12 amino acids (*126, 127*). Among the 12 residues in the second Ca^{2+} binding loop (site II) of cNTnC, residues D65, D67, S69, D73, T71, and E76 at positions 1, 3, 5, 7, 9, 12 are involved in coordination to the calcium (*8, 110*). Since the interaction of these residues with each other and the Ca^{2+}-binding pocket itself are critical regulators of the contractile process, we also analyzed the MD simulation trajectories of cNTnC(L48Q)•Ca^{2+}•cTnI$_{147-163}$ and cNTnC•Ca^{2+}•cTnI$_{147-163}$ to examine how the L48Q substitution influences Ca^{2+} binding at cNTnC site II. The distances between the center of mass of Ca^{2+} and the Ca^{2+}-coordinating residues were calculated and averaged over time to evaluate the overall stability of the Ca^{2+} binding site (Figures 3.8.A and B). Variability was not significant at any of the Ca^{2+} coordinating residues, with the exception of S69, in the WT simulations. The L48Q simulations showed no significant perturbation at any residues, indicative of a very stable Ca^{2+} binding site.

Detailed coordinating information was obtained by investigating the changes in the distances between center of mass of Ca^{2+} and individual Ca^{2+}-binding atoms, shown by examples in Figure 3.7.C. Interestingly, in the 60 ns simulation snapshot of the WT cNTnC•Ca^{2+}•cTnI$_{147-163}$complex, D67-OD1, E76-OE2 and S69-OG (atoms shown as red spheres in Figure 3.7.D) pointed away from the Ca^{2+} ion. However, for the cNTnC(L48Q)•Ca^{2+}•cTnI$_{147-163}$ complex, only D65-OD2 pointed away from the Ca^{2+} ion. Figure 3.7.C summarizes the average distances between these atoms and Ca^{2+} throughout

the simulations. When compared to the average distances between Ca^{2+} and these atoms from the original 40 structures in the 1mxl NMR ensemble and those in model 18 from 1mxl (data not shown), D67OD1 and E76OE2 were closer to Ca^{2+} for the L48Q variant than WT, suggesting possible improved interactions between Ca^{2+} and these coordinating residues in L48Q. This change within the calcium binding site in the L48Q variant observed by MD simulations is consistent with our observed experimental measurements of increased Ca^{2+} binding affinity for the L48Q cTnC variant (Figure 3.1).

3.3. Discussion

Calcium binding to the regulatory domain of cardiac troponin C (cNTnC) causes a conformational change that exposes a hydrophobic surface to which troponin I (cTnI) binds, prompting a series of protein-protein interactions that culminate in muscle contraction. A number of cTnC variants that alter the Ca^{2+}-sensitivity of the thin filament have been linked to disease. Tikunova and Davis have engineered a series of cNTnC mutations that altered Ca^{2+} binding properties and studied the effects on the Ca^{2+} sensitivity of the thin filament and contraction(*68*). One of the mutations they engineered, the L48Q variant, resulted in a pronounced increase in cNTnC Ca^{2+} binding affinity and Ca^{2+} sensitivity of cardiac muscle force development. In this work, we sought structural and mechanistic explanations for the increased Ca^{2+} sensitivity of contraction for the L48Q cNTnC variant, using an array of biophysical techniques.

The combination of structural and functional information has been valuable for understanding the biochemical and biophysical mechanisms of proteins. Here we have used a highly integrative approach by combining fluorescence spectroscopy, micro-calorimetry and molecular dynamics simulations to determine the molecular

consequences of an L48Q mutation on the conformation and dynamics of cTnC, as well as its interaction with cTnI upon Ca^{2+} binding. We found that the L48Q mutation enhanced binding of both Ca^{2+} and cTnI to cTnC. Molecular dynamics simulations suggest that the mutation disrupts a network of crucial hydrophobic interactions so that the closed form of cNTnC is destabilized. Later, results from our collaborators indicated that NMR chemical shift and relaxation data provided evidence that the cNTnC hydrophobic core is more exposed with the L48Q variant. The findings emphasize the importance of cNTnC's conformation in the regulation of contraction and suggest that mutations in cNTnC that alter myofilament Ca^{2+} sensitivity can do so by modulating Ca^{2+} and cTnI binding.

It is important to elucidate the effects of cTnC modifications on its interactions with cTnI that may contribute to the change in cooperative myofilament activation. As such, knowledge of how the L48Q cTnC variant influences the cTnC-cTnI interaction will help in understanding molecular mechanisms of how altered cTn protein-protein interaction lead to changes in Ca^{2+} sensitivity of myofilament contraction (*75*). Our steady state fluorescence spectroscopy results indicate that interactions with cTnI, L48Q cTnC underwent greater conformational changes than the control indicated by the increased fluorescence signal in both the presence and absence of Ca^{2+}. This increase in the L48Q cTnC-cTnI interaction suggests a strengthening of the Ca^{2+} signaling pathway between cTn subunits and tropomyosin (and actin) such that at any given sub-saturating Ca^{2+} concentration, more myosin binding sites on thin filaments are available. This (for L48QcTnC) is demonstrated in myofibrils and demembranated cardiac muscle as a faster rate of myosin binding and force development at all sub-maximal (but not maximal) Ca^{2+}

activations (*75*). Greater myosin binding is also demonstrated by a prolonged slow phase of relaxation in cardiac myofibrils (*75*), which is thought to reflect the rate of decay of the attached myosin population during relaxation (*128*). Finally, in terms of cooperative mechanisms of contractile force production, we have demonstrated that myosin binding to actin plays a larger role in cardiac vs. skeletal muscle thin filament activation (*75, 129-131*) and that the apparent cooperativity of activation (the slope, n_H, of the force-pCa curve) is reduced by L48Q cTnC (*75*). The greater conformational change of L48Q cTnC upon binding Ca^{2+} and cTnI binding might lead to the exposure of the hydrophobic patch at lower concentrations of Ca^{2+} than for native cTnC. This may result in a lower dependence on allosteric activation of thin filaments by myosin in myofilaments containing L48Q cTnC.

The MD simulations demonstrate how the L48Q mutation causes the opening of cNTnC, with the B-helix swinging away from the hydrophobic core of cNTnC and remaining in that position till throughout multiple 70 ns simulations. The MD simulations predicted a decrease of approximately $10°$ in the AB interhelical angle of cNTnC(L48Q)•Ca^{2+}. This magnitude of change is consistent with a recent study that used couple of different computational methods in combination with NMR data to predict that the AB angle of cNTnC(L48Q)•Ca^{2+} would go from ~130 to ~120$°$(*125*). This structural impact is most likely the result of changing the hydrophobic Leu to the hydrophilic Gln at position 48 at the end of the B-helix. L48 makes key hydrophobic contacts with the side-chains of residues on the A-helix, such as F20, A23, and F27 (Figure 3.6). Overall, the results presented herein suggest the L48Q mutation modulates Ca^{2+} sensitivity of cTnC

and myofilament contraction by disrupting the structure of cNTnC, destabilizing the closed conformation of cNTnC.

In terms of the Ca^{2+}-sensitivity of cTnC, our solution spectrofluorimetry measurements demonstrate that the Ca^{2+} binding affinity (K_a) is increased by the L48Q variant for both cTnC in isolation and the cTn complex, as previously reported (15). This increase is due primarily to a slower rate of Ca^{2+} dissociation (k_{off}), as measured for isolated cTnC, whole cTn and reconstituted thin filaments (15, 17). S69 was the least stable Ca^{2+} coordinating residue in the WT cNTnC MD simulations. In contrast, D67 and E76 (in addition to S69) in site II were more tightly coordinated with Ca^{2+} in the L48Q variant relative to WT cNTnC (Figures 3.8.C, D). Similar results have been reported for MD simulations of other EF-hand Ca^{2+} binding proteins, parvalbumin and its variants (*132*), although the simulations were too short (300 ps) to make confident conclusions. This work represents the first study of the dynamic behavior of cNTnC in apo, Ca^{2+} saturated and cTnI$_{147-163}$ bound states in multiple long (70ns) MD simulations. L48 is located at the end of helix B (Figure 3.4.A), and is too distant to directly affect Ca^{2+} binding at site II. Instead L48Q causes local changes that are propagated to the calcium site. Interestingly, the Cα RMSD of C and D helices calculated from all MD simulations are 1.59 ± 0.06 Å for L48Q (6 runs) and 1.88 ± 0.07 Å for WT (5 runs), showing that these helices are more stable in L48Q. The exposure of the hydrophobic surface requires the B and C helices to move away from the N, A, and D helix bundle, and L48Q catalyzes the lifting movement of helix B (**Movie 1&2** Supporting Information)**.** This decreases the energetic barrier of opening, enhancing both Ca^{2+} and cTnI binding.

Furthermore, we collaborated with another group at University of Alberta to perform NMR studies on L48Q cTnC variant. They measured the affinity of L48Q cNTnC for Ca^{2+}, and the affinity of cNTnC·Ca^{2+} for $cTnI_{147-163}$ using NMR spectroscopy. Their results showed that Ca^{2+} bound to L48Q cNTnC with a K_D of 0.6μM, which is lower than the dissociation constant for WT cNTnC (~2.6 μM), indicating an increased Ca^{2+} binding affinity to cNTnC compared with WT. This is consistent with our results using fluorescence spectroscopy, where we demonstrated that the K_D for Ca^{2+} also decreased following the L48Q substitution as compared to WT. Our MD simulations suggest that this increase in Ca^{2+} binding affinity might be related to the increased interaction between several Ca^{2+} coordinating residues with Ca^{2+}. Consistent with our results that L48Q increased cTnC-cTnI interaction, they also found that the affinity of $cTnI_{147-163}$ to L48Q cNTnC·Ca^{2+} is approximately two times higher than that measured for WT, K_d ~ 61 μM (L48Q) vs ~150 μM (WT) by NMR. The K_D that we observed was lower than that determined by the Sykes group, however (K_D: ~170nM for L48Q vs ~200nM for WT). This might be due to the fact that full cTnI has 210 residues and has several regions that interact with cTnC (both at N and C domains) than those used in the MD simulations and NMR studies. In their NMR study, only $cTnI_{147-163}$, a short segment, is used to assess the cTnI binding to the hydrophobic patch of (L48Q) cNTnC•Ca^{2+}, which specifically relates to the interaction between cTnI and cTnC at these residues alone. They further compared the amide chemical shifts of D73, E66, L29, G34, G68, and T71 from cNTnC(L48Q)•Ca^{2+} with the shifts of the closed state, cNTnC•Ca^{2+} and two open states, cNTnC•Ca^{2+}•$cTnI_{147-163}$ and cNTnC•Ca^{2+}•bepridil (*133*). The average of chemical shifts suggest that cNTnC(L48Q)•Ca^{2+} is in a conformation somewhere

between the closed and open states, closer to the closed state. Furthermore, cNTnC(L48Q) was found to dimerize more readily than cNTnC•Ca^{2+} but less than sNTnC•2Ca^{2+}, which also supports the notion that L48Q stabilizes a slightly more open state of cNTnC.

Although many physiological and animal model studies have revealed the functional changes between native and disease-associated cTnC mutations that may underlie the pathogenesis of heart disease, there is little information available about the structural consequences of the change in the interaction of cTnI with cTnC caused by these substitutions. Our results provide the structural, dynamic and functional effects of the L48Q mutation of cTnC on cTnC-cTnI interactions and emphasize the importance of the conformational change in the regulatory domain of cNTnC in cardiac muscle regulation.

3.4. Conclusions

In this work, we sought structural and mechanistic explanations for the increased Ca^{2+} sensitivity of contraction for the L48Q cNTnC variant, using an array of biophysical techniques. We found that the L48Q mutation enhanced binding of both Ca^{2+} and cTnI to cTnC. Molecular dynamics simulations suggest that the mutation disrupts a network of crucial hydrophobic interactions so that the closed form of cNTnC is destabilized. NMR chemical shift and relaxation data provided support that the cNTnC hydrophobic core is more exposed with the L48Q variant as provided by our collaborators. The findings emphasize the importance of cNTnC's conformation in the regulation of contraction and suggest that mutations in cNTnC that alter myofilament Ca^{2+} sensitivity can do so by modulating Ca^{2+} and cTnI binding.
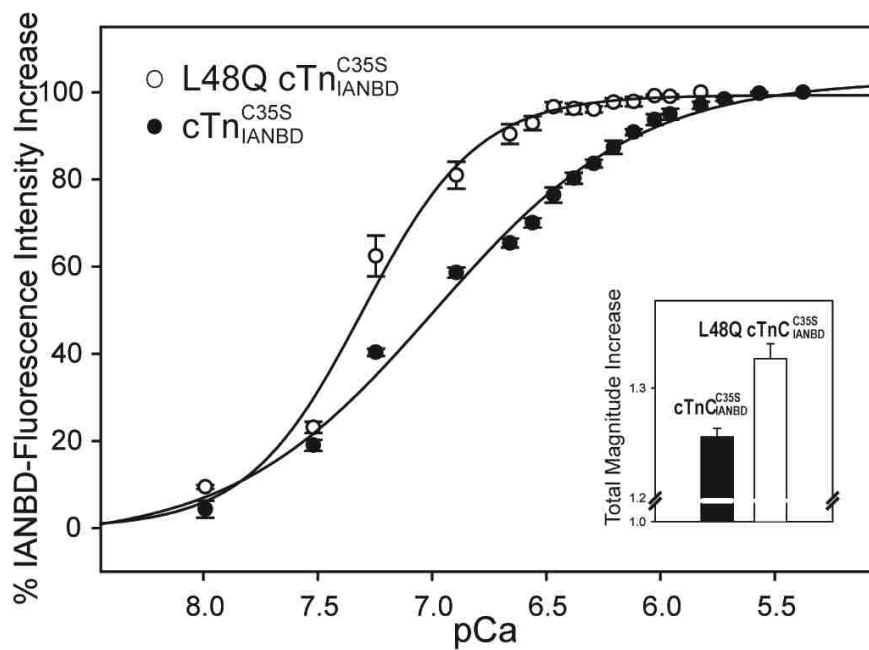
Figure 3.1. Effects of L48Q on the Ca^{2+} dependent changes in the fluorescence of cTn_{IANBD}^{C35S} complexes. ($\circ$) Ca^{2+} binding to L48Q cTn_{IANBD}^{C35S}; ($\bullet$) Ca^{2+} binding to cTn_{IANBD}^{C35S}. Inset graph, effects of L48Q on the total magnitude IANBD fluorescence increase. Excitation was at 490 nm and the emission was monitored at 530 nm. The error bars represent the standard error of 3-5 experiments. $p<0.05$
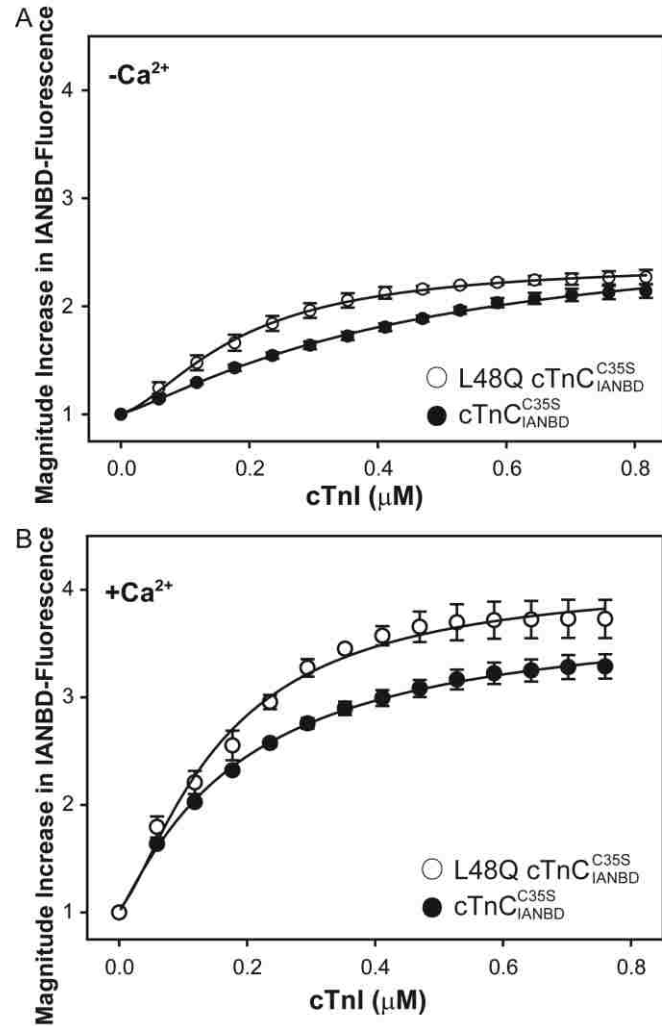
Figure 3.2. Effect of L48Q on the binding of cTnI to $cTnC_{IANBD}^{C35S}$. The binding was determined by measuring the changes in IANBD fluorescence emission intensity of $cTnC_{IANBD}^{C35S}$ titrating with cTnI in A. the absence of Ca^{2+} ($p<0.05$) and B. the presence of Ca^{2+}: (○) L48Q $cTnC_{IANBD}^{C35S}$; (●) $cTnC_{IANBD}^{C35S}$. Excitation was at 490nm and the emission was monitored at 530nm. The error bars represent the standard error of 3-5 experiments.
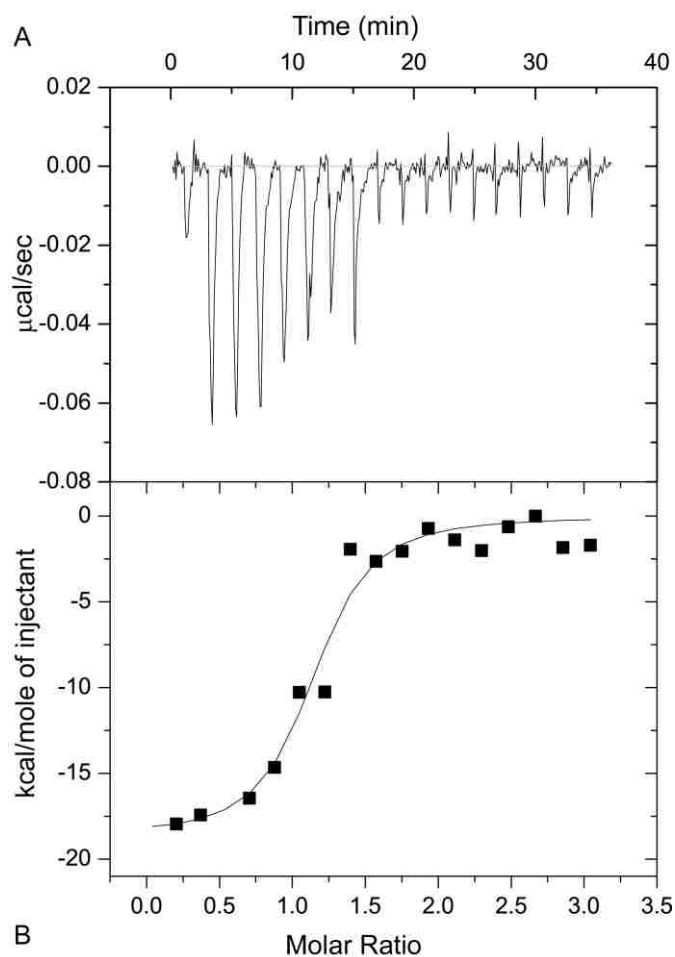
Figure 3.3. Microcalorimetric titration of cTnI with cTnC(L48Q) in the presence of Ca^{2+}. A, an example trace of the titration of 3 μM cTnI with 50 μM - 70 μM cTnC(L48Q) at 30 ℃. B, Integrated heats for each injection obtained from the raw data in panel A *versus* the molar ratio of cTnC(L48Q) to cTnI. The data were fit to the data using a 1:1 binding model, the fit is shown by the solid line.
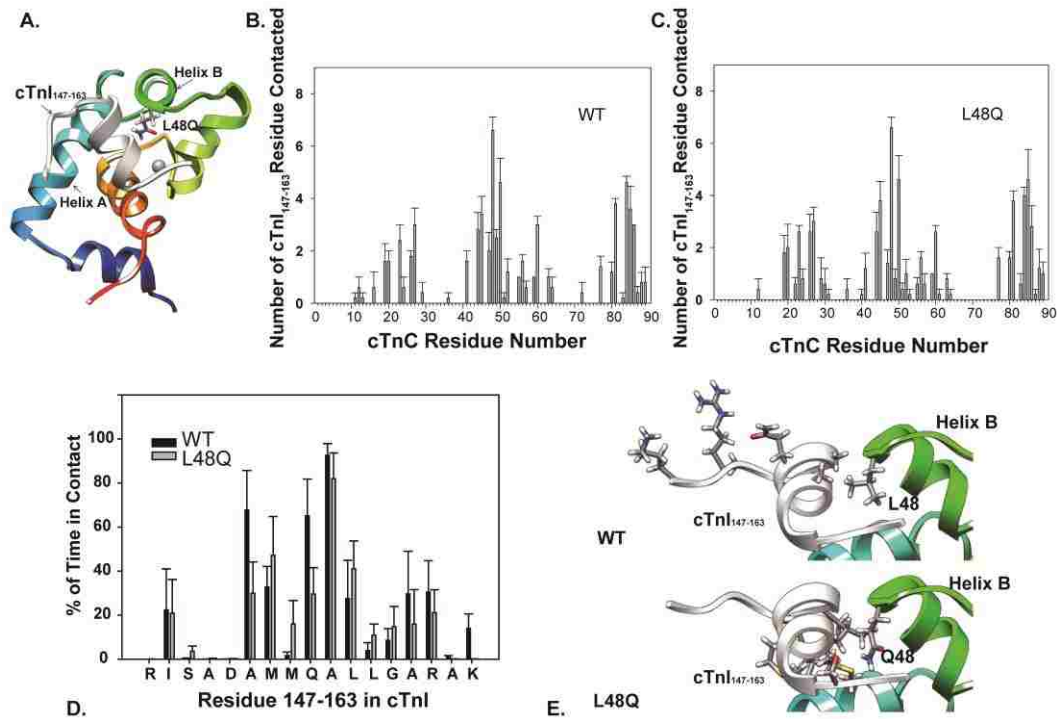
Figure 3.4. Interactions between cNTnC and cTnI$_{147-163}$. A. Structure of cNTnC(L48Q)•Ca^{2+}•cTnI$_{147-163}$ (modified from pdb: 1mxl) with residue Q48 shown in sticks, cTnI$_{147-163}$ in white, helix A in cyan and helix B in green. B and C. Number of cTnI$_{147-163}$ residues that contact cNTnC (number of contact pairs) for WT and L48Q. The error bars represent the standard error from 3-5 runs of simulations. D. Percentage of time of residue 48 in cTnC in contact with residues in cTnI$_{147-163}$. E. Residues in cTnI showing increased percentage of time in contact with residue 48 in WT and L48Q.

A. cNTnC Ca^{2+} cTnI$_{147-163}$

Helix B

Helix A

L48Q   t = 0ns   t = 60ns

WT   t = 0ns   t = 60ns

B. cNTnC Ca^{2+}

Helix A   Helix B

L48Q

60 ns

0 ns

WT

C. cNTnC apo

L48Q

WT

D.

WT

60 ns

0 ns

L48Q

Helix B

Helix A

Helix B

Helix A

cNTnC apo

+ Ca^{2+}

Helix B

Helix A

Helix B

Helix A

cNTnC Ca^{2+}

+ cTnI$_{147-163}$

Helix B

Helix A

Helix B

Helix A

cNTnC Ca^{2+} cTnI$_{147-163}$

E.

Cα RMSD Helix A + B (Å)

WT

L48Q

cNTnC·Ca^{2+}·cTnI$_{147-163}$ cNTnC·Ca^{2+} cNTnC apo

F.   cNTnC Ca^{2+}

t = 0ns   WT   t = 60ns   L48Q   t = 60ns

66

Figure 3.5. Effects of L48Q on the mobility of helix B in cNTnC. A. Snapshots from cNTnC(L48Q)•Ca^{2+}•$cTnI_{147-163}$ and cNTnC•Ca^{2+}•$cTnI_{147-163}$ simulations (run1, at 0ns and 60ns). B. Ca^{2+} Saturated State: cNTnC(L48Q)•Ca^{2+} (upper) *versus* cNTnC•Ca^{2+} (0 ns gray, 60 ns cyan). C. Apo State: cNTnC(L48Q) (upper) *versus* cNTnC. L48 and Q48 are shown in sticks. D. A/B helices truncated from structures at 0 ns (gray) and 60 ns (cyan) for cNTnC•Ca^{2+} (left), cNTnC(L48Q) Ca^{2+} (middle), and NTnC(L48Q) •Ca^{2+}•$cTnI_{147-163}$ (right). The helices are shown rotated 90° right from the structures in panels A-C to better view the A/B helix angle. E. Cα RMSD for Helices A and B of L48Q (white) and WT (black) averaged over all simulations of cNTnC•Ca^{2+}•$cTnI_{147-163}$, cNTnC•Ca^{2+} and cNTnC apo. F. Surface rendering of cNTnC•Ca^{2+} for structures from the WT (0, left; and 60 ns, middle) and L48Q (60 ns, right) simulations. The hydrophobic residues (F20, A23, F24, I26, F27, I36, L41, V44, L48, L57, M60, F77, M80, M81) are colored red with the rest of the protein in white.
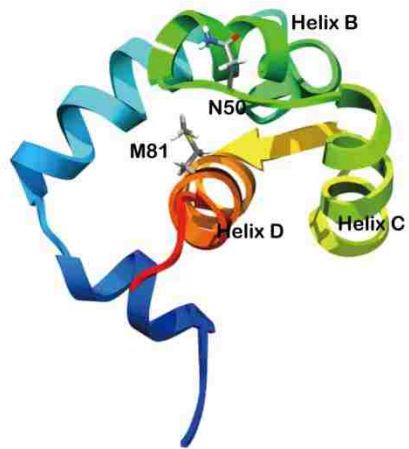
Figure 3.6. Residue N50 and M80 in cNTnC indicating the opening of the cNTnC.
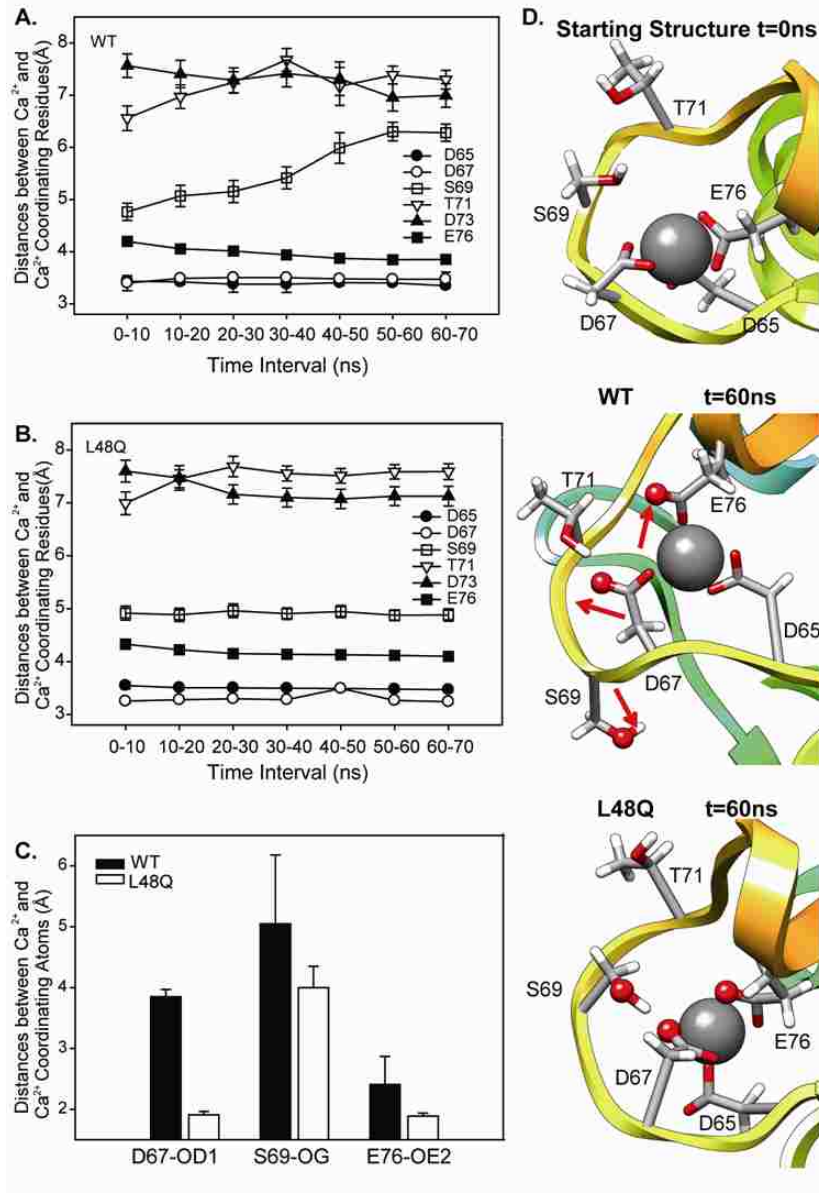
Figure 3.7. Ca^{2+} binding pocket at site II. A and B. Average distances between Ca^{2+} coordinating residues over 10 ns windows. C. Distances between Ca^{2+} and Ca^{2+} coordinating residues: D67, S69 and E76. D. Snapshots from L48Q (run1) and WT (run1) simulations showing the Ca^{2+} binding site compared with the starting structure (top), WT t=60 ns (middle), and L48Q t=60 ns (bottom) with Ca^{2+} coordinating residues shown in sticks and atoms from panel C shown in spheres.

69

Table 3.1. Interhelical angles (°) of helices A and B in cNTnC.

Protein Structures	cNTnC apo	cNTnC•Ca^{2+}	cNTnC•Ca^{2+}•cTnI$_{147-163}$	Bepridil
PDB code	1spy	1ap4	1mxl	1dtl
Exp. NMR[#]	140±3	132±3	102±5	92
WT*	103±7	98±8	107±6	-
L48Q*	97±8	89±7	87±7	-

[#] Averaged from the NMR ensembles from (*23, 25, 133*).

*Averaged from multiple runs of simulations (0-70ns).

Table 3.2. Total (main-chain and side-chain) SASA of the selected hydrophobic patch residues in cNTnC*

	WT (Å^2)	L48Q (Å^2)
Apo cNTnC	611±39	685±38
cNTnC•Ca^{2+}	630±43	642±39
cNTnC•Ca^{2+}•cTnI$_{147-163}$	722±42	748±39

*Averaged from multiple (n ≥3) simulations at last 45-70ns.

Table 3.3. Distances between residue M81 and N50 in cNTnC (Å).

Protein Structures	cNTnC apo	cNTnC•Ca^{2+}	cNTnC•Ca^{2+} •cTnI$_{147-163}$
PDB code	1spy	1ap4	1mxl
Exp. NMR[#]	10	8	17.5
WT*	10.66±1.3	9.81±1.3	16.11±1.5
L48Q*	13.54±1.9	11.66±1.9	17.97±1.3

[#] Averaged from the NMR ensembles from (*23, 25*).

*Averaged from multiple runs of simulations (0-70ns).

Chapter 4

Structural and Functional Consequences of Cardiac Troponin C L57Q and I61Q Ca^{2+}-Desensitizing Variants

4.1. Introduction

Cardiac muscle contraction is tightly controlled by the influx and efflux of Ca^{2+} from the cytosol of cardiomyocytes. Cardiac troponin C (cTnC) belongs to the EF-hand protein family and is the Ca^{2+}-binding subunit of cardiac troponin (cTn) which regulates Ca^{2+}-sensitive contraction. The N-terminus of cTnC (cNTnC) has only one physiological Ca^{2+} trigger site with lower affinity ($\sim 10^5 M^{-1}$), which differs from the two sites in fast skeletal muscle TnC (sNTnC). Ca^{2+} binding to cNTnC initiates thin filament activation in cardiac muscle, subsequent to force generation and contraction (for reviews, see (*2, 137*)). The C-terminus contains Ca^{2+} binding sites III and IV, which have higher Ca^{2+} binding affinity, and it is commonly accepted that these two sites play a mainly structural role in anchoring the proteins within the cTn complex. When Ca^{2+} binds to cTnC, the switch region of cTnI (from residues 147-163) interacts with cNTnC, resulting in reduced interaction of the inhibitory region of cTnI with actin. This allows increased mobility of tropomyosin (Tm), which exposes the myosin binding sites on actin and allows crossbridge interactions to ultimately generate force.

In recent years, numerous mutations have been identified in cTn subunits that are

associated with cardiomyopathies (*49, 121*) and also with alterations in Ca^{2+} sensitivity of force generation in cardiomyocytes from hearts of animal models and humans expressing these mutations (*138, 139*). Functional studies of Dilated Cardiomyopathy (DCM) mutations in thin filament regulatory proteins generally demonstrate a decrease in the Ca^{2+} sensitivity of force development in demembranated muscle preparations, suggesting a fundamentally functional change at the level of the sarcomere (*140, 141*). Recently, mutations in cTnC have been identified as being associated with DCM, and shown to decrease the Ca^{2+} sensitivities of force generation and cardiac myofibrillar ATPase activation (*142*). Moreover, significant loss in Ca^{2+} sensitivity of force generation in demembranated cardiac muscle from the hearts of cTnC mutations in knock-in mice that develop DCM, suggesting a correlation between Ca^{2+} desensitization of the cardiac myofilament and the pathogenesis of dilated cardiomyopathy (*16*). However, this decrease in Ca^{2+} sensitivity of force development may not be the disease causing agent itself, and could be associated with the progression and severity of these diseases over time. Moreover, there are relatively few mutations in cTnC that have been found in patients, and there is a lack of scientific knowledge on how rare mutations might lead to cardiac muscle dysfunction. Knowledge of both the molecular and clinical pathogenesis of cardiomyopathies is necessary to achieve the ultimate goal of using genotype information to help diseased patients.

Others (*72-74, 143*) and we (*144*) have been using site-directed mutagenesis of recombinant cTnC to develop and study how affect troponin function and the regulation of contractile properties of cardiac myofilaments. In this study we have focused on two

cTnC variants, cTnC (L57Q) and cTnC (I61Q), both of which are located on helix C within the N domain of cTnC to determine how they affect the molecular level structure of cTnC, it's interaction with the switch peptide of cTnI, and the correlative functional changes of these two proteins. The effects of these two variants were originally reported for the skeletal muscle system (*72, 73*), as the analogous L58Q and I62Q skeletal TnC (sTnC), and demonstrated a decreased Ca^{2+} binding affinity. In the heart, Parvatiyar *et al.* (*76*) found that I61Q cTnC decreased both Ca^{2+} sensitivity of skinned porcine papillary contraction and ATPase sensitivity, while L57Q showed a substantial decrease in the Ca^{2+} sensitivity of myofilament contraction. We have confirmed that I61Q cTnC reduces the Ca^{2+} sensitivity of force development, and reported that it also slows the rate of thin filament activation, making it the limiting process in force development of myofibrils, while having no effect on maximal relaxation kinetics (*75*).

While the consequences of these, and other cTnC mutations, have begun to be characterized in terms of their effect on mechanical performance of cardiac muscle, the protein structure-function changes that underlie these effects on contractile properties are not known. Here, we provide detailed characterization of structure-function relationships for L57Q and I61Q cTnC, resulting in a framework for determining similarities and differences with other cTnC mutations, especially those that have been identified as associated with DCM. Thus, the information gained from these engineered cTnC variants has considerable merit, as neither L57Q nor I61Q cTnC has been identified in patients, but they result in similar changes in function of cardiac muscle. To understand how the L57Q and I61Q variants influence Ca^{2+} binding at site II, the subsequent effects on the interaction with cTnI, and the structural changes which are associated with these changes,

we have used an integrative approach to study the structure and function of cTnC both in solution and *in silico.* We coupled biochemical experiments and all-atom explicit solvent molecular dynamics (MD) simulations to probe the relationship between molecular structure, movement, and function. Steady-state and stopped flow fluorescence spectroscopy confirmed that a decrease in Ca^{2+} affinity for recombinant cTnC and cTn complexes containing the L57Q or I61Q variants, and the binding of cTnI to cTnC was also reduced. MD simulations of protein constructs containing the regulatory domain of cTnC (cNTnC) in the Ca^{2+} saturated state complexed with the switch region of cTnI (residues 147-163) suggest that I61Q disrupted the key hydrophobic interactions between helices B and C in cNTnC and formed new interactions with the residues on the Ca^{2+} binding loop, which in turn decreased cTnI and Ca^{2+} binding to cNTnC.

4.2 Results and Discussion

4.2.1. Effects of L57Q and I61Q cTnC variants on the binding of Ca^{2+} to cTn complexes

We have shown previously that trabeculae exchanged with cTn containing recombinant cTnC (I61Q) (I61Q cTn) have reduced Ca^{2+} sensitivity of contraction (pCa_{50}) and thin filament activation kinetics (*75*). Trabeculae exchanged with L57Q cTn also have decreased Ca^{2+} sensitivity of force compared to WT cTn (manuscript in preparation, or abstract). To explore the molecular mechanism of how these single amino acid substitutions in cTnC affect cTn function that regulates the contractile properties of cardiac muscle, here we focus on the interaction between these two cTnC variants with their two ligands, Ca^{2+} and cTnI.

First, to investigate Ca^{2+} binding affinity to cTn complexes containing the cTnC

74

variants using steady state fluorescence spectroscopy, a C35S mutation was introduced, allowing site specific labeling at Cysteine 84 of cTnC with the fluorescence probe IANBD. Figure 4.1 shows representative wavelength scans for 0.6 μM cTnC alone (blue trace) and an increase in fluorescence with addition of Ca^{2+} (red trace), indicating that Ca^{2+} binding induces a conformational change in cNTnC that leads to an increase in the hydrophobicity of the environment around the IANBD-labeled cysteine, resulting in an increased in the fluorescence signal. We also tested D65A $cTnC_{IANBD}^{C35S}$, which disrupts Ca^{2+} binding at site II of cTnC(*145*). Our results indicated that, not surprisingly, the fluorescence signal decreased upon addition of Ca^{2+} due to the dilution of the concentration of fluoro-probe in the system (data not shown). Thus, an increase in IANBD fluorescence is associated with the increased binding of Ca^{2+} to cTnC.

The total magnitude of fluorescence signal increase was significantly less for isolated cTnC (I61Q) $_{IANBD}^{C35S}$ compared to the control $cTnC_{IANBD}^{C35S}$, ~1.15 fold (for I61Q) *vs*. ~1.25 fold (for control), as shown in the inset graph of Figure 2. cTnC (L57Q) also showed a lower increase in fluorescence (~1.21 fold). The results suggest that the regulatory domain of cTnC $_{IANBD}^{C35S}$ underwent a smaller conformational change in the cTnC (I61Q) and cTnC (L57Q) variants, suggesting less exposure of hydrophobic residues compared to control cTnC.

The Ca^{2+} binding affinities of cTn complexes were determined from the data in Figure 4.2, and they are reported as the pCa that elicited half-maximal increase in fluorescence (pCa_{50}). L57Q and I61Q decreased Ca^{2+} binding affinity, as indicated by reduction of pCa_{50} by ~0.28 and ~0.84 pCa units, respectively (pCa 6.58±0.01 for L57Q cTn_{IANBD}^{C35S} and 6.15 ±0.01 for I61Q cTn_{IANBD}^{C35S}). Similar results were reported for

analogous positional mutations of L57Q and I61Q cTnC in skeletal TnC by Tikunova and Davis *et al.* using steady-state fluorescence measurements with a different labeling system. They reported decreased Ca^{2+} binding affinity in both of the variants, but especially for sTnC (I62Q) with a dramatic decrease of ~0.9 pCa units shifting the pCa_{50} to the right (*73*).

4.2.2. Effects of cTnC (L57Q) on Ca^{2+} dissociation rates

The Ca^{2+} dissociation rate (k_{off}) of whole cTn (with WT cTnI, cTnT) and the thin filament (with cTn, actin and cTm) was determined with stopped-flow fluorimetry using Quin-2 as a reporter for free Ca^{2+}. We have previously reported the k_{off} for I61Q cTnC (*16*). Table 4.1 summarizes the results for L57Q compared to WT and I61Q. In both Tn and thin filament studies, k_{off} was faster for I61Q than WT cTn, as well as any other variants that have been tested. k_{off} for L57Q was faster than WT but not as fast as I61Q cTn. The relative order of increasing k_{off} was maintained for measurements of recombined thin filaments, but the rates were all faster compared to cTn alone. This is consistent with previous reports from Davis and Tikunova (*11, 12*) for analogous mutations in sTnC. Moreover, the disease-related cardiac contractile protein mutations have been shown to change the rate of Ca^{2+} dissociation from TnC (*31, 32*).

4.2.3. Effects of cTnC(L57Q) and cTnC(I61Q) variants on cTnC-cTnI interaction

To study the affinity of the cTnC variants for cTnI, IANBD-labelled cTnC was titrated with cTnI in the presence and absence of Ca^{2+}. As shown in Figure 4.3A, I61Q cTnC had reduced interactions with cTnI in both apo ($K_D= 328\pm22nM$) and Ca^{2+} saturated states ($K_D=241\pm12nM$). In contrast, L57Q cTnC was similar to WT cTnC in

the apo state (K_D=271±17nM). However, in the Ca^{2+} saturated states the affinity of cTnI for L57Q cTnC (K_D=228±9nM) was reduced to a similar level as I61Q (Figure 4.3B).

4.2.4 MD simulation

To investigate the structural changes that may explain the experimental observed effects on Ca^{2+} and cTnI binding to cTnC, multiple (n≥3) independent MD simulations at neutral pH and 15 °C were performed for WT, L57Q and I61Q cNTnC•Ca^{2+}•cTnI$_{147-136}$ complexes (70ns each). After the initial equilibration period, the Cα RMSDs generally reached a plateau at ~4 Å (WT 4.2±0.2 Å, L57Q 3.9±0.6 Å, and I61Q 4.1±0.7 Å), suggesting that all systems were stable.

The MD simulations with the chosen fragments of the cTnI-cTnC complex allow for the visualization of interactions between the mutated residue and the rest of the protein as well changes in conformation that may result in altered cTnI-cTnC interaction. Residue L57 and I61 are both on helix C with 61 closer to the Ca^{2+} binding site and 57 nearer to helix B (Figure 4.4).

4.2.4.(a) Effects of I61Q substitution on the mobility of helix B and C in cNTnC

The simulation of the I61Q cNTnC•Ca^{2+}•cTnI$_{147-136}$ complex helices B and C moved apart, as shown in Figure 4.5. This movement did not occur for any of the WT cNTnC•Ca^{2+}•cTnI$_{147-136}$ complex simulations nor in any of L57Q simulations, suggesting that I61Q has influence on the mobility of helices B and C. For all simulations there were no significant differences in movement of these helices for L57Q *vs*. WT cTnC. Interestingly, the movement between helices B and C for I61Q was very different from what was observed in a previous study of cTnC(L48Q), where

movement of helix B away from the rest of the protein facilitated the exposure of the hydrophobic patch and stabilized the open state of cNTnC (*20*).

In order to quantify helical movements in the I61Q cNTnC•Ca^{2+}•cTnI$_{147\text{-}136}$ simulations and compare with WT as well as the L57Q cTnC variant simulations, we analyzed the center of mass distances between helices B and C within cNTnC (COMdist BC), as summarized in Table 4.2. Results indicate that the averaged COMdist BC for the last 25 ns from multiple runs of simulations increased about 1.6 Å for I61Q, ~0.33 Å greater than for the WT (1.27±0.35 Å).

4.2.4.(b) Effects of cTnC (L57Q) and cTnC(I61Q) on the contacts between helices B and C of cNTnC

Contacts between helices B and C were further analyzed to determine how intra-molecular interactions were disrupted by the L57Q or I61Q variants of cTnC. A contact between a pair of residues was defined on the basis of whether any one of the atoms in the first residue was below a set cutoff distance (see Methods section) to atoms in the next residue (*33*). The percentage of time in contact of each pair was calculated by taking the percentage of structures in which two specified residues were in contact over the 70ns simulation period. In the WT simulation, the following residue pairs between helices B and C were in contact during more than 30% of the total simulation time: L41−L57, L41−M60, L41−I61, G42−L57, M45−L57, and M45−M60. These residues are all hydrophobic residues and contribute to the major interactions between helices B and C (Figure 4.6). For L57Q, the results averaged over multiple simulations suggest that the percentage of time in contact between residues M45 and Q57 decreased by ~ 26% compared to WT. For I61Q, the contact times between all the pairs discussed above were

generally decreased (L41− L57 ↓6%; L41 − M60 ↓ 9%; L41 − Q61↓ 15%; G42 − L57 ↓17%, M45 − L57 ↓2%, and M45 − M60 ↓10%) compared to WT. As such, the I61Q variant caused a decrease in hydrophobic interactions between helices B and C. Furthermore, as residues L41, L57, and M60 are known to contribute to the formation of the hydrophobic patch (*20*), it is possible that the disruption of the hydrophobic interactions introduced by I61Q or L57Q affected the interaction between cNTnC and cTnI$_{147-163}$, which provides a structural explanation for the experimental observations that we described in the solution studies.

4.2.4.(c) Effects of I61Q substitution on the Ca^{2+} binding loop

Residue 61 is at the end of helix C and close to the Ca^{2+} binding loop. The contacts between residue 61 and residues on the loop (V64, D65, E66, D67, G68, S69, G70, T71, V72, D73 to F74) were monitored and screened. The results indicated that the side chain of Q61 could form hydrogen bonds with these residues. As summarized in Table 3, I61Q formed a backbone hydrogen bond with residue G70 on the Ca^{2+} binding loop ~14% of the simulation time (Figure 4.7). Moreover, the percentage of time a hydrogen bond was formed between residue 61 and D65 decreased from 74.1±9.2 % to 34.3±15.4 % due to the I61Q substitution. It was reduced even further for L57Q, to only 16.9±12.0 %. These results suggest that the reason for the experimentally observed decrease in Ca^{2+} binding affinity for the I61Q and L57Q variants may be due to the destabilization of the Ca^{2+} binding loop by formation of hydrogen bond interactions between the variant residues and those in the binding loop.

Another deduction from these results is that V64 and D65 form constant hydrogen bond contacts with residue 61, which provides another explanation for the

severe loss/disruption of Ca^{2+} binding ability for D65A and V64Q cTnC variants in structural detail (data not shown).

4.4. Conclusions

In summary, we have characterized the structure and function of cTnC variants L57Q and I61Q with a progressing decrease in Ca^{2+} binding affinity. This was associated with an increased Ca^{2+} dissociation rate in both whole cTn complex and reconstituted thin filament studies(*16*). The L57Q variant was intermediate between WT and I61Q cTnC and also did not alter cTnC-cTnI interaction in the absence of Ca^{2+}, while it was reduced in the presence of Ca^{2+}. In contrast, I61Q decreased the cTnC-cTnI interaction in both the absence and presence of Ca^{2+}. This difference in the absence of Ca^{2+} suggests a greater structural change in cNTnC may occur with the I61Q mutation than the L57Q mutation. The MD simulations revealed that the decreased Ca^{2+} binding induced by I61Q might be due to destabilization of the Ca^{2+} binding site through interruption of intra-molecular interactions when residue 61 forms new hydrogen bonds with G70 on the Ca^{2+} binding loop. Furthermore, the experimentally observed interruption of the cTnC-cTnI interaction caused by L57Q or I61Q is due to the disruption of key hydrophobic interactions between helices B and C in cNTnC. Our study provides a molecular basis of how single mutations in the C helix of cTnC can reduce Ca^{2+} binding affinity and cTnC-cTnI interaction, which may provide useful insights for a better understanding of cardiomyopathies and future gene-based therapies.
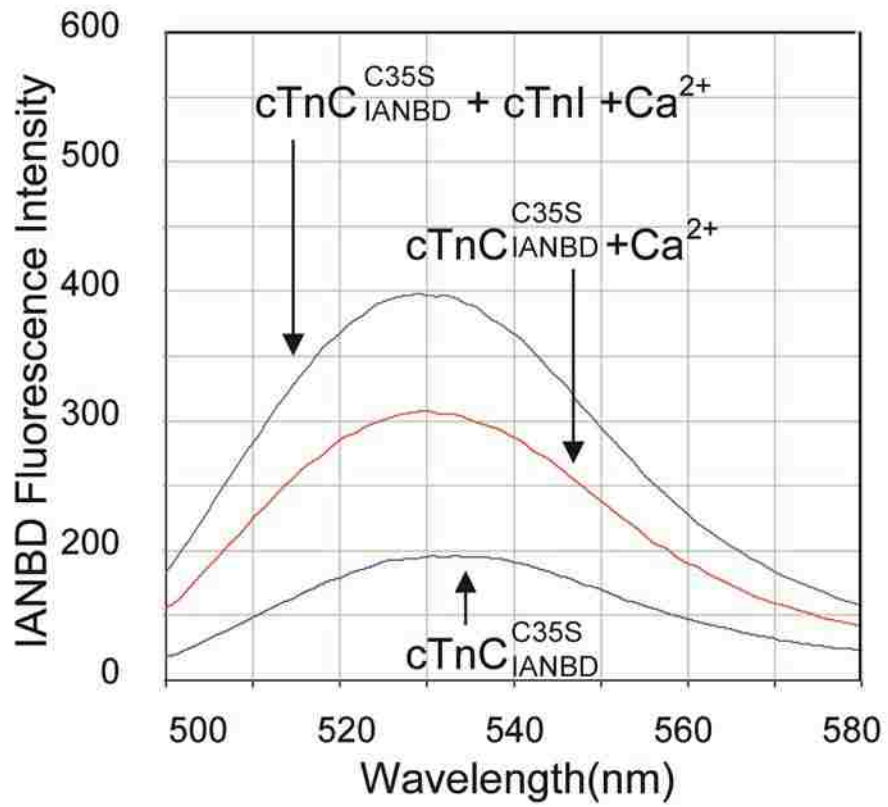
Figure 4.1 Representatives of the IANBD emission spectra of the $cTnC_{IANBD}^{C35S}$ (blue), $cTnC_{IANBD}^{C35S} \bullet Ca^{2+}$ (red) and $cTnC_{IANBD}^{C35S} \square Ca^{2+} \bullet cTnI$ (green).
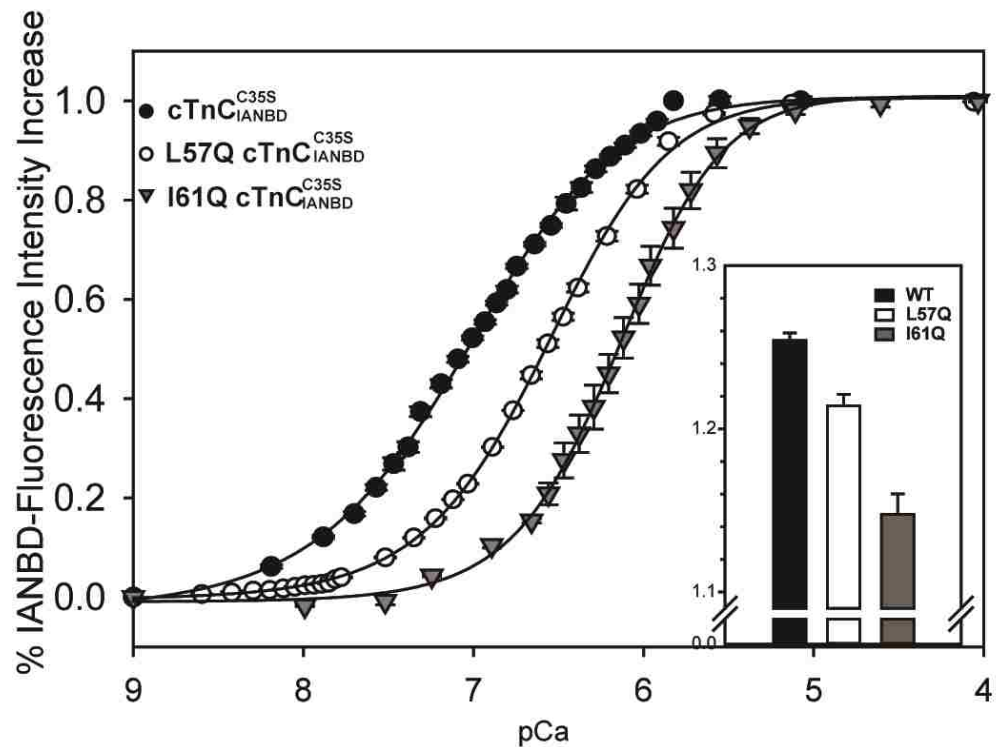
Figure 4.2. Effects of L57Q and I61Q cTnC on the Ca^{2+} dependent changes in the fluorescence of cTn_{IANBD}^{C35S} complexes. ($\bullet$) Ca^{2+} binding to cTn_{IANBD}^{C35S} ;($\circ$) Ca^{2+} binding to L57Q cTn_{IANBD}^{C35S}; ($\blacktriangledown$) Ca^{2+} binding to I61Q cTn_{IANBD}^{C35S}. Inset graph: the magnitude of IANBD fluorescence increase of $cTnC_{IANBD}^{C35S}$ and other variants. Buffer conditions were 20mM MOPS, pH 7.0, 150mM KCl, 3mM $MgCl_2$, 2mM EGTA and 1mM DTT; 15°C; Tn complex concentration was 0.6μM. Excitation was at 490nm and the emission was monitored at 530nm. The error bars represent the standard error of 3-5 experiments. P<0.05 as compared to control protein.
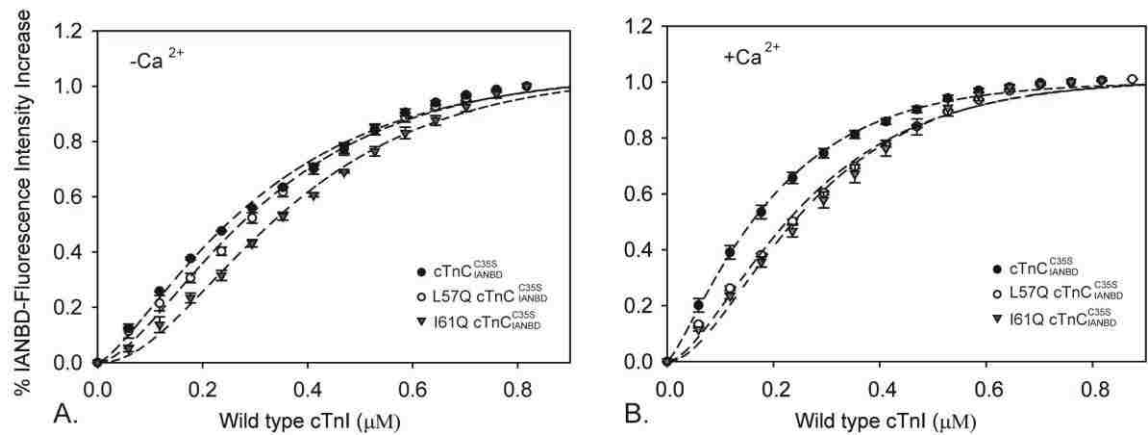
Figure.4.3. Effects of L57Q and I61Q cTnC on the binding of cTnI to cTnC $_{IANBD}^{C35S}$. The binding was determined by measuring the changes in IANBD fluorescence emission intensity of cTnC$_{IANBD}^{C35S}$ titrating with cTnI in **(A)** the absence of Ca^{2+} and **(B)** the presence of Ca^{2+}. ($\circ$) cTnC$_{IANBD}^{C35S}$ ($\bullet$) L48Q cTnC$_{IANBD}^{C35S}$. Buffer conditions were 20mM MOPS, pH 7.0, 150mM KCl, 3mM MgCl$_2$, 2mM EGTA and 1mM DTT; 15°C; Tn complex concentration was 0.6μM. Excitation was at 490nm and the emission was monitored at 530nm. The error bars represent the standard error of 3-5 experiments. P<0.05 as compared to control protein.
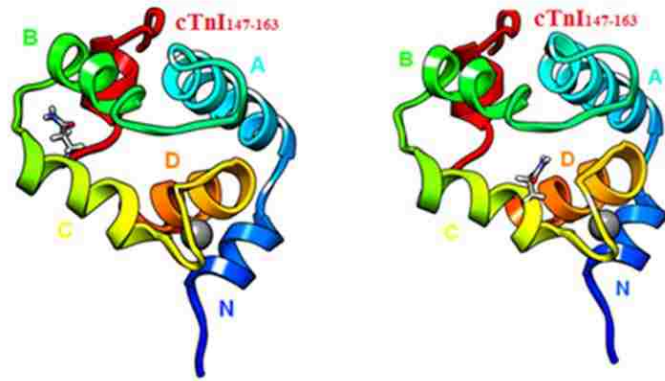
A. L57Q   **B. I61Q**

Figure.4.4. Variant position in the cNTnC●Ca^{2+} ●cTnI$_{147\text{-}163}$. (A) L57Q on helix-C; (B) I61Q on helix-C. cNTnC: Helix-N (blue 4-10), Helix-A(cyan 14-28), Helix-B(green 41-48), Helix-C(yellow 54-64),Helix-D (orange 74-82), cTnI$_{147\text{-}163}$(red) and Ca^{2+} (grey).
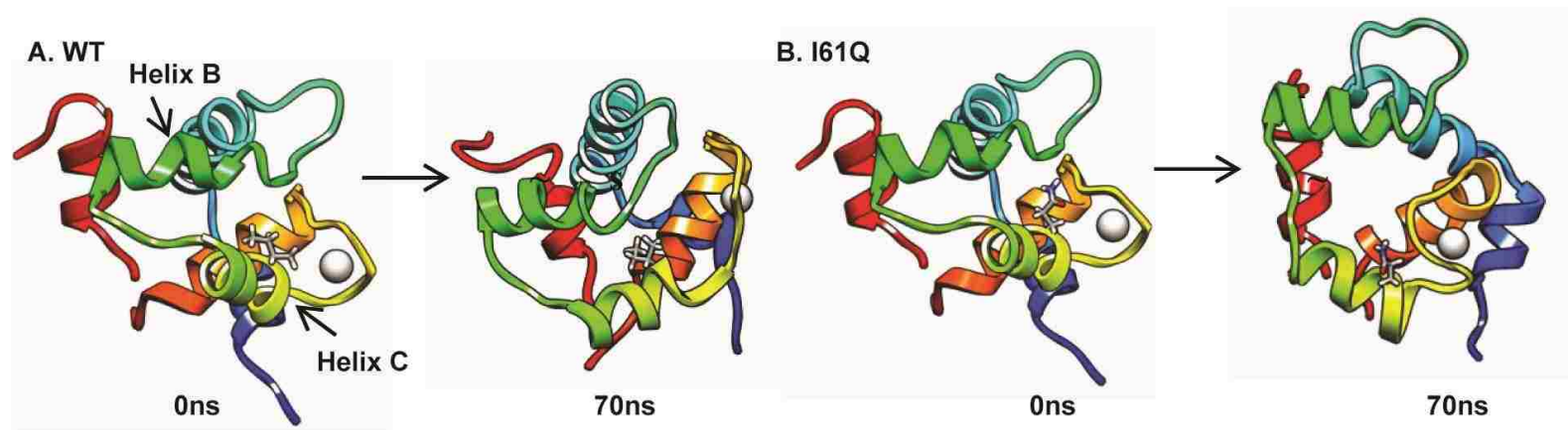
Figure.4.5. Snapshots from simulations showing motion between helix B and C at 0ns and 70ns. ((A) WT; (B) I61Q)

A. WT

Helix-B

G42

M45

L41

L57

I61

M60

Helix-C

t=0ns

t=70ns

B. L57Q

G42

M45

L41

Q57

I61

M60

t=0ns

t=70ns

C. I61Q

G42

M45

L41

Q61

L57

M60

t=0ns

Q61

t=70ns
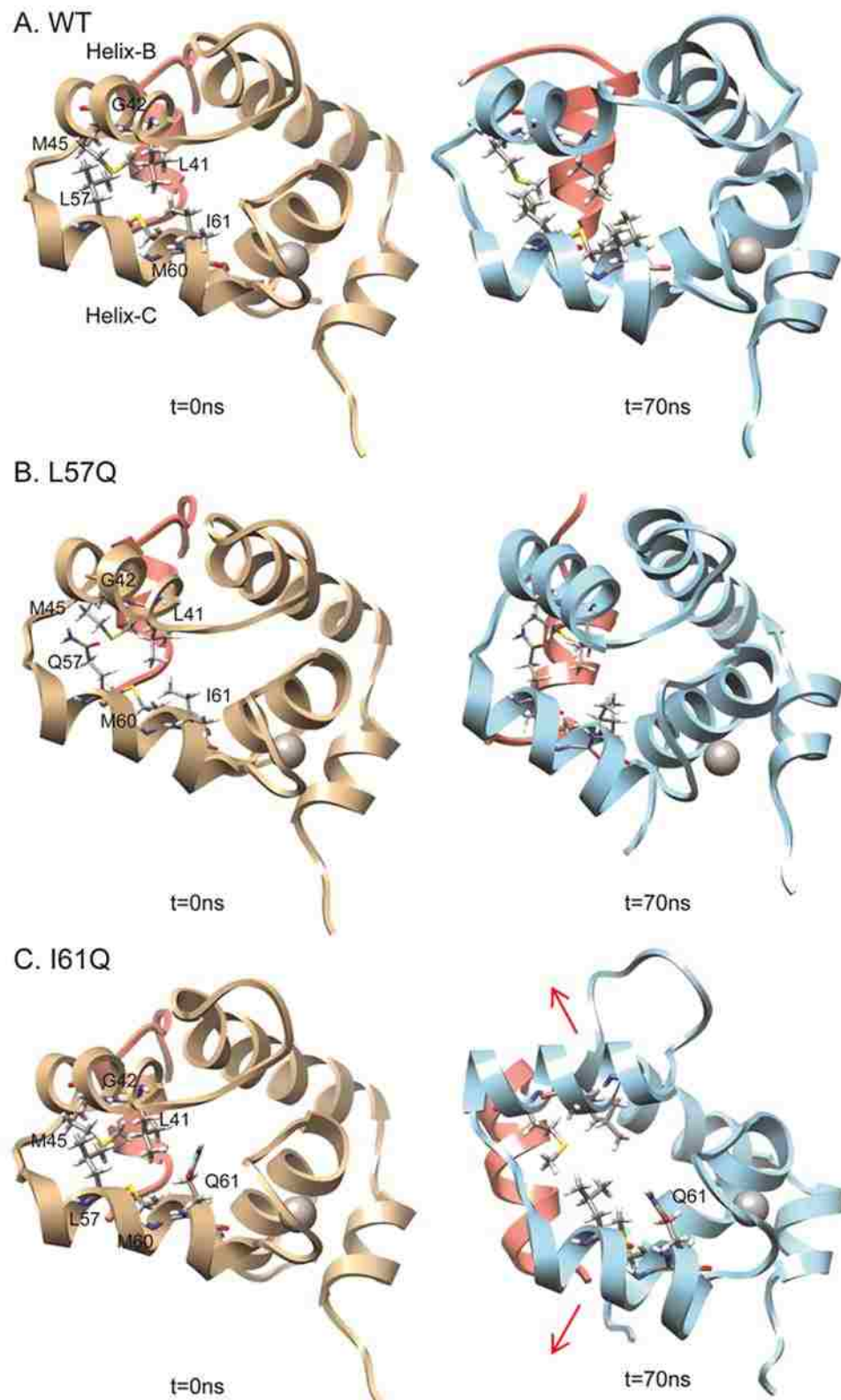
Figure 4.6. Disruption of cTnC(I61Q) and cTnC (L57Q) on the interactions between helices B (residues 41-48) and C (residues 54-64) of cNTnC. WT (shown in panel A) simulations results suggest that the following residues pairs between helices B and C were in contact during more than 30% of the total simulation time: L41 *vs.* L57, L41 *vs.* M60, L41 *vs.*I61, G42 *vs.* L57, M45 *vs.*L57, and M45 *vs.* M60. For L57Q (shown in panel B), contact time between M45 and Q57 was decreased for 26% compared to WT; For I61Q (shown in panel C), helices B and C apart from each other, generally, contact times between all the pairs listed above were decreased (L41 *vs.* L57 ↓6%; L41 *vs.* M60 ↓ 9%; L41 *vs.*Q61↓ 15%; G42 *vs.* L57 ↓17%, M45 *vs.*L57↓2%, and M45 *vs.*M60 ↓10%.) compared to WT.
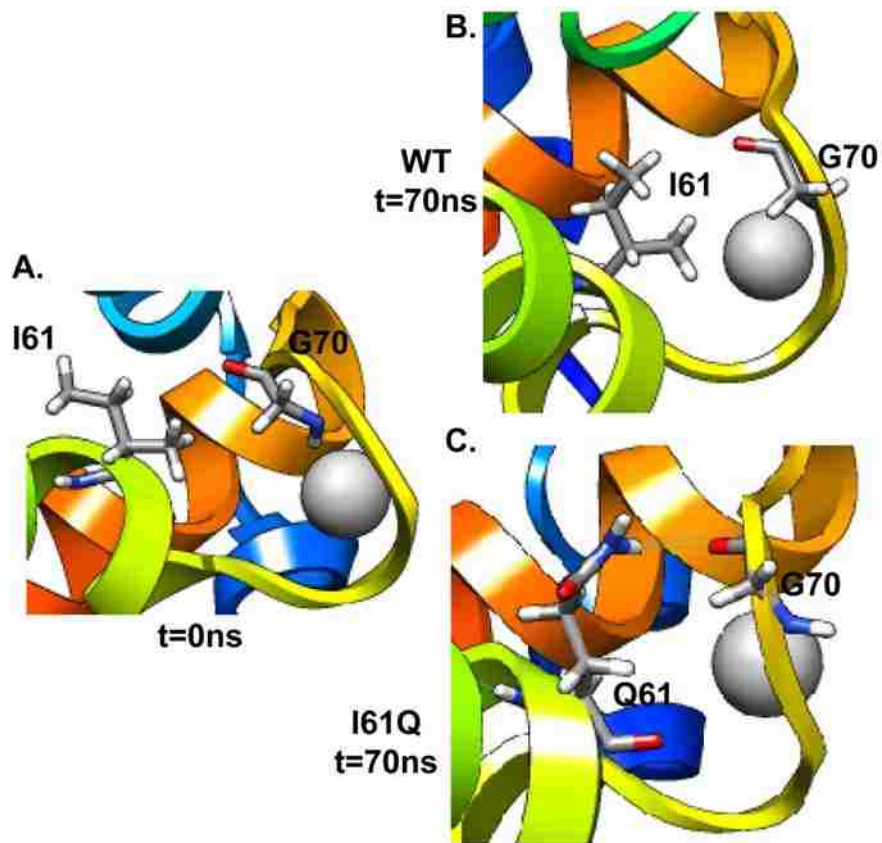
Figure.4.7. Snapshots from I61Q and WT simulations for Ca^{2+} binding site II at 0ns (A)

and 70ns ((B) WT; (C) I61Q).

Table 4.1. Summary of Ca^{2+} dissociation rate (k$_{off}$) from cTnC in whole cTn complex or in reconstituted thin filaments by stopped-flow spectroscopy with Quin-2 fluorescence at 15 °C.

	cTn Complex [a] Ca^{2+} k$_{off}$ (s^{-1})	Thin filament[†] Ca^{2+} k$_{off}$ (s^{-1})
WT[#]	29.7±0.5	75.4±4.8
L57Q	51.8±2.1* (n=5)	74.1±11.6 (n=5)
I61Q(75) [#]	67.0±9.3	237.7 ±30.5

[a]*Tn complexes (6 uM) +100 uM Quin-2)*
[†]*Thin Filament (5.4 uM cTn, 42 uM skel Actin, 6 uM Tm) +100 uM Quin-2)*
[#]WT and I61Q data reported by Kreutziger *et al.* (*75*), cited here for comparison with L57Q cTnC. P < 0.05

Table 4.2. RMSD-Cα (*10-70ns*) for all simulations

cNTnC•Ca^{2+}•cTnI$_{147-136}$ (PDB:1mxl)	WT	L57Q	I61Q
	n=6	*n=5*	*n=6*
	4.19±0.2	3.90±0.60	4.06±0.69

Table4.3. Distances between helices B and C.

	Avg. Comdist from NMR ensembles Å	Avg. Comdist at 0ns (in min.pdb) Å	Comdist BC helices (45-70ns) Å	ΔComdist BC helices* Å
WT	13.73±0.29	13.57±0.00	14.71±0.29	1.27±0.35
L57Q	-	13.50±0.02	14.60±0.32	1.48±0.35
I61Q	-	13.57±0.02	15.24±0.26	1.60±0.30
* ΔComdist BC helices= Avg.Comdist (45-70ns)-Avg.Comdist at 0ns				

Table 4.4 Percentage of time in hydrogen bond contact between residue 61 and residues

in Ca^{2+} binding loop

	WT	L57Q	I61Q
V64	4.1±1.2 %	5.8±0.02 %	2.2 ±1.0 %
D65	74.1±9.2 %	16.9±12.0 %	34.3±15.4 %
S69	-	-	3.7±2.8 %
G70	-	-	14.0±6.2 %
T71	-	-	0.3±0.1%

Chapter 5

Modulation of cTnC Variants Function by the N-extension Region of cTnI − Effects of PKA Phosphorylation on the Ca^{2+} Binding Affinity and cTnC-cTnI Interaction

5.1. Introduction

The regulation of cardiac muscle contraction by calcium is also modulated by the Protein kinase A (PKA) mediated phosphorylation during β-adrenergic stimulation. PKA phosphorylates the thin filament protein, cTnI, which has two PKA specific substrates at S23 and S24 in the cardiac unique N-extension region (for reviews (*28, 148, 149*)). The phosphorylation of cTnI at these two sites resulted in a reduction of myofilament Ca^{2+} sensitivity of contraction (*46, 150, 151*), and an increase in relaxation rate and cross bridge cycle kinetics (*44, 45*). These effects may be critical when the contractile demands of the heart are increased. Alterations in cTnI phosphorylation status have been reported in patients during end-stage heart failure (*152*). More functional significance of cTnI phosphorylation under physiological and pathophysiological conditions have been reviewed by Layland *et al* (*47*).

Biophysical and structural studies suggest that PKA phospohryaltion of cTnI may exert their functional effects by altering the global cTnI structure (intramolecular) and protein-protein interactions in the thin filament (intermolecular). The interactions of cTnI

with other thin filament proteins are discussed in Chapter 1 (section 1.3.2, Figures 1.2 and 1.3). The N-extension of cTnI binds weakly to the regulatory domain of cTnC (cNTnC) (*153-155*) in the absence of PKA phosphorylation, which influences the conformational change within cNTnC by stabilizing an 'open' conformation that exposes the hydrophobic patch. However, this interaction between cNTnC and the N-extension of cTnI is further weakened when PKA phosphorylation occurs, shifting the conformational equilibrium within cNTnC to the 'closed' state and resulting in reduced Ca^{2+} affinity of cNTnC. NMR studies reveal that these effects may be caused by a repositioning of the N-extension of cTnI to cNTnC during PKA phosphorylation, which induces a bending of the end region of the N-extension (residues 33-42), and an intramolecular electrostatic interaction between the inhibitory and the N-extension regions of cTnI (*29*). This demonstrated a linkage between the inhibitory region and the N-extension of cTnI, which is further supported by evidence that a HCM related mutation in the inhibitory region, R145G cTnI, has been shown to be insensitive to PKA phosphorylation of cTnI at S23/S24 (*156*). These observations suggest that PKA phosphorylation could modulate the interactions of cTnC with cTnI, and cTnI with actin, in both apo (Ca^{2+}-free) and Ca^{2+}-boundsaturated states. Taken together, PKA phosphorylation of cTnI may alter both the Ca^{2+} binding properties of cTnC by weakening its interaction with cNTnC and crossbridge formation by disrupting the interactions between the inhibitory region of cTnI with actin (in apo state) and cTnC (in Ca^{2+} saturated state).

Recently, many HCM and DCM related mutations in cTnC were reported to blunt or abolish the Ca^{2+} desensitization induced by PKA phosphorylation of cTnI (*15, 52, 157, 158*), including L29Q, G159D, and E134D cTnC. However, it is still unclear if this

failure in response to PKA phosphorylation during β-adrenergic stimulation is a common mechanism among cardiomyopathy related cTnC mutations, and/or if it is an adaptive changes during the development of the disease. In this work, we investigated how PKA phosphorylation regulates the Ca^{2+} binding affinities of the cTnC variants, and the interaction between these cTnC variants with cTnI. These studies could provide important clues for developing molecular approaches aimed at modifying cardiac muscle contraction and relaxation, which may help explain the underlying mechanisms involved and the potential therapeutic strategies for various cardiomyopathies.

As such, the Ca^{2+} binding affinity of the cTnC-cTnI complex or whole cTn-complex upon PKA phosphorylation, and the differences between PKA phosphorylated and non-phosphorylated cTnI binding affinities to cTnC, were systematically examined using steady-state fluorescence spectroscopy.

5.2. Results

5.2.1. Effects of cTnC variants on the Ca^{2+} binding to $cTnC_{IANBD}^{C35S}$ in the presence of PKA phosphorylation.

PKA phosphorylation of cTnI was produced using a cTnC affinity column according to the protocol provided generously by Dr. Dong (Washington State University) and verified by both Pro-Q phosphoprotein stain (Invitrogen) and western blot (Figure 2.1). To test how PKA phosphorylation affects the Ca^{2+} binding affinity to cTnC variants, we first used reconstituted $cTnC_{IANBD}^{C35S}$ – cTnI complexes with isolated PKA phosphorylated cTnI. Changes in the fluorescence intensities of the environmentally sensitive probe IANBD labeled $cTnC^{C35S}$ were monitored. The results are shown in

Figure 5.1 and Table 5.1. Similar to the results found in studying the Ca^{2+} binding to non-phosphorylated $cTnC_{IANBD}^{C35S}$-cTnI complexes, in the presence of PKA phosphorylation, L48Q still showed an increased Ca^{2+} binding affinity, while L57Q and I61Q showed a decrease, compared to the control. Table 5.1 also lists the Ca^{2+} sensitivity of the fluorescence signal (reported as pCa at half-maximal fluorescence increase) for both non-phosphorylated and phosphorylated $cTnC_{IANBD}^{C35S}$-cTnI complexes. By comparing these two groups, it is clear that in the PKA-treated groups there was a decrease in the Ca^{2+} affinity to $cTnC_{IANBD}^{C35S}$ as indicated by a rightward shift (decrease) in the Ca^{2+} sensitivity of the fluorescence signal for ~0.1 pCa unit. This result is consistent with that reported by Dong *et al* [159, 160] who observed a decreased Ca^{2+} binding affinity using IAANS fluorescence spectroscopy.

We further tested PKA phosphorylation of cTnI on the Ca^{2+} binding to whole Tn complex. As shown in Figure 5.2, the pCa at half-maximal increase in IANBD fluorescence was 6.70±0.01 for the control cTn_{IANBD}^{C35S} complex, which is ~0.29 pCa unit rightward shift (decrease in Ca^{2+} sensitivity) compared with non-phosphorylated control (pCa 6.99±0.03), indicating a decrease in Ca^{2+} binding affinity with PKA phosphorylation. A similar trend was found for L48Q, shifting pCa from 7.31±0.03 (L48Q cTn_{IANBD}^{C35S} complex) to 6.96±0.01 with PKA phosphorylation of cTnI. These results suggest that PKA phosphorylation of cTnI is sufficient to significantly decrease the Ca^{2+} affinity of both L48Q and WT cTn complex. The reduction of Ca^{2+} binding affinity of L48Q cTn complex induced by cTnI PKA phosphorylation appeared to fall in line with control cTn complexes in the absence of PKA (6.96±0.01 vs 6.99±0.03).

The fluorescence-Ca^{2+} relationships of cTn complexes containing either L57Q or I61Q cTnC in the presence of PKA phosphorylation is shown in Figure 5.3. In strong contrast to L48Q cTnC, the Ca^{2+} binding affinities of these two variants were not further reduced by PKA phosphorylation. In the presence of PKA, L57Q cTn complex exhibited a half-maximal increase in IANBD fluorescence with a pCa_{50} of 6.61±0.01, which did not differ statistically from the non-phosphorylation state of this variant which exhibited a pCa_{50} of 6.57±0.01. I61Q cTnC, similarly, showed a pCa_{50} of 6.23±0.02 in the presence of PKA phosphorylation, and a pCa_{50} of 6.15±0.01 in the absence of PKA phosphorylation. These results suggest that L57Q and I61Q cTnC blunt PKA phosphorylation effect on Ca^{2+} binding to whole cTn complexes (see Table 5.2).

5.2.2. Effects of cTnC variants on cTnC-cTnI interaction upon PKA phosphorylation of cTnI in the presence and absence of Ca^{2+}.

To further assess how PKA phosphorylation modulates the interaction of cTnI with these cTnC variants, we monitored the binding of isolated PKA phosphorylated cTnI to both apo and Ca^{2+} saturated $cTnC_{IANBD}^{C35S}$ variants. The dissociation constant, K_D, for phos-cTnI binding to cTnC derived from normalized IANBD fluorescence change was increased for all variants compared with WT cTnI, indicating a decreased interaction (Table 5.3).

Moreover, phosphorylation decreased total conformational change induced by binding of cTnI to $cTnC_{IANBD}^{C35S}$ in the absence of Ca^{2+} as shown in Figure 5.4A. Consistent with wild type cTnI-cTnC interaction results we found as discussed in Chapter 3 and 4, for all cTnC variants PKA phosphorylated cTnI binding to Ca^{2+} saturated cTnC

underwent a greater conformational change. Upon binding to phos-cTnI total magnitude increase in IANBD fluorescence for L48Q increased by ~1.6 fold when cTnC was saturated with Ca^{2+} (magnitude 3.28±0.03 in Ca^{2+} saturated state vs 2.05±0.06 in apo state). Interestingly, L48Q, I61Q and control cTnC showed more reduction in conformational change induced by PKA phosphorylation in the Ca^{2+} saturated state, while L57Q showed no significant conformational change effects under both conditions. These results suggest that PKA phosphorylation may decrease cTnI binding affinity to cTnC especially at saturating Ca^{2+} for wild type, L48Q and I61Q cTnC. Functional studies support these findings that show enhanced Ca^{2+} dissociation kinetics following PKA treatment. Previous studies show that PKA phosphorylation of cTnI decreases Ca^{2+} sensitivity of force and increases the rate of relaxation in skinned cardiac muscles (*44, 45, 149, 161, 162*).

In this study PKA phosphorylation of Ca^{2+}-saturated L48Q and control cTnC proteins induced a ~12% and ~11% decrease in total conformational change, respectively (L48Q cTnC from 3.73±0.18 to 3.28±0.03 vs control cTnC from 3.29±0.11 to 2.93±0.10 fold increase in IANBD-Fluorescence). PKA phosphorylation appeared to reduce cTnC and cTnI interaction to a greater degree for L48Q as indicated by about 150nM increase in K_D value, which was only about 10nM for WT cTnC (see Table 5.3). These results suggest that PKA phosphorylation decreased the interactions between cTnC-cTnI for L48Q to a greater extent than the for the control, indicating that the increased cTnI binding induced by L48Q might be compromised during the PKA phosphorylation of cTnI.

5.3. Discussion

Ca^{2+} binding is considered as the trigger of activation of the thin filament leading to the force generation and the change in the cTnC-cTnI interaction is the linkage between the activation and deactivation states. The cTnC-TnI interaction is also regulated during β-adrenergic stimulation, via PKA mediated phosphorylation of S23, 24 of the cardiac specific N-terminal extension of TnI. Previous studies have utilized amino acid substitutions to mimic different states of phosphorylation, e.g. using aspartic acid (D) substitution (*163*) to mimic phosphorylation and alanine (A) substitution(*164*) to prevent phosphorylation at specific sites. However, these substitutions do not always recapitulate the effects of phosphorylation as the modification of the proteins is needed. Thus, the validity of these amino acid substitutions in terms of mimicking phosphorylation is not well known. Thus, in this study, we used real PKA phosphorylated cTnI prepared by cTnC affinity column to study the effects of PKA phosphorylation.

We have previously discussed the structural and functional consequences of L48Q, L57Q and I61Q cTnC variants. Further investigations of the effects of these variants on the contractile performance in intact cardiomyocytes were also pursued using adenovirus based gene delivery, which is discussed in Chapter 6 (for L57Q and I61Q). However, how these variants response to PKA phosphorylation is not yet well studied. Recently, HCM associated mutation L29Q cTnC cTnC(*158*), and DCM related mutation G159D cTnC (*165*) were reported to blunt the Ca^{2+} desensitization that is considered as a common consequence of PKA phosphorylation of cTnI. In contrast, A8V cTnC and E134D(*19)*, both HCM linked mutations, did not abolish the Ca^{2+} desensitization effect and the acceleration of the rate of dissociation of Ca^{2+} from cNTnC in the presence of a cTnI phosphomimick (S23/S24D). These disease related cTnC mutations are located in

different regions of cTnC and response differently to PKA phosphorylation of cTnI: A8V is on the helix N; L29Q is on the dysfunctional Ca^{2+} binding site I; E134D is on the helix G close to the Ca^{2+} binding site III in the C-domain; G159D is at the C-terminus of cTnC. In this study, we showed that L48Q, L57Q and I61Q, which are all located in the regulatory domain of cTnC, also responded differently to the PKA phosphorylation of cTnI.

Here, we found that L48Q cTnC, known to increase Ca^{2+} binding affinity, similar to the HCM linked mutation A8V cTnC with increased Ca^{2+} sensitivity, did not blunt the Ca^{2+} desensitization effect introduced by PKA phosphorylation of cTnI. The Ca^{2+} binding sensitivities of IANBD fluorescence for L48Q and control cTn were reduced by the same extent upon cTnI PKA phosphorylation, both showed ~0.3 pCa decrease in Ca^{2+} sensitivity, though L48Q showed higher Ca^{2+} binding affinity to cTnC than the control regardless of the cTnI phosphorylation status. However, PKA phosphorylation appeared to reduce cTnC-cTnI interaction to a greater extent for L48Q compared to control cTnC (see Table 5.3) in both apo and Ca^{2+} saturated states. It is possible that L48Q alters interactions of the cNTnC with N-extension of cTnI upon PKA phosphorylation, ultimately affecting the cTnC-cTnI interactions within the cTn complex. These results suggest that the increase in Ca^{2+} binding affinity for L48Q may not counterbalance the reduction in the cTnC-cTnI interaction by PKA phosphorylation. Furthermore, PKA phosphorylation might compromise the increased cTnI binding induced by L48Q cTnC. We have previously discussed in Chapter 3 that L48Q increases the binding of the switch region of cTnI to cNTnC by stabilizing the open state of the regulatory domain of cTnC induced by the substitution of L to Q at residue 48. This is also supported by NMR using

cTnI$_{147-163}$ and cNTnC from our collaborators as described in Chapter 3. Increased binding of cTnI$_{147-163}$ has been considered to associate with decreased inhibition of cTnI on actin. The more efficiently the switch region of cTnI binds to cNTnC, the more efficiently the inhibitory region of cTnI is pulled away from actin, likely accelerating the rate of crossbridge formation and detachment (*166*). In the case of L48Q cTnC, the drastic effect of PKA phosphorylation on the cTnC-cTnI interaction (supported by our data) might be due to the perturbed modulation of the cTnI$_{147-163}$ binding characteristics with cNTnC during PKA phosphorylation. Physiological data for L48Q cTnC are not available yet to confer if this effect induced by the PKA phosphorylation of cTnI would be transferred to the inhibitory region of cTnI, leading to changes in its inhibition of actin, rates of cross-bridge formation and relaxation. Experiments aimed at these aspects are beyond the scope of this project.

L57Q and I61Q, located on the helix C of the regulatory domain of cTnC, however, blunted the Ca^{2+} desensitization effect of cTnI PKA phosphorylation. Our Ca^{2+} binding affinity studies indicated that the PKA phosphorylation did not further desensitize Ca^{2+} binding to cTn complexes that containing either L57Q or I61Q cTnC, respectively. However ~0.1 pCa unit decrease in Ca^{2+} sensitivity was found in Ca^{2+} binding to cTnC-cTnI complex in the presence of cTnI PKA phosphorylation for both I61Q and L57Q, which was not seen in the studies of Ca^{2+} binding to whole cTn complexes. This could be explained by the fact that cTnT plays an important role in regulating Ca^{2+} activated force generation by interacting with other subunits in cTn complex and Tm (*2*). These results suggest that PKA phosphorylation of cTnI has no obvious effects on the Ca^{2+} binding properties to L57Q and I61Q cTn complexes.

However, our studies of cTnC-cTnI interaction of these two variants indicate that PKA phosphorylation of cTnI disturbed the interactions between cTnC-cTnI in both absence and presence of Ca^{2+}. In the presence of PKA phosphorylation, a small, but statistically significant decrease in the affinity of cTnI for cTnC●Ca^{2+} was found for the control cTnC (ΔK_D= ~10nM compared to the non-phosphorylated condition). The K_D of cTnC●Ca^{2+} for cTnI was determined to be 296±18 nM in the absence of PKA phosphorylation and 395±20 nM in the presence of PKA phosphorylation for L57Q cTnC, ΔK_D= ~100nM. The affinity of cTnI for I61Q cTnC was reduced to a greater extent than L57Q, indicated by ΔK_D=~200nM (from 321±26 nM (no PKA) to 532±45 nM (PKA phosphorylated)). These results suggest that L57Q and I61Q enhanced the effect of PKA phosphorylation on the cTnC-cTnI interaction compared to the wild type cTnC. We have shown previously that the introduction of either L57Q or I61Q mutation brings the change in cTnC-cTnI interaction *per se*, and here we found that this interaction was further modulated differently by PKA phosphorylation compared to the control cTnC. The combined effects of altered interaction between cTnI and cTnC and perturbed modulation of the cTnI affinity to L57Q or I61Q cTnC by PKA phosphorylation may result in the development of impaired cardiac contractility, which will be discussed in Chapter 7.

5.4. Conclusions

Here, we have focused on studying how PKA phosphorylation modulates the Ca^{2+} binding properties and cTnC-cTnI interactions of the cTnC variants, L48Q, L57Q, and I61Q. L48Q cTnC did not affect the Ca^{2+} desensitization of cTn complex induced by PKA phosphorylation, while L57Q and I61Q abolished this effect indicated by no change in the Ca^{2+} binding affinity to cTn complexes in the presence of cTnI PKA

phosphorylation. PKA phosphorylation appears to affect the cTnC-cTnI interaction to a greater degree for all cTnC variants studied compared to the control cTnC in both presence and absence of Ca^{2+}. These PKA phosphorylation related characteristics of the cTnC variants brings crucial insights for the understanding certain HCM or DCM associated with altered Ca^{2+} sensitivities of contraction.
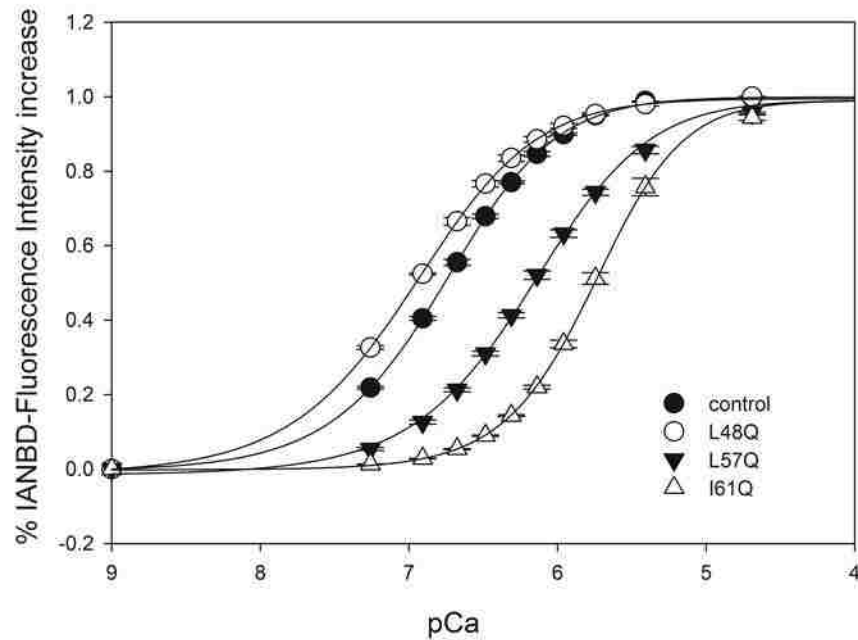
Figure 5.1. Ca^{2+} binding to cTnC$_{IANBD}^{C35S}$ and PKA phosphorylated cTnI complexes. (○) L48Q cTnC$_{IANBD}^{C35S}$-cTnI (PKA phosphorylated) complex (n=3); (●) cTnC$_{IANBD}^{C35S}$-cTnI (PKA phosphorylated) complex (n=3); (▼) L57Q cTnC$_{IANBD}^{C35S}$-cTnI (PKA phosphorylated) complex; (△) I61Q cTnC$_{IANBD}^{C35S}$-cTnI(PKA phosphorylated). Excitation was at 490nm and the emission was monitored at 530nm. The error bars represent the standard error of 3 experiments.
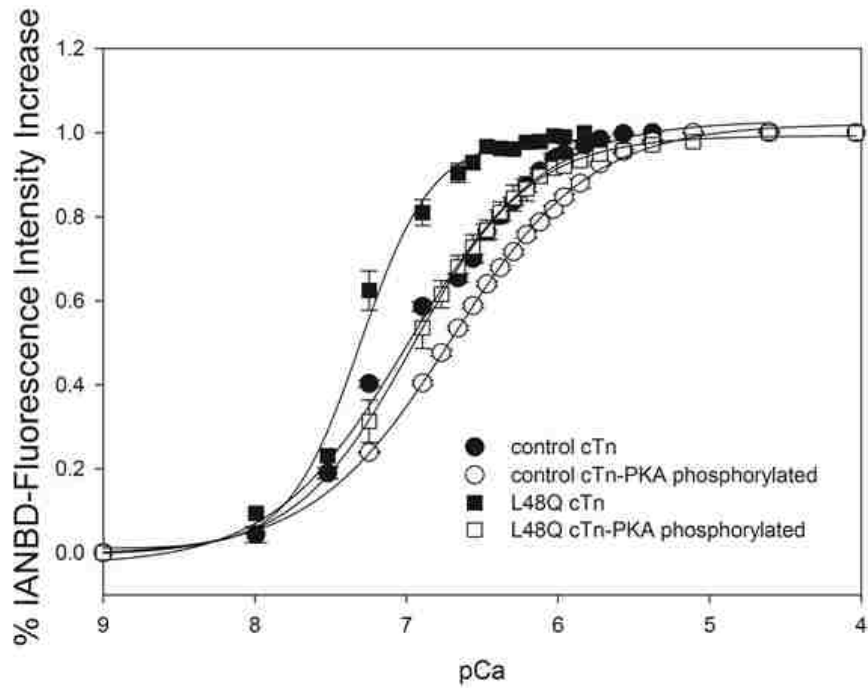
Figure 5.2. Effects of L48Q on Ca^{2+} binding to cTn_{IANBD}^{C35S} complex and its modulation by PKA phosphorylation. (●) cTn_{IANBD}^{C35S} complex; (○) PKA phosphorylated cTn_{IANBD}^{C35S} complex; (■) L48Q cTn_{IANBD}^{C35S} complex; (□) PKA phosphorylated L48Q cTn_{IANBD}^{C35S} complex. Excitation was at 490nm and the emission was monitored at 530nm. The error bars represent the standard error of 3 experiments.
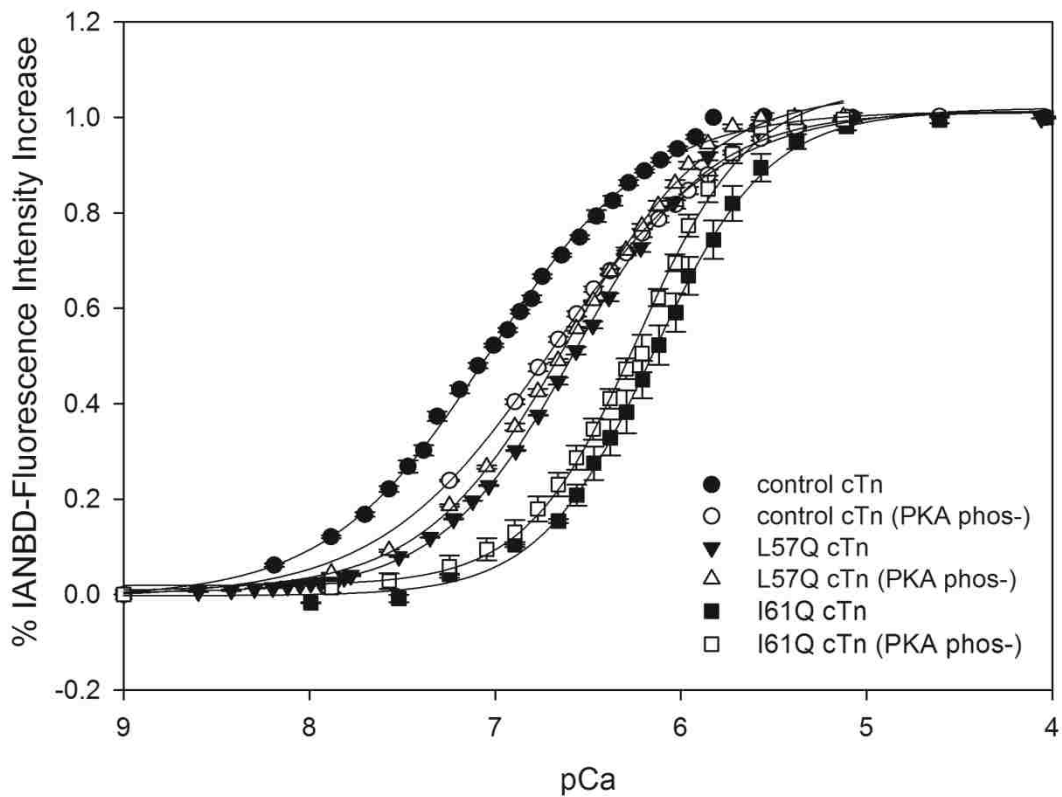
Figure 5.3. Effects of L57Q and I61Q on Ca^{2+} binding to cTn_{IANBD}^{C35S} complex and its modulation by PKA phosphorylation. ($\bullet$) cTn_{IANBD}^{C35S} complex; ($\circ$) PKA phosphorylated cTn_{IANBD}^{C35S} complex; ($\blacktriangledown$) L57Q cTn_{IANBD}^{C35S} complex; ($\triangle$) PKA phosphorylated L57Q cTn_{IANBD}^{C35S}; ($\blacksquare$) I61Q cTn_{IANBD}^{C35S} complex; ($\square$) PKA phosphorylated I61Q cTn_{IANBD}^{C35S} complex. Excitation was at 490nm and the emission was monitored at 530nm. The error bars represent the standard error of 3 experiments. P<0.05.
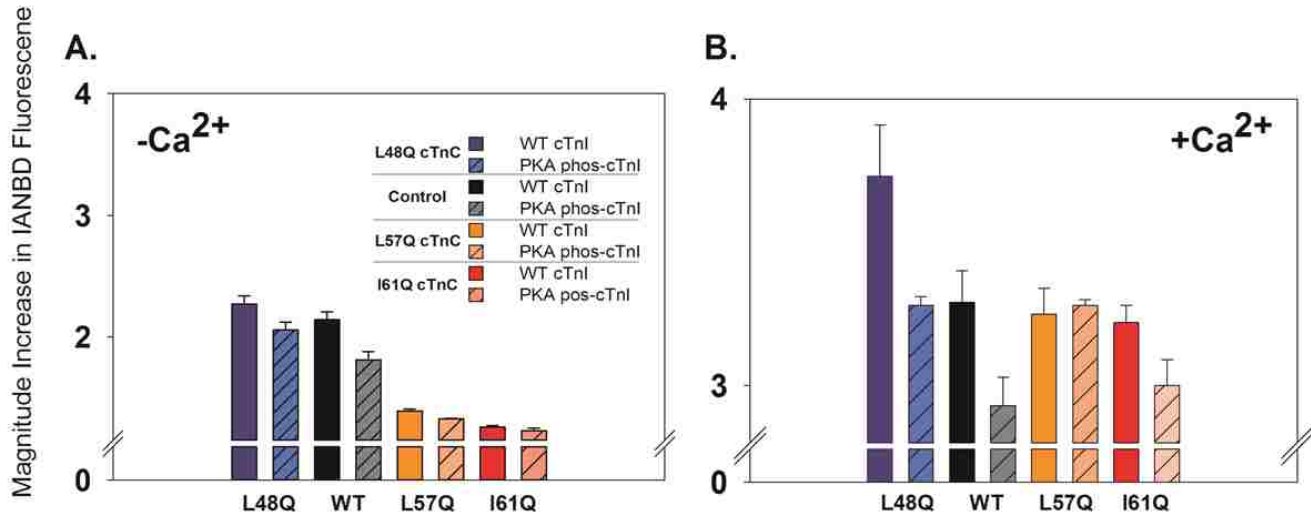
Figure 5.4. Total magnitude increase in IANBD fluorescence of WT or PKA phosphorylated cTnI binding to cTnC variants in the absence (Panel A) and presence (Panel B) of Ca^{2+}.

Table 5.1. Summary of Ca^{2+} binding parameters for cTnI or phos-cTnI and cTnC complexes

	cTnI+cTnC$_{IANBD}^{C35S}$	n_H	PKA phos-cTnI+cTnC$_{IANBD}^{C35S}$	n_H
L48Q	7.02±0.01*	1.10±0.03	6.96±0.01*	1.08±0.02*
Control	6.86±0.01	1.16±0.01	6.76±0.01	1.17±0.02
L57Q	6.28±0.01*	1.25±0.03*	6.18±0.01*	1.09±0.01*
I61Q	5.85±0.01*	1.26±0.02*	5.76±0.01*	1.42±0.03*

$P < 0.05$ as compared to the control cTnC-cTnI complex.

Table 5.2. Summary of Ca^{2+} binding parameters for cTn or PKA phosphorylated-cTn complexes

	cTn$_{IANBD}^{C35S}$	n_H	PKA phos-cTn$_{IANBD}^{C35S}$	n_H
L48Q	7.31±0.03*	1.83±0.02*	6.96±0.01*	1.12±0.02*
Control†	6.99±0.03	1.16±0.01	6.70±0.01	0.94±0.02
L57Q	6.57±0.01*	1.19±0.02	6.61±0.01*	1.12±0.04*
I61Q	6.15±0.01*	1.41±0.01*	6.23±0.02*	1.44±0.07*

†The non-phosphorylated control cTn data in Figure 5.2 and 5.3 are from different set of experiments and are proved to be consistent with each other as indicting by unchanged pCa50 and n_H values. * $p < 0.05$ as compared to the control cTnC-cTnI complex.

Table 5.3. Summary of binding parameters for WT cTnI or PKA

phosphorylated cTnI to apo / Ca^{2+} saturated cTnC.

	Ca^{2+} saturated- cTnC$_{IANBD}^{C35S}$		apo- cTnC$_{IANBD}^{C35S}$	
	K_D (wt cTnI) nM	K_D (phos-cTnI) nM	K_D(cTnI wt) nM	K_D (phos-cTnI) nM
L48Q	174±8*	319±14*	140±7*	746±93*
WT	198±5	207±5	455±50	673 ±53
L57Q	296±18*	395±20*	419±41*	861 ± 103*
I61Q	321±26*	532±45*	515±22*	2370±884*

* $p < 0.05$ as compared to the control cTnC-cTnI complex.

Chapter 6

Effects of L57Q and I61Q cTnC Variants on Intact Cardiomyocyte Contraction and Relaxation

6.1. Introduction

Our solution studies (Chapter 3-5) indicated that increasing (e.g. L48Q cTnC) or decreasing (e.g. L57Q or I61Q cTnC) Ca^{2+} binding affinity in whole cTn resulted in increased and decreased cTnC-cTnI interaction, respectively. This strengthening (or weakening) of the cTnC-cTnI interaction could sensitize (or desensitize) a positive feedback effect of crossbridges on Ca^{2+} binding to cTnC and contribute to the changes in Ca^{2+} sensitivity of force generation. This proposed mechanism is supported by a recent report from Kreutziger *et al*. They used exchanged cardiac myofibrils and demembranated trabeculae to study the influences of L48Q and I61Q cTnC on the cooperative thin filament activation and the kinetics of tension generation and relaxation (75)[Error! Bookmark not defined.]. Results showed that L48Q cTnC increased Ca^{2+} sensitivity of ension without affecting the activation kinetics but prolonged slow phase relaxation duration at maximal activating Ca^{2+}, and I61Q cTnC slowed the rate of thin filament activation and decreased the Ca^{2+} sensitivity of myofilament contraction. More recently, our lab have demonstrated that L48Q increases intact myocyte contractility without affecting relaxation or Ca^{2+} transients (Feest *et al,* paper in preparation). Thus, we

hypothesize that if L48Q cTnC increases cardiac myocytes contractility through increased Ca^{2+} sensitivity of force generation *($\uparrow Ca^{2+}$ binding affinity, $\downarrow Ca^{2+}$ dissociation rate, $\uparrow$cTnC-cTnI interaction)*, then cTnC variants with decreased Ca^{2+} sensitivity *($\downarrow Ca^{2+}$ binding affinity, $\uparrow Ca^{2+}$ dissociation rate, $\downarrow$cTnC-cTnI interaction)*, such as L57Q and I61Q, may decrease the extent and rate of shortening, and increase the rate of relaxation in intact cardiomyocytes. Experiments with L48Q have been conducted by a post-doctoral fellow and a graduate student in our research group (with a manuscript in preparation). Thus, this work focused on cultured cardiomyocytes transduced with viral constructs containing DNA for the L57Q and I61Q cTnC variants. These *in vitro* experiments allowed us to first characterize effects of the L57Q and I61Q cTnC variants at the intact cell level in the absence of neuro-hormonal signaling and systemic viral-mediated responses (such as immune response and inflammation) *in situ*. Cultured adult cardiomyocytes provided a useful platform on which to make the variety of measurements, including contractility, intracellular Ca^{2+} transients and metabolism, and protein isoform content, which allowed us to study how these parameters might be affected by altered myofilament Ca^{2+} sensitivity. Adult cardiomyocytes will also enable an easier transition to *in situ* models being developed in our lab. Knowledge of how adult rat cardiomyocytes respond to incorporation of these cTnC variants into myofilaments is also a necessary precursor before moving to *in vivo* animal models.

For these studies, we used cultured intact adult rat cardiomyocytes and viral gene transfer approaches to incorporate cTnC variants into the myofilaments. We used the IonOptix imaging system to make measurements of cell shortening and relaxation using. Viral constructs contained DNA for green fluorescent protein (GFP) in order to

qualitatively monitor transduction levels. The DNA for cTnC variants contained a poly-His tag code that will allow measurement of the amount of variant incorporated into myofilaments (vs. native protein without the His-tag). Following the contractile measurements, cellular protein analysis techniques were performed to determine the effect of the treatment on protein isoforms and phosphorylation status. The IonOptix microscopy hardware and software system allowed simultaneous measures of cell length using edge detection, sarcomere length (SL) using dark/light pixel intensity and fast Fourier analysis, and Fura-2 ratiometric fluorescence capture for probing Ca^{2+} transients. Measures of shortening and relaxation for individual adult rat cardiomyocytes in culture were made after 48 hours of incubation with vectors containing WT cTnC, L57Q, and I61Q cTnC. Higher cardiomyocyte density cultures treated with WT cTnC, L57Q cTnC or I61Q cTnC were processed to determine the protein content and phosphorylation levels.

6.2 Results and Discussion

6.2.1 Cardiomyocyte mechanics

To determine the effects of the L57Q and I61Q cTnC variant on contractile function, ventricular cardiomyocytes were isolated from adult rats and transduced with adenovirus. The recombinant adenovirus was driven by CMV vector and contained GFP as a reporter protein to identify successful transduction of the cardiomyocytes. The cardiomyocytes were treated with adenovirus containing [I61Q cTnC + GFP], [L57Q cTnC + GFP], or [WT cTnC + GFP] after isolation and cultured for 48 hours. Nearly 100% transfection efficiency was achieved as identified using florescence microscopy, which is consistent with our previous studies (paper in preparation). Cell viability was not

affected by virus as the cardiomyocytes survival did not differ among treated and non-treated groups. Previous studies have shown either a slight depression in function with GFP (*167*) or no change (*168*). Since we expect the contractility of L57Q and I61Q cTnC transduced cells to be compromised due to decreased Ca^{2+} sensitivity, any potential depression effects from GFP expression might confound our results. Therefore, we have made all of our comparisons to cardiac myocytes overexpressing WT cTnC instead of non-treated cells in this study.

Table 6.1 lists the basic cell characteristics for WT, L57Q and I61Q cTnC transduced cells. Of note, the isolated cardiomyocytes measured in our experiments were unloaded, presenting a potential limitation. Unloaded cardiomyocytes exhibit shorter sarcomere lengths and faster cross-bridge cycling (*169, 170*). Nevertheless, we propose to study two independent cTnC variants under identical experimental conditions where their influences could be compared with controls and with one another, thereby enabling us to isolate the effects of each independent variant.

Representative contraction/relaxation recordings of isolated adult cardiomyocytes field stimulated at 0.5 HZ are shown in Figure 6.1 A. Figure 6.1 B and C summarize the changes in fractional shortening (FS), shortening velocity (V_{short}), relaxation rate (V_{rel}) and 90% time to relaxation (RT_{90}) for both L57Q and I61Q as a percentage change relative to WT transduced cells. I61Q transduced cardiomyocytes had significantly decreased extent (↓54.2%) and rate of shortening (↓53.0%), and increased relaxation times (↑18.3%) compared to WT. L57Q also showed ~27% and ~29.1% reduction in FS and V_{short}, respectively, while the RT_{90} (relaxation) was increased ~5.4% compared with WT. However, the effects of L57Q were not as significant as the effects of the I61Q

variant. Interestingly, results from experiments with L48Q transduced myocytes showed that L48Q cTnC significantly increased the extent and rate of shortening, while relaxation times were unaffected (Feest *et al* paper in preparation). These results demonstrate that the contractility of L57Q and I61Q transduced cardiomyocytes was compromised as compared to WT transduced cardiomyocytes

6.2.2. Cardiomyocyte Ca^{2+} transients

Given the tight relationship between contractility and Ca^{2+} kinetics, myocyte intracellular Ca^{2+} concentration was probed to determine whether the transduced cTnC variants with altered Ca^{2+} binding affinity would influence the Ca^{2+} handling in intact cardiomyocytes. Representative Ca^{2+} transients indicated by Fura-2 fluorescence recordings of isolated cells field stimulated at 0.5HZ are shown in Figure 6. 2. A. We found that the baseline, the amplitude (peak), and the 90% time to baseline of Fura2 fluorescence were all significantly decreased for I61Q cTnC transduced cells compared with control cells (WT cTnC) (Figure 6.2.B). L57Q cTnC transduced cells also had a reduction in peak Ca^{2+} transient and longer fluorescence decay times (RT_{90}), but these effects were more pronounced with I61Q cTnC. The Ca^{2+} transient baseline was not affected for L57Q cTnC but decreased about 15% for I61Q cTnC compared to WT cTnC. However, the Ca^{2+} transient (both baseline and peak) was not changed for L48Q cTnC transduced myocytes (Feest *et al,* paper in preparation). These results suggest that cTnC variants that have increased/decreased Ca^{2+} binding affinity (as discussed in Chapter 3&4) have different effects on Ca^{2+} handling in intact cardiomyocytes.

6.2.3. Contractile response to stimulation frequencies

Because heart rate changes in response to the demands of human body, it is

important to determine if L57Q or I61Q cTnI affects the cellular response to increased stimulation frequency. Figure 6.3 shows the effects of increased stimulation frequency (from 0.5 to 1.0 to 2.0 Hz) on fractional shortening (6.3.A), shortening velocity (6.3.B), relaxation velocity (6.3.C), and time to 90% relaxation (6.3.D). The cardiomyocytes mechanics are also summarized in Table 6.2, 6.3 and 6.4, respectively. The contractile response to different pacing frequency was similar between L57Q and control groups. L57Q cardiomyocytes showed moderate depression of contraction at all frequencies compared to control cells, while the contraction of I61Q transduced cardiomyocytes was significantly more depressed than L57Q and WT at 0.5 and 1 Hz. However, at higher frequency (2 Hz) I61Q cells were not potentiated, indicated by the results that the fractional shortening, the shortening velocity and the relaxation shortening were all elevated to nearly the same level as L57Q transduced cells. The time to 90% relaxation were shortened with increasing stimulation frequency in all groups (Figure 6.3.D).

Figure 6.4 summarizes the effects of stimulation frequency on Ca^{2+} transients from cardiomyocytes transduced with I61Q or L57Q cTnC. All groups of cells had a slight increase in baseline and peak Ca^{2+} at all frequencies. In particular, the peak Ca^{2+} was significantly decreased for I61Q cTnC transduced myocytes. Time to 50% and 90% relaxation were similar between groups at all stimulation frequencies, which indicated there was no effect of I61Q or L57Q cTnC expression on Ca^{2+} decay properties.

6.2.4. Contractile efficiency of transduced cells

We further analyzed the contractile efficiency of the transduced cells by looking at the value of fractional shortening divided by the peak Ca^{2+} transient, which gives a measure of the percentage of contraction per calcium released for these variants. As

shown in Figure 6.5.A at 0.5 Hz, I61Q cTnC transduced cells shortened less for a given amount of Ca^{2+} release, which is likely indicative of decreased Ca^{2+} sensitivity of contraction. L57Q also shortened less per a given Ca^{2+} release compared to control myocytes, but not as much as I61Q. Conversely, L48Q cTnC cells contracted more per Ca^{2+} release (Feest *et al* paper in preparation). These results using intact cardiomyocytes studies correlate well with our previous studies of cTnC variants with different Ca^{2+} affinity (Figure 3.1 and Figure 4.1) and Ca^{2+} sensitivity of force in exchanged muscle fibers (75)[Error! Bookmark not defined.]. Figure 6.5.B illustrates the calculated contractile fficiency at all stimulation frequencies. Interestingly, I61Q cTnC transduced cells demonstrated similar Ca^{2+} sensitivity to control cardiomyocytes at higher frequencies, maintaining responsiveness to increasing stimulation frequencies.

Our results suggest that I61Q cTnC severely decreased the extent and rate of cardiomyocyte shortening, and both the baseline and peak Ca^{2+} transients. This suggests that I61Q cTnC (decreased Ca^{2+} binding affinity) likely disrupted normal sarcoplasmic reticulum (SR) function. L57Q cTnC also showed a slight decrease, though not statistically significant, in contractility and Ca^{2+} transient properties.

We did not observe a change in thin filament protein stoichiometry, as assessed by Ruby-stain and SDS-PAGE. This is consistent with previous evidences that the stoichiometry(171) of this filament proteins was maintained after adenoviral and transgenic overexpression thin filament proteins(172-174).

Functional studies for DCM linked mutations in sarcomeric proteins have shown altered (generally decreased) Ca^{2+} sensitivity of myofilaments and impaired myocardial contractility. There is also evidence that heart disorder such as cardiomyopathies and

heart failure can result in altered SR function (*90, 175*). However, little is known about how or if the myofilament is communicating with the SR, and whether these myofilament alterations are causative, consequential, or coincidence to the development of the disease phenotype. I61Q cTnC has decreased Ca^{2+} binding affinity, which significantly decreased shortening rate and magnitude when expressed in intact cells as expected. The reduction of the Ca^{2+} transient amplitude and time to decay in I61Q cTnC cells might be explained by a decrease in SERCA activity (at 0.5 and 1.0 Hz) as decreased SERCA activity is known to reduce SR Ca^{2+} stores (*176*). A reduction in SR Ca^{2+} stores could reduce the amount of Ca^{2+} released during contraction, which would be indicated by decreased Ca^{2+} peak amplitude for I61Q cTnC transduced cells. Such interplay between myofilaments and the SR might be due to altered phosphorylation profiles of the myofilament and SR proteins, but the mechanism of which is beyond the scope of this project and awaits future study.

6.3. Conclusions

In conclusion, our studies demonstrate that I61Q cTnC (decreased Ca^{2+} binding affinity) reduced the Ca^{2+} transient amplitude and time to decay, and impaired contraction compared to control cardiomyocytes. L57Q also disrupted the cell shortening and intracellular Ca^{2+} , albeit to a smaller degree than I61Q cTnC and was not statistically significant. This suggests that there is some 'communication' between myofilaments and the SR. These experiments demonstrate the potential of using our cTnC variants to study how altered myofilament Ca^{2+} binding might affect SR function, other intracellular Ca^{2+} buffers, and gene regulation. The knowledge of how these processes couple with each other provides critical information for understanding the mechanisms of

cardiomyopathies that are associated with abnormal Ca^{2+} sensitivity, as well aid in designing specific therapeutics to treat cardiomyopathies.
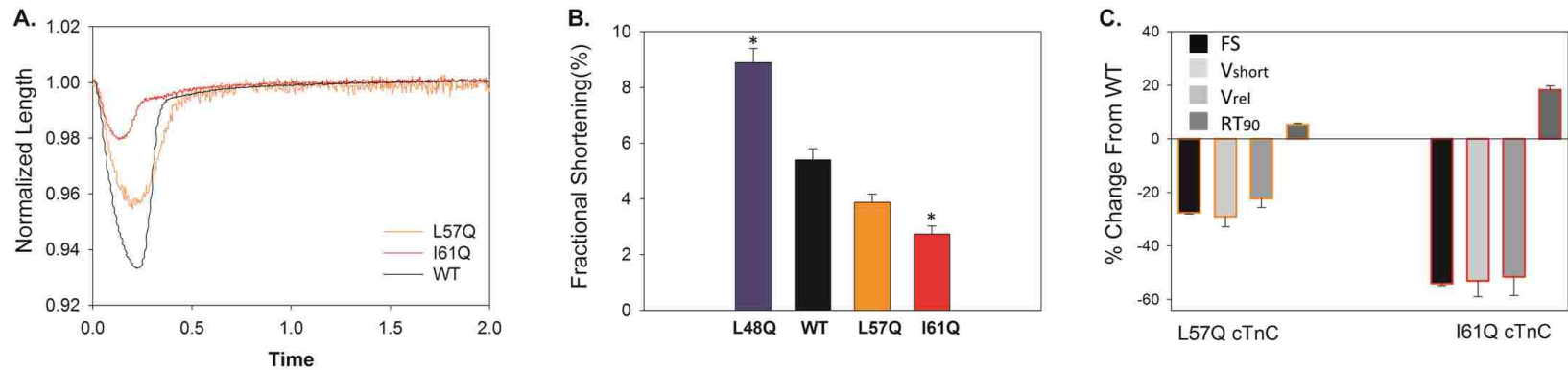
Figure 6.1 Contraction and relaxation measurements of fieled-stimulated rat adult cardiomyocytes (AV-transduced variant + GFP) at 0.5 Hz. A. Representative cardiomyocyte shorteing traces from WT cTnC (black), L57Q cTnC (orange), I61Q cTnC (red) transduced cardiomyocytes; B. Fractional Shortening (FS) for L48Q(data courtesy from Dr. Steve Korte), WT, L57Q, I61Q cTnC. C. Summary data for L57Q&I61Q cTnC % change over WT cTnC for fractional shortening (FS), shortening velocity(Vshort), relaxation rate(Vrel), and 90% time to relaxation(RT90) * = p<0.05 as compared to WT cTnC
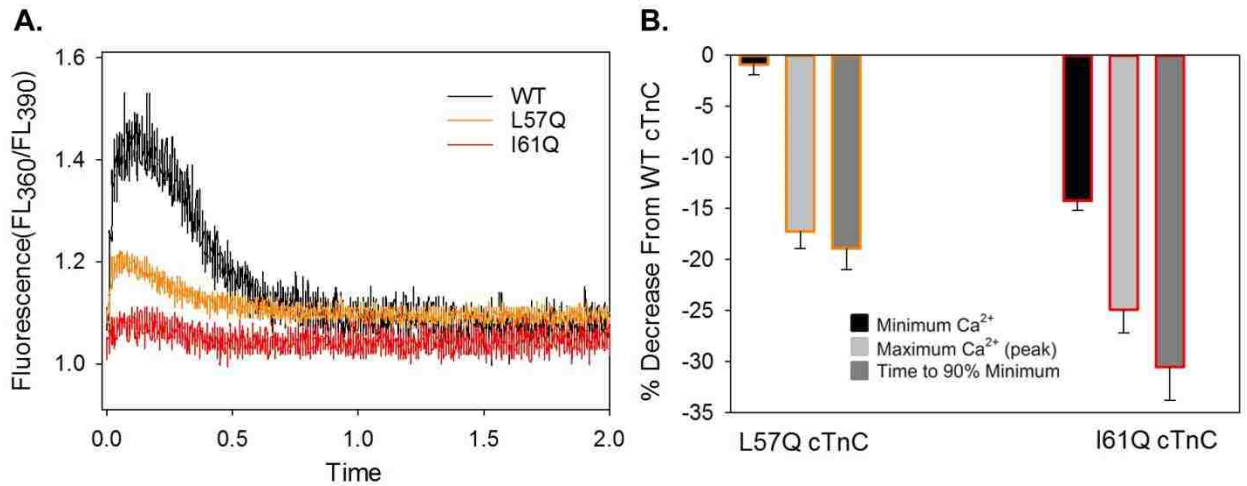
Figure 6.2. Contraction and relaxation measurements of filed-stimulated rat adult

cardiomyocytes (AV-transduced variant + GFP)

(A). Representative cardiomyocyte Ca^{2+} transients traces from WT cTnC(black), L57Q cTnC(orange), I61Q cTnC(red) transduced cardiomyocytes; (B). Summary data for L57Q&I61Q cTnC % decrease over WT cTnC for baseline Fura2 fluorescence (Min.Fura2 FL), amplitude Fura2 fluorescence (Max. Fura2 FL) and 90% time to baseline fluorescence (FL RT_{90}).
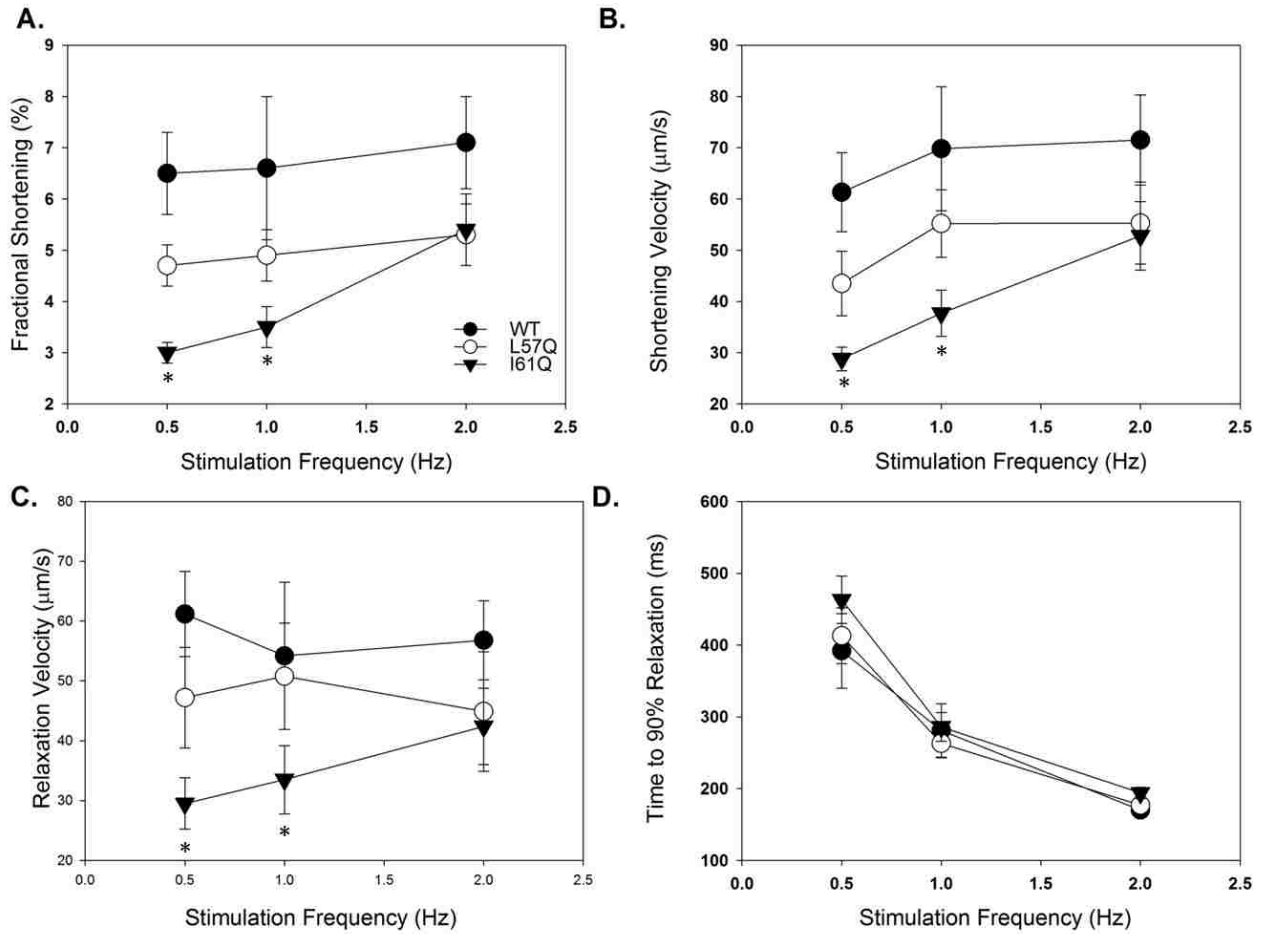
Figure 6.3. Effect of stimulation frequency on contractile properties. L57Q transduced myocytes (open circles) and I61Q transduced myocytes (closed triangles) respond similarly to stimulation frequency as WT transduced (closed circles) but show reduced fractional shortening (A), shortening velocity (B) and relaxation velocity (C) at all frequencies (0.5, 1, 2 Hz). Time to 90% relaxation (D) is similar between groups, with time to relaxation shortening as stimulation frequency increases. * = p < 0.05 as compared to WT transduced.
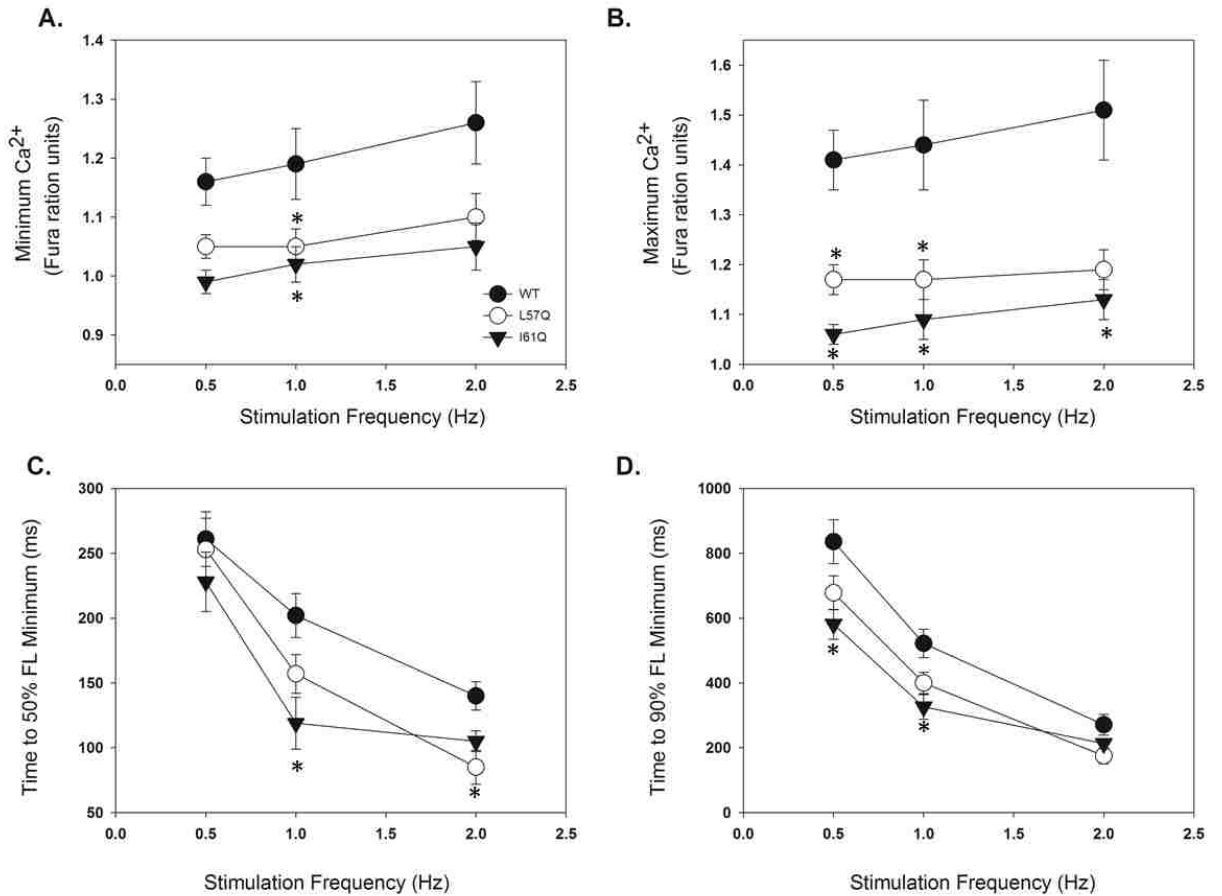
Figure 6.4. Effect of stimulation frequency on Ca^{2+} handling properties. L57Q transduced myocytes (open circles) and I61Q transduced myocytes (closed triangles) respond similarly to stimulation frequency as WT transduced myocytes (closed circles) in minimal (A) and maximal (B) fura fluorescence, while WT transduced myocytes showed higher level of fura fluorescence than I61Q and L57Q transduced myocytes at all frequencies (0.5, 1, 2 Hz). As with cardiomyocytes relaxation, Ca^{2+} transient decay time (DT) to 50% (C) and 90% (D) is shortened with increased stimulation frequency for all groups. * = p < 0.05 as compared to WT transduced.
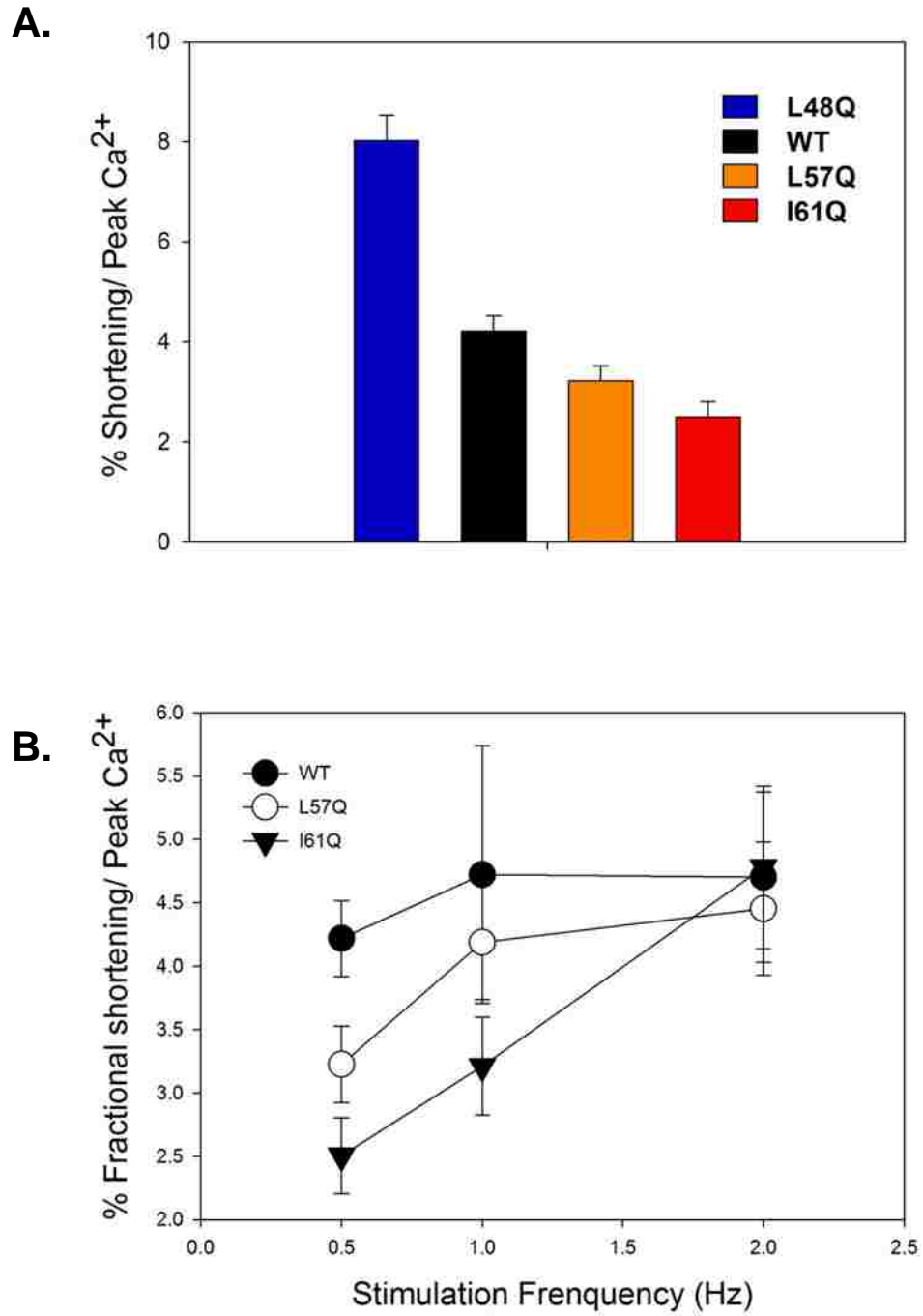
Figure 6.5. Contractile efficiency for cTnC variants transduced myocytes. I61Q cTnC transduced cells rescued Ca^{2+} sensitivity of cardiomyocytes contraction at 2 Hz.

Table 6.1. Cell characteristics

	N	n	SL (μm)	Cell length (μm)
Control (WT cTnC)	7	45	1.67 ± 0.02	89.5 ± 3.3
L57Q cTnC	7	45	1.67 ± 0.02	83.8 ± 1.8
I61Q cTnC	7	50	1.66 ± 0.02	83.3 ± 2.0

N = number of hearts, n = number of cardiomyocytes.

Table 6.2. Contractile and Ca^{2+} transient values for 0.5 Hz stimulation.

	Fractional Shortening (%)	Maximal Shortening Rate (μm/s)	Maximal Relaxation Rate (μm/s)	RT_{50} (ms)	RT_{90} (ms)	Minimal Ca^{2+} (Fura ratio units)	Maximal Ca^{2+} (Fura ratio units)	DT_{50} (ms)	DT_{90} (ms)
Control (WT cTnC)	6.5 ± 0.8	61.3± 7.7	61.2 ± 7.1	134 ± 22	392± 52	1.16 ± 0.04	1.41 ± 0.06	261 ± 21	836 ± 68
L57QcTnC	4.7±0.4	43.5±6.3	47.2±8.4	142±14	413±39	1.05±0.02	1.17±0.03*	253±24	678±52
I61QcTnC	3.0±0.2*	28.8±2.3*	29.5±4.3*	142±14	463±33	0.99±0.02	1.06±0.02*	228±23	581±46*

* $P < 0.05$ as compared to WT for all groups.

Table 6.3. Contractile and Ca^{2+} transient values for 1 Hz stimulation.

	Fractional Shortening (%)	Maximal Shortening Rate (μm/s)	Maximal Relaxation Rate (μm/s)	RT_{50} (ms)	RT_{90} (ms)	Minimal Ca^{2+} (Fura ratio units)	Maximal Ca^{2+} (Fura ratio units)	DT_{50} (ms)	DT_{90} (ms)
Control (WT cTnC)	6.8± 1.4	69.8 ± 12.1	54.2 ± 12.3	106 ± 13	281 ± 37	1.19 ± 0.06	1.44 ± 0.09	202 ± 17	522 ± 44
L57Q TnC	4.9±0.5	55.2±6.6	50.8±8.9	108 ± 13	263 ± 20	1.05±0.03*	1.17±0.04*	157±15	400±33
I61Q cTnC	3.5±0.4*	37.7±4.5*	33.5±5.7*	109±8	286±20	1.02±0.03*	1.09±0.04*	119±20*	326±38*

* $P < 0.05$ as compared to WT for all groups.

Table 6.4. Contractile and Ca^{2+} transient values for 2 Hz stimulation.

	Fractional Shortening (%)	Maximal Shortening Rate (μm/s)	Maximal Relaxation Rate (μm/s)	RT_{50} (ms)	RT_{90} (ms)	Minimal Ca^{2+} (Fura ratio units)	Maximal Ca^{2+} (Fura ratio units)	DT_{50} (ms)	DT_{90} (ms)
Control (WT cTnC)	7.1 ± 0.9	71.5 ± 8.8	56.8 ± 6.6	98 ± 6	170 ± 9	1.26± 0.07	1.51 ± 0.1	140 ±11	271 ± 32
L57Q TnC	5.3±0.6	55.3±8.0	44.9±10.0	91±6	177±8	1.10±0.04	1.19±0.04	85±13*	175±24
I61Q cTnC	5.4±0.7	52.8±6.7	42.4±6.4	96±5	194±8	1.05±0.04	1.13±0.04*	105±8	213±15

* $P < 0.05$ as compared to WT for all groups.

Chapter 7

Designing and Using Engineered cTnC variants to Correct Disease Induced Abnormal Ca^{2+} Binding Sensitivities

---

7.1. Introduction

The abnormal response of cardiac thin filament proteins to Ca^{2+} can lead to severe cardiac dysfunctions. Functional studies of disease related mutations commonly showed alterations in the Ca^{2+} sensitivity of cTnC and force development (for reviews, (*49, 177*)). There are several transgenic animal studies demonstrating that the hypertrophic or restrictive phenotypes could be rescued by correcting the disrupted Ca^{2+} sensitivity (*65, 178, 179*). The ability of rescuing/correcting the abnormal Ca^{2+} sensitivity was considered as an important part of an integrative approach to ultimately improve cardiac function for patients with cardiomyopathies (*121*).

cTnC plays a central role as the Ca^{2+} sensor for the thin filament activation as well as the whole process of muscle contraction and relaxation. Targeting cTnC to change the Ca^{2+} sensitivity of the thin filament has more considerable merit than altering the overall intracellular Ca^{2+} handling. There are no drugs available so far that directly targeting cTnC (*180*). A recent study using steady state Ca^{2+} binding affinity and actomyosin ATPase acitivity measurements indicated that engineered cTnC construct S69DcTnC (decreased Ca^{2+} binding affinity) could correct thin filament Ca^{2+} binding

sensitivity of R192H cTnI (RCM related), and M45QcTnC or M45Q/S69D cTnC could correct the deducted Ca^{2+} sensitivity of a DCM linked mutation, ΔK210 cTnT (*181*).

In previous chapters we have characterized the biochemical, structural and physiological properties of L57Q and I61Q cTnC variants. Here, we studied the effects of these variants on the Ca^{2+} binding properties of a disease related model. We have chosen a HCM associated mutation, R145GcTnI, to testify if our cTnC variants with decreased Ca^{2+} binding affinity could correct or rescue the abnormal Ca^{2+} binding sensitivity induced by the disease mutation. Importantly, we have designed and developed a novel variant, L48A cTnC, which is expected to have influence on the cTnC-cTnI interaction, but more moderate effect on the Ca^{2+} binding property compared to either L57Q or I61Q cTnC. The design rationale is discussed together with the experimental results.

7.2. Results and Discussion

7.2.1. Effects of L57Q and I61Q cTnC on the Ca^{2+} binding to cTn complexes containing HCM R145G cTnI mutation

Figure 7.1 shows the Ca^{2+} binding studies for a series of reconstituted cTn complexes. We found that R145G cTnI caused an increase in the Ca^{2+} binding affinity compared with the control cTnC. This is consistent with previous studies that R145G cTnI increased Ca^{2+} binding sensitivity to the thin filament(*54*). Table 7.1 summarizes the Ca^{2+} binding parameters for all cTn complexes studied in this work. Interestingly, when combined L57Q cTnC to the cTn complex containing R145G cTnI (Figure 7.1.A), the Ca^{2+} binding sensitivity exhibited a decrease (rightward shift) for about 0.5 pCa unit, indicating that the increased Ca^{2+} sensitivity of a HCM mutation were significantly deducted by a cTnC variant with decreased Ca^{2+} binding affinity. The pCa_{50} for the cTn

complex with both L57Q cTnC and R145GcTnI, however, was still distinguishable from the control protein, by about ~0.2 pCa with decrease in Ca^{2+} sensitivity. I61Q cTnC, differently from L57Q, when reconstituted in to cTn complex containing R145GcTnI, still showed a dramatic deduction in Ca^{2+} binding, which may be too severe to rescue any depressed contraction in the heart. Another cTnC variant with more tunable Ca^{2+} binding effect, with moderate decreased Ca^{2+} binding affinity on the thin filament would be appreciated to have a better correct effect on a HCM related model.

7.2.2. *Design and characterization of the L48A cTnC variant*

As a cTnC variant with moderate change in Ca^{2+} binding affinity is desired, we designed and developed a new variant by substituting leucine with alanine at residue 48 of cTnC and performed MD simulations on this variant. We chose residue 48 on cNTnC because based on the simulation results on the structure of cNTnC$\bullet$Ca^{2+}$\bullet$cTnI$_{147\text{-}163}$ that 48 position is very important in the interaction between cNTnC and the switch region of cTnI (as shown in Figure 3.4.B and Figure 7.3). Briefly, any inter-residue pairs that show $\geq$ 20% of total time in contact have been counted. The results from multiple simulations show that L48 contacts the greatest number of residues in cTnI$_{147\text{-}163}$ (Figure7.2.A), indicating that this site is likely plays an important role in the dynamics of the cTnI-cTnC interaction. A similar result was found for the L48Q, L48A, L57Q and I61Q simulations (Figure 7.2.B-E). In Figure 7.2.F, a representative contact map for the WT showing the fraction of time in contact between residues in cNTnC and cTnI$_{147\text{-}163}$ during a 70ns simulation indicates that at position 48 in cNTnC there are more constant contacts than the other residues in cNTnC. These results indicate the importance of the amino acid 48 position of cNTnC for the binding of cTnI$_{147\text{-}163}$.

The reason why we chose to use alanine substitution at residue L48 is because alanine is one of the structurally simpler amino acids that has non-bulky, chemical inert, methyl group (*182*). This methyl group of alanine maintains the secondary structure preferences that many of the other amino acids possess (*182*). The technique 'alanine scanning' has been widely used in both molecular and computational biology to determine the contribution of a specific residue to the structure or function for a given protein, and to determine whether the side chain of a specific residue is critical for the bioactivity of the given molecule (*182, 183*). Thus, we designed and developed the L48A cTnC variant and characterized the binding properties of Ca^{2+} and cTnI to cTnC(L48A) in solution using steady-state fluorescence spectroscopy.

As shown in Figure 7.3, the Ca^{2+} sensitivity of the fluorescence signal (reported as pCa at half-fluorescence increase) was barely shifted for L48A cTn_{IANBD}^{C35S}, pCa 6.96 ± 0.01 vs. 7.04 ± 0.03 (for control cTn_{IANBD}^{C35S}). However, when we further examined the effect of L48A cTnC on the interaction between cTnC-cTnI in both presence and absence of Ca^{2+}, the total magnitude increase in IANBD fluorescence were significantly decreased by L48A cTnC, compared to the control cTnC. These results suggest that the cTnC-cTnI interaction was disrupted by L48A cTnC as expected, which was probably due to the direct interruption of the interaction at the switch region-cNTnC interface.

7.2.3. Effects of L48A cTnC on the Ca^{2+} binding to cTn complexes containing HCM R145G cTnI mutation

Our study showed that L48A cTnC altered cTnC-cTnI interaction without dramatically affecting the Ca^{2+} binding affinity to the whole cTn complex. To testify if this variant would properly correct the abnormal Ca^{2+} binding affinity that caused by

R145G cTnI, we reconstituted cTn complex that containing R145GcTnI with L48A cTnC. The results are summarized in Table 7.1 and shown in Figure 7.3. Promisingly, cTn (L48AcTnC+R145GcTnI) complex exhibited a Ca^{2+} binding sensitivity and cooperativity that were about the same as compared to the control cTn complex. Thus, the increased Ca^{2+} binding sensitivity of a HCM linked mutation could be corrected by a proper engineered cTnC variant.

7.3. Conclusions

The increased Ca^{2+} binding sensitivity caused by HCM related mutations in the contractile proteins could be corrected by engineered cTnC variants with proper Ca^{2+} binding properties. L48A cTnC was designed with moderate effect on the Ca^{2+} binding but significant influence on the cTnC-cTnI interaction. In addition to testify the idea of correcting the disease caused abnormal Ca^{2+} sensitivity using engineered cTnC variants, our study here also brings novel insights for designing cTnC that directly targeting at the cTnC-cTnI binding interface.
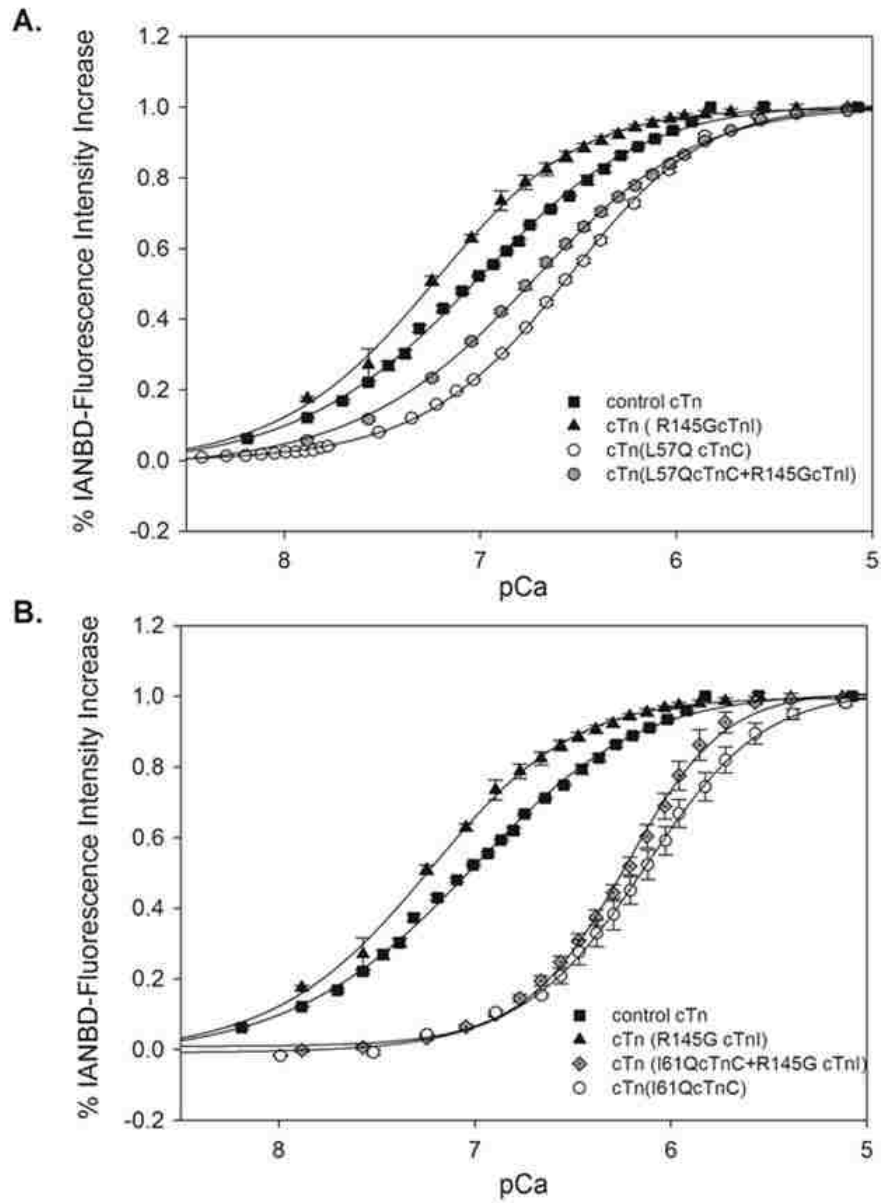
Figure 7.1. HCM linked cTnI(R145G) mutation induced increased Ca^{2+} binding sensitivity can be altered through engineered cTnC variants with decreased Ca^{2+} binding affinity . The normalized Ca^{2+} binding sensitivity as a function of pCa is shown. (■) Ca^{2+} binding to cTn $_{IANBD}^{C35S}$ (control); (▲) cTn $_{IANBD}^{C35S}$ (R145GcTnI). Panel A: (○) cTn $_{IANBD}^{C35S}$ (L57QcTnC); (●) cTn $_{IANBD}^{C35S}$ (R145cTnI + L57QcTnC). Panel B: (○) cTn$_{IANBD}^{C35S}$(I61QcTnC), (◆) cTn$_{IANBD}^{C35S}$ (R145cTnI+I61QcTnC). Each data point represents

129

the mean ± S.E.M. of 3 to 5 titrations fit with hill sigmoid equation. The IANBD fluorescence was excited at 490 nm and monitored at a fixed wavelength near the peak emission at ~ 530nm.

Figure 7.2. Interactions between cNTnC and $cTnI_{147-163}$-Number of $cTnI_{147-163}$ residues that contacted with cTnC. (A): WT; (B): L48Q; (C): L48A; (D): L57Q and (E):I61Q; (G): Example of WT simulation contact map (fraction of time in contact). (A) and (B) are the same as shown in Figure 3.4.B and C.
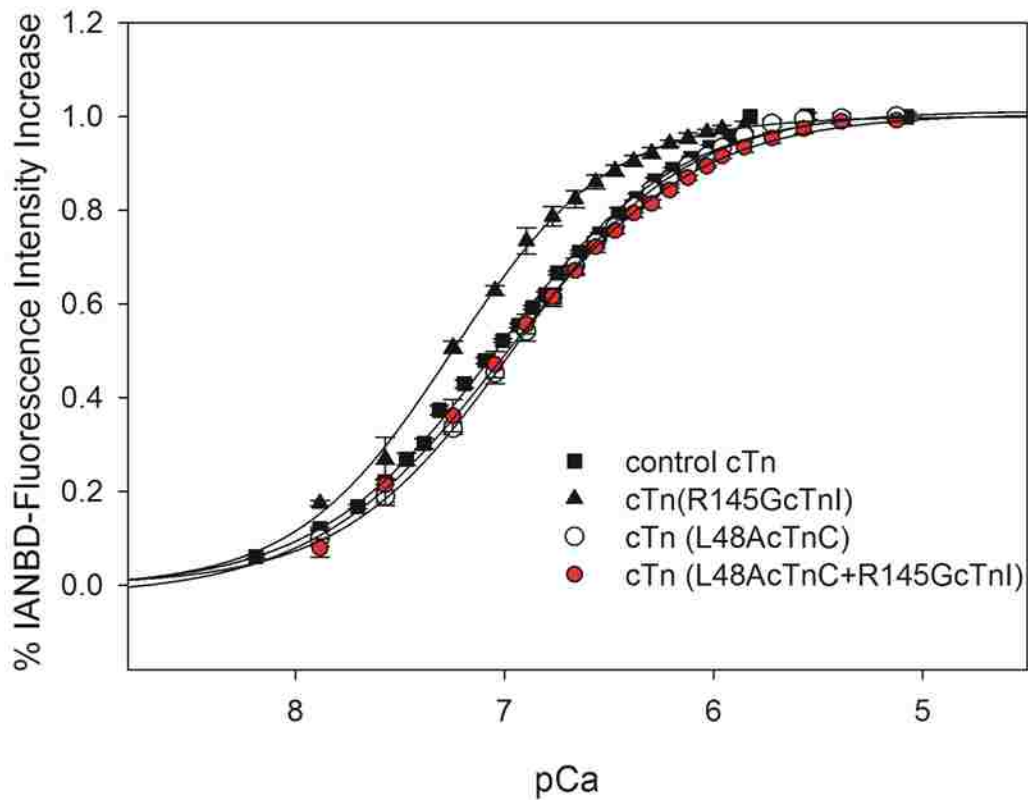
Figure 7.3. L48A cTnC variant corrected the increased Ca^{2+} binding sensitivity induced by HCM linked cTnI (R145G) mutation. The normalized Ca^{2+} binding sensitivity as a function of pCa is shown. (■) Ca^{2+} binding to cTn_{IANBD}^{C35S} (control); (▲) cTn_{IANBD}^{C35S} (R145GcTnI); (○) cTn_{IANBD}^{C35S}(L48A cTnC); (●) cTn_{IANBD}^{C35S}(L48AcTnC+R145cTnI). Each data point represents the mean $\pm$ S.E.M. of 3 to 5 titrations fit with hill sigmoid equation. The IANBD fluorescence was excited at 490 nm and monitored at a fixed wavelength near the peak emission at ~ 530nm.

Table 7.1. Ca^{2+} binding parameters for cTn complexes containing R145G cTnI and cTnC variants.

	R145G cTnI	Control	L57Q cTnC	I61Q cTnC	L48A cTnC	L57QcTnC + R145GcTnI	I61QcTnC + R145GcTnI	L48AcTnC + R145GcTnI
pCa$_{50}$	7.25±0.01*	7.04±0.02	6.57±0.01*	6.15±0.01*	6.96±0.01	6.76±0.01*	6.24±0.01*	7.00±0.01
n$_H$	1.16±0.03	1.16±0.01	1.19±0.02	1.41±0.01*	1.06±0.02	1.02±0.02	1.71±0.06*	0.95±0.02*

*p < 0.05 as compared to control cTn

Chapter 8

Future Directions

The ultimate goals of this research are to determine if cTnC variants (1) will result in HCM and DCM phenotypes, providing insights for the mechanisms underlying the connection between genotype and phenotype, and (2) can reduce or reverse hypertrophic/dilated signaling that results from the pathological myofilament protein mutations, and be used as therapeutic genes for the treatment of HCM or DCM. Thus, after characterizing these cTnC variants in vitro (solution and intact cardiomyocytes) as discussed (Chapter 3-7), the effects of these variants on contractile function of HCM and DCM animal models will be studied in more detail. Then, we can progress to *in situ* whole heart gene therapy that would improve contraction without altering relaxation in disease animal models (e.g. using L48Q to treat DCM or infarcted hearts). That relaxation is impaired in I61Q cTnC transduced cells according to our preliminary studies implies a possible disruption in the diastolic function and may limit its application for the treatment of heart disease (e.g.HCM). However, it has particular value in studying whether altered Ca^{2+} signaling in myofilament contraction is causal for the development of disease phenotypes. Our lab is currently developing these cTnC variant animal models in transgenic mice. Thus, cultured cardiomyocytes, intact/demembranated trabeculae, and whole heart mechanics from these transgenic mice can be studied. Additionally, as cTnC

variants with decreased Ca^{2+} binding affinity, such as I61Q and L57Q cTnC, also show a reduction in Ca^{2+} transients, we will use them as novel reagents to study how altered myofilament activity influences SR and mitochondrial function in more detail. Besides, we designed and tested L48A cTnC variant using both MD simulations and biochemical solution experiment, and future studies of this variant would be focus on physiological functional characterization in muscle fibers, intact cardiomyocytes and if possible, animal models.

Computationally, MD simulation studies will be further continued to design new variants with altered Ca^{2+} binding affinity or protein-protein interaction within cTn. Furthermore, larger scale models (e.g. whole cTn complex) will be built based on the publically available structures. Simulation for these models will be performed to monitor interactions between other myofilament proteins, which could be compiled afterwards with the results we found from cNTnC•Ca^{2+}•$cTnI_{147-163}$ simulations. This completed overall picture, from the structural point of view, will assist in the interpretation of the physiological data. On the other side, we (discussed in Chapter 7) and others (*181*) have demonstrated that engineered cTnC variants with altered Ca^{2+} binding affinities were able to affect the contractile function in cardiomyocytes and correct the disease related aberrant steady state Ca^{2+} binding. However, the molecular mechanism underlying the thin filament Ca^{2+} sensitizing/desensitizing abilities remains unclear. Besides, these studies will bring important implications with respect to the design of Ca^{2+} sensitizer or desensitizer, either cTnC itself or cardiotonic drugs that targets cTnC. MD simulations enable to extend the resolution of our molecular understanding of changes in thin filament or whole sarcomere function to the atomic level.

List of References

1. Association, A. H. (2003) Heart Facts pAll Americans http://www.americanheart.org/downloadable/heart/1046365800849HFAAFS.pdf (1046365800820)

2. Gordon, A. M., Homsher, E., and Regnier, M. (2000) Regulation of contraction in striated muscle, *Physiol. Rev. 80*, 853-924.

3. Gillis, T. E., Martyn, D. A., Rivera, A. J., and Regnier, M. (2007) Investigation of thin filament near-neighbour regulatory unit interactions during force development in skinned cardiac and skeletal muscle, *J Physiol 580*, 561-576.

4. McKillop, D. F., and Geeves, M. A. (1993) Regulation of the interaction between actin and myosin subfragment 1: evidence for three states of the thin filament, *Biophys J 65*, 693-701.

5. Lehman, W., Hatch, V., Korman, V., Rosol, M., Thomas, L., Maytum, R., Geeves, M. A., Van Eyk, J. E., Tobacman, L. S., and Craig, R. (2000) Tropomyosin and actin isoforms modulate the localization of tropomyosin strands on actin filaments, *J Mol Biol 302*, 593-606.

6. Vibert, P., Craig, R., and Lehman, W. (1997) Steric-model for activation of muscle thin filaments, *J Mol Biol 266*, 8-14.

7. Takeda, S., Yamashita, A., Maeda, K., and Maeda, Y. (2003) Structure of the core domain of human cardiac troponin in the Ca(2+)-saturated form, *Nature 424*, 35-41.

8. Herzberg, O., and James, M. N. (1985) Structure of the calcium regulatory muscle protein troponin-C at 2.8 A resolution, *Nature 313*, 653-659.

9. Li, M. X., Wang, X., and Sykes, B. D. (2004) Structural based insights into the role of troponin in cardiac muscle pathophysiology, *J Muscle Res Cell Motil 25*, 559-579.

10. Dvoretsky, A., Abusamhadneh, E. M., Howarth, J. W., and Rosevear, P. R. (2002) Solution structure of calcium-saturated cardiac troponin C bound to cardiac troponin I, *J Biol Chem 277*, 38565-38570.

11. van Eerd, J. P., and Takahashi, K. (1975) The amino acid sequence of bovine cardiac tamponin-C. Comparison with rabbit skeletal troponin-C, *Biochem Biophys Res Commun 64*, 122-127.

12. Gordon, A. M., Homsher, E., and Regnier, M. (2000) Regulation of contraction in striated muscle, *Physiol Rev 80*, 853-924.

13. Putkey, J. A., Sweeney, H. L., and Campbell, S. T. (1989) Site-directed mutation of the trigger calcium-binding sites in cardiac troponin C, *J Biol Chem 264*, 12370-12378.

14. Sweeney, H. L., Brito, R. M., Rosevear, P. R., and Putkey, J. A. (1990) The low-affinity Ca2(+)-binding sites in cardiac/slow skeletal muscle troponin C perform distinct functions: site I alone cannot trigger contraction, *Proc Natl Acad Sci U S A 87*, 9538-9542.

15. Biesiadecki, B. J., Kobayashi, T., Walker, J. S., John Solaro, R., and de Tombe, P. P. (2007) The troponin C G159D mutation blunts myofilament desensitization induced by troponin I Ser23/24 phosphorylation, *Circ Res 100*, 1486-1493.

16. Gagne, S. M., Li, M. X., McKay, R. T., and Sykes, B. D. (1998) The NMR angle on troponin C, *Biochem Cell Biol 76*, 302-312.

17. Sia, S. K., Li, M. X., Spyracopoulos, L., Gagne, S. M., Liu, W., Putkey, J. A., and Sykes, B. D. (1997) Structure of cardiac muscle troponin C unexpectedly reveals a closed regulatory domain, *Journal of Biological Chemistry 272*, 18216-18221.

18. Gasmi-Seabrook, G. M., Howarth, J. W., Finley, N., Abusamhadneh, E., Gaponenko, V., Brito, R. M., Solaro, R. J., and Rosevear, P. R. (1999) Solution structures of the C-terminal domain of cardiac troponin C free and bound to the N-terminal domain of cardiac troponin I, *Biochemistry 38*, 8313-8322.

19. Mercier, P., Spyracopoulos, L., and Sykes, B. D. (2001) Structure, dynamics, and thermodynamics of the structural domain of troponin C in complex with the regulatory peptide 1-40 of troponin I, *Biochemistry 40*, 10063-10077.

20. Lindhout, D. A., and Sykes, B. D. (2003) Structure and dynamics of the C-domain of human cardiac troponin C in complex with the inhibitory region of human cardiac troponin I, *J Biol Chem 278*, 27024-27034.

21. Finley, N. L., Howarth, J. W., and Rosevear, P. R. (2004) Structure of the Mg2+-loaded C-lobe of cardiac troponin C bound to the N-domain of cardiac troponin I: comparison with the Ca2+-loaded structure, *Biochemistry 43*, 11371-11379.

22. Gagne, S. M., Tsuda, S., Li, M. X., Smillie, L. B., and Sykes, B. D. (1995) Structures of the troponin C regulatory domains in the apo and calcium-saturated states, *Nat Struct Biol 2*, 784-789.

23. Spyracopoulos, L., Li, M. X., Sia, S. K., Gagne, S. M., Chandra, M., Solaro, R. J., and Sykes, B. D. (1997) Calcium-induced structural transition in the regulatory domain of human cardiac troponin C, *Biochemistry 36*, 12138-12146.

24. Dong, W. J., Xing, J., Villain, M., Hellinger, M., Robinson, J. M., Chandra, M., Solaro, R. J., Umeda, P. K., and Cheung, H. C. (1999) Conformation of the regulatory domain of cardiac muscle troponin C in its complex with cardiac troponin I, *J Biol Chem 274*, 31382-31390.

25. Li, M. X., Spyracopoulos, L., and Sykes, B. D. (1999) Binding of cardiac troponin-I147-163 induces a structural opening in human cardiac tropoin-C, *Biochemistry 38*, 8289-8298.

26. Martins, S. M., Chapeaurouge, A., and Ferreira, S. T. (2002) Equilibrium unfolding and conformational plasticity of troponin I and T, *Eur J Biochem 269*, 5484-5491.

27. Perry, S. V. (1999) Troponin I: inhibitor or facilitator, *Mol Cell Biochem 190*, 9-32.

28. Solaro, R. J., Rosevear, P., and Kobayashi, T. (2008) The unique functions of cardiac troponin I in the control of cardiac muscle contraction and relaxation, *Biochem Biophys Res Commun 369*, 82-87.

29. Howarth, J. W., Meller, J., Solaro, R. J., Trewhella, J., and Rosevear, P. R. (2007) Phosphorylation-dependent conformational transition of the cardiac specific N-extension of troponin I in cardiac troponin, *J Mol Biol 373*, 706-722.

30. Pearlstone, J. R., and Smillie, L. B. (1985) The interaction of rabbit skeletal muscle troponin-T fragments with troponin-I, *Can J Biochem Cell Biol 63*, 212-218.

31. Syska, H., Wilkinson, J. M., Grand, R. J., and Perry, S. V. (1976) The relationship between biological activity and primary structure of troponin I from white skeletal muscle of the rabbit, *Biochem J 153*, 375-387.

32. Talbot, J. A., and Hodges, R. S. (1981) Synthetic studies on the inhibitory region of rabbit skeletal troponin I. Relationship of amino acid sequence to biological activity, *J Biol Chem 256*, 2798-2802.

33. Tung, C. S., Wall, M. E., Gallagher, S. C., and Trewhella, J. (2000) A model of troponin-I in complex with troponin-C using hybrid experimental data: the inhibitory region is a beta-hairpin, *Protein Sci 9*, 1312-1326.

34. Brown, L. J., Sale, K. L., Hills, R., Rouviere, C., Song, L., Zhang, X., and Fajer, P. G. (2002) Structure of the inhibitory region of troponin by site directed spin labeling electron paramagnetic resonance, *Proc Natl Acad Sci U S A 99*, 12765-12770.

35. Ertz-Berger, B. R., He, H., Dowell, C., Factor, S. M., Haim, T. E., Nunez, S., Schwartz, S. D., Ingwall, J. S., and Tardiff, J. C. (2005) Changes in the chemical and dynamic properties of cardiac troponin T cause discrete cardiomyopathies in transgenic mice, *Proc Natl Acad Sci U S A 102*, 18219-18224.

36. Manning, E. P., Tardiff, J. C., and Schwartz, S. D. (2011) A model of calcium activation of the cardiac thin filament, *Biochemistry 50*, 7405-7413.

37. Li, M. X., Robertson, I. M., and Sykes, B. D. (2008) Interaction of cardiac troponin with cardiotonic drugs: a structural perspective, *Biochem Biophys Res Commun 369*, 88-99.

38. Endoh, M. (2001) Mechanism of action of Ca2+ sensitizers--update 2001, *Cardiovasc Drugs Ther 15*, 397-403.

39. Sorsa, T., Heikkinen, S., Abbott, M. B., Abusamhadneh, E., Laakso, T., Tilgmann, C., Serimaa, R., Annila, A., Rosevear, P. R., Drakenberg, T., Pollesello, P., and Kilpelainen, I. (2001) Binding of levosimendan, a calcium sensitizer, to cardiac troponin C, *J Biol Chem 276*, 9337-9343.

40. Pollesello, P., Ovaska, M., Kaivola, J., Tilgmann, C., Lundstrom, K., Kalkkinen, N., Ulmanen, I., Nissinen, E., and Taskinen, J. (1994) Binding of a new Ca2+ sensitizer, levosimendan, to recombinant human cardiac troponin C. A molecular modelling, fluorescence probe, and proton nuclear magnetic resonance study, *J Biol Chem 269*, 28584-28590.

41. Solaro, R. J., Wolska,B.M., Arteaga G.M., Martin, A.F., Buttrick, P., deTombe, P. (2002) Modulation of thin filament activity in long and short term regulation of cardiac function In *Molecular Control Mechanisms in Striated Muscle Contraction* (R.J. Solaro, R. L. M. E., Ed.), Kluwer Academic Publishers.

42. Dong, W. J., Jayasundar, J. J., An, J., Xing, J., and Cheung, H. C. (2007) Effects of PKA phosphorylation of cardiac troponin I and strong crossbridge on conformational transitions of the N-domain of cardiac troponin C in regulated thin filaments, *Biochemistry 46*, 9752-9761.

43. al-Hillawi, E., Bhandari, D. G., Trayer, H. R., and Trayer, I. P. (1995) The effects of phosphorylation of cardiac troponin-I on its interactions with actin and cardiac troponin-C, *Eur J Biochem 228*, 962-970.

44. Zhang, R., Zhao, J., Mandveno, A., and Potter, J. D. (1995) Cardiac troponin I phosphorylation increases the rate of cardiac muscle relaxation, *Circ Res 76*, 1028-1035.

45. Zhang, R., Zhao, J., and Potter, J. D. (1995) Phosphorylation of both serine residues in cardiac troponin I is required to decrease the Ca2+ affinity of cardiac troponin C, *J Biol Chem 270*, 30773-30780.

46. Kentish, J. C., McCloskey, D. T., Layland, J., Palmer, S., Leiden, J. M., Martin, A. F., and Solaro, R. J. (2001) Phosphorylation of troponin I by protein kinase A accelerates relaxation and crossbridge cycle kinetics in mouse ventricular muscle, *Circ Res 88*, 1059-1065.

47. Layland, J., Solaro, R. J., and Shah, A. M. (2005) Regulation of cardiac contractile function by troponin I phosphorylation, *Cardiovasc Res 66*, 12-21.

48. Towbin, J. A. (2009) Hypertrophic cardiomyopathy, *Pacing Clin Electrophysiol 32 Suppl 2*, S23-31.

49. Willott, R. H., Gomes, A. V., Chang, A. N., Parvatiyar, M. S., Pinto, J. R., and Potter, J. D. (2010) Mutations in Troponin that cause HCM, DCM AND RCM: what can we learn about thin filament function?, *J Mol Cell Cardiol 48*, 882-892.

50. Tardiff, J. C. (2005) Sarcomeric proteins and familial hypertrophic cardiomyopathy: linking mutations in structural proteins to complex cardiovascular phenotypes, *Heart Fail Rev 10*, 237-248.

51. Parvatiyar, M. S., Landstrom, A. P., Figueiredo-Freitas, C., Potter, J. D., Ackerman, M. J., and Pinto, J. R. (2012) A mutation in TNNC1-encoded cardiac troponin C, TNNC1-A31S, predisposes to hypertrophic cardiomyopathy and ventricular fibrillation, *J Biol Chem*.

52. Albury, A. N., Swindle, N., Swartz, D. R., and Tikunova, S. B. (2012) Effect of hypertrophic cardiomyopathy-linked troponin C mutations on the response of reconstituted thin filaments to calcium upon troponin I phosphorylation, *Biochemistry 51*, 3614-3621.

53. Liu, B., Tikunova, S. B., Kline, K. P., Siddiqui, J. K., and Davis, J. P. (2012) Disease-related cardiac troponins alter thin filament ca(2+) association and dissociation rates, *PLoS One 7*, e38259.

54. Kobayashi, T., and Solaro, R. J. (2006) Increased Ca2+ affinity of cardiac thin filaments reconstituted with cardiomyopathy-related mutant cardiac troponin I, *J Biol Chem 281*, 13471-13477.

55. Robinson, P., Griffiths, P. J., Watkins, H., and Redwood, C. S. (2007) Dilated and hypertrophic cardiomyopathy mutations in troponin and alpha-tropomyosin have opposing effects on the calcium affinity of cardiac thin filaments, *Circ Res 101*, 1266-1273.

56. Gomes, A. V., Harada, K., and Potter, J. D. (2005) A mutation in the N-terminus of troponin I that is associated with hypertrophic cardiomyopathy affects the Ca(2+)-sensitivity, phosphorylation kinetics and proteolytic susceptibility of troponin, *J Mol Cell Cardiol 39*, 754-765.

57. Gomes, A. V., and Potter, J. D. (2004) Cellular and molecular aspects of familial hypertrophic cardiomyopathy caused by mutations in the cardiac troponin I gene, *Mol Cell Biochem 263*, 99-114.

58.   Gomes, A. V., and Potter, J. D. (2004) Molecular and cellular aspects of troponin cardiomyopathies, *Ann N Y Acad Sci 1015*, 214-224.

59.   Kruger, M., Zittrich, S., Redwood, C., Blaudeck, N., James, J., Robbins, J., Pfitzer, G., and Stehle, R. (2005) Effects of the mutation R145G in human cardiac troponin I on the kinetics of the contraction-relaxation cycle in isolated cardiac myofibrils, *J Physiol 564*, 347-357.

60.   Rust, E. M., Albayya, F. P., and Metzger, J. M. (1999) Identification of a contractile deficit in adult cardiac myocytes expressing hypertrophic cardiomyopathy-associated mutant troponin T proteins, *J Clin Invest 103*, 1459-1467.

61.   Tardiff, J. C., Factor, S. M., Tompkins, B. D., Hewett, T. E., Palmer, B. M., Moore, R. L., Schwartz, S., Robbins, J., and Leinwand, L. A. (1998) A truncated cardiac troponin T molecule in transgenic mice suggests multiple cellular mechanisms for familial hypertrophic cardiomyopathy, *J Clin Invest 101*, 2800-2811.

62.   Tardiff, J. C., Hewett, T. E., Palmer, B. M., Olsson, C., Factor, S. M., Moore, R. L., Robbins, J., and Leinwand, L. A. (1999) Cardiac troponin T mutations result in allele-specific phenotypes in a mouse model for hypertrophic cardiomyopathy, *J Clin Invest 104*, 469-481.

63.   Tardiff, J. C., Hewett, T. E., Factor, S. M., Vikstrom, K. L., Robbins, J., and Leinwand, L. A. (2000) Expression of the beta (slow)-isoform of MHC in the adult mouse heart causes dominant-negative functional effects, *Am J Physiol Heart Circ Physiol 278*, H412-419.

64.   Javadpour, M. M., Tardiff, J. C., Pinz, I., and Ingwall, J. S. (2003) Decreased energetics in murine hearts bearing the R92Q mutation in cardiac troponin T, *J Clin Invest 112*, 768-775.

65.   Du, C. K., Morimoto, S., Nishii, K., Minakami, R., Ohta, M., Tadano, N., Lu, Q. W., Wang, Y. Y., Zhan, D. Y., Mochizuki, M., Kita, S., Miwa, Y., Takahashi-Yanaga, F., Iwamoto, T., Ohtsuki, I., and Sasaguri, T. (2007) Knock-in mouse model of dilated cardiomyopathy caused by troponin mutation, *Circ Res 101*, 185-194.

66. Du, J., Liu, J., Feng, H. Z., Hossain, M. M., Gobara, N., Zhang, C., Li, Y., Jean-Charles, P. Y., Jin, J. P., and Huang, X. P. (2008) Impaired relaxation is the main manifestation in transgenic mice expressing a restrictive cardiomyopathy mutation, R193H, in cardiac TnI, *Am J Physiol Heart Circ Physiol 294*, H2604-2613.

67. Wang, Y., Pinto, J. R., Solis, R. S., Dweck, D., Liang, J., Diaz-Perez, Z., Ge, Y., Walker, J. W., and Potter, J. D. (2012) Generation and functional characterization of knock-in mice harboring the cardiac troponin I-R21C mutation associated with hypertrophic cardiomyopathy, *J Biol Chem 287*, 2156-2167.

68. Tikunova, S. B., and Davis, J. P. (2004) Designing calcium-sensitizing mutations in the regulatory domain of cardiac troponin C, *J Biol Chem 279*, 35341-35352.

69. Davis, J. P., Norman, C., Kobayashi, T., Solaro, R. J., Swartz, D. R., and Tikunova, S. B. (2007) Effects of Thin and Thick Filament Proteins on Calcium Binding and Exchange with Cardiac Troponin C, *Biophysical Journal 92*, 3195-3206.

70. Kass, D. A., and Solaro, R. J. (2006) Mechanisms and use of calcium-sensitizing agents in the failing heart, *Circulation 113*, 305-315.

71. Pearlstone, J. R., Borgford, T., Chandra, M., Oikawa, K., Kay, C. M., Herzberg, O., Moult, J., Herklotz, A., Reinach, F. C., and Smillie, L. B. (1992) Construction and characterization of a spectral probe mutant of troponin C: application to analyses of mutants with increased Ca2+ affinity, *Biochemistry 31*, 6545-6553.

72. Tikunova, S. B., Rall, J. A., and Davis, J. P. (2002) Effect of hydrophobic residue substitutions with glutamine on Ca(2+) binding and exchange with the N-domain of troponin C, *Biochemistry 41*, 6697-6705.

73. Davis, J. P., Rall J.A., Alionte C., Tikunova S.B. (2004) Mutations of Hydrophobic Residues in the N-terminal Domain of Troponin C Affect Calcium Binding and Exchange with the Troponin C-Troponin I96-148 Complex and Muscle Force Production, *Journal of Biological Chemistry 279*, 17348-17360.

74. Tikunova, S. B., Liu, B., Swindle, N., Little, S. C., Gomes, A. V., Swartz, D. R., and Davis, J. P. (2010) Effect of calcium-sensitizing mutations on calcium

binding and exchange with troponin C in increasingly complex biochemical systems, *Biochemistry 49*, 1975-1984.

75. Kreutziger, K. L., Piroddi, N., McMichael, J. T., Tesi, C., Poggesi, C., and Regnier, M. (2011) Calcium binding kinetics of troponin C strongly modulate cooperative activation and tension kinetics in cardiac muscle, *J. Mol. Cell. Cardiol. 50*, 165-174.

76. Parvatiyar, M. S., Pinto, J. R., Liang, J., and Potter, J. D. (2010) Predicting cardiomyopathic phenotypes by altering Ca2+ affinity of cardiac troponin C, *J. Biol. Chem. 285*, 27785-27797.

77. Karplus, M., and McCammon, J. A. (2002) Molecular dynamics simulations of biomolecules, *Nat Struct Biol 9*, 646-652.

78. van der Kamp, M. W., Shaw, K. E., Woods, C. J., and Mulholland, A. J. (2008) Biomolecular simulation and modelling: status, progress and prospects, *J R Soc Interface 5 Suppl 3*, S173-190.

79. Daggett, V. (2006) Protein Folding−Simulation, *Chemical Reviews 106*, 1898-1916.

80. Elcock, A. H. (2006) Molecular Simulations of Cotranslational Protein Folding: Fragment Stabilities, Folding Cooperativity, and Trapping in the Ribosome, *PLoS Comput Biol 2*, e98.

81. Ritchie, D. W. (2008) Recent progress and future directions in protein-protein docking, *Curr Protein Pept Sci 9*, 1-15.

82. Moitessier, N., Englebienne, P., Lee, D., Lawandi, J., and Corbeil, C. R. (2008) Towards the development of universal, fast and highly accurate docking/scoring methods: a long way to go, *Br J Pharmacol 153 Suppl 1*, S7-26.

83. Beckstein, O., Biggin, P. C., Bond, P., Bright, J. N., Domene, C., Grottesi, A., Holyoake, J., and Sansom, M. S. (2003) Ion channel gating: insights via molecular simulations, *FEBS Lett 555*, 85-90.

84. Gilson, M. K., and Zhou, H. X. (2007) Calculation of protein-ligand binding affinities, *Annu Rev Biophys Biomol Struct 36*, 21-42.

85. Durrant, J. D., and McCammon, J. A. (2011) Molecular dynamics simulations and drug discovery, *BMC Biol 9*, 71.

86. Taft, C. A., Da Silva, V. B., and Da Silva, C. H. (2008) Current topics in computer-aided drug design, *J Pharm Sci 97*, 1089-1098.

87. Mulholland, A. J. (2008) Computational enzymology: modelling the mechanisms of biological catalysts, *Biochem Soc Trans 36*, 22-26.

88. van der Kamp, M. W., and Daggett, V. (2010) Pathogenic mutations in the hydrophobic core of the human prion protein can promote structural instability and misfolding, *J Mol Biol 404*, 732-748.

89. Guinto, P. J., Manning, E. P., Schwartz, S. D., and Tardiff, J. C. (2007) Computational characterization of mutations in cardiac troponin T known to cause familial hypertrophic cardiomyopathy, *Journal of Theoretical and Computational Chemistry 06*, 413-419.

90. Haim, T. E., Dowell, C., Diamanti, T., Scheuer, J., and Tardiff, J. C. (2007) Independent FHC-related cardiac troponin T mutations exhibit specific alterations in myocellular contractility and calcium kinetics, *J Mol Cell Cardiol 42*, 1098-1110.

91. Lim, C. C., Yang, H., Yang, M., Wang, C. K., Shi, J., Berg, E. A., Pimentel, D. R., Gwathmey, J. K., Hajjar, R. J., Helmes, M., Costello, C. E., Huo, S., and Liao, R. (2008) A novel mutant cardiac troponin C disrupts molecular motions critical for calcium binding affinity and cardiomyocyte contractility, *Biophys J 94*, 3577-3589.

92. Hamelberg, D., Mongan, J., and McCammon, J. A. (2004) Accelerated molecular dynamics: a promising and efficient simulation method for biomolecules, *J Chem Phys 120*, 11919-11929.

93. Lindert, S., Kekenes-Huskey, P. M., Huber, G., Pierce, L., and McCammon, J. A. (2012) Dynamics and Calcium Association to the N-Terminal Regulatory Domain of Human Cardiac Troponin C: A Multiscale Computational Study, *Journal of Physical Chemistry B*.

94. Pinto, J. R., Parvatiyar, M. S., Jones, M. A., Liang, J., Ackerman, M. J., and Potter, J. D. (2009) A functional and structural study of troponin C mutations related to hypertrophic cardiomyopathy, *J Biol Chem 284*, 19090-19100.

95. Slupsky, C. M., and Sykes, B. D. (1995) NMR solution structure of calcium-saturated skeletal muscle troponin C, *Biochemistry 34*, 15953-15964.

96. Pettersen, E. F., Goddard, T. D., Huang, C. C., Couch, G. S., Greenblatt, D. M., Meng, E. C., and Ferrin, T. E. (2004) UCSF chimera - A visualization system for exploratory research and analysis, *J. Comput. Chem. 25*, 1605-1612.

97. Dong, W. J., Rosenfeld, S. S., Wang, C. K., Gordon, A. M., and Cheung, H. C. (1996) Kinetic studies of calcium binding to the regulatory site of troponin C from cardiac muscle, *J. Biol. Chem. 271*, 688-694.

98. Pearlstone, J. R., Chandra, M., Sorenson, M. M., and Smillie, L. B. (2000) Biological function and site IICa2+-induced opening of the regulatory domain of skeletal troponin C are impaired by invariant site I or II Glu mutations, *J. Biol. Chem. 275*, 35106-35115.

99. Li, M. X., Corson, D. C., and Sykes, B. D. (2002) Structure determination by NMR. Isotope labeling, *Methods Mol. Biol. 173*, 255-265.

100. Martyn, D. A., Regnier, M., Xu, D., and Gordon, A. M. (2001) Ca2+ - and cross-bridge-dependent changes in N- and C-terminal structure of troponin C in rat cardiac muscle, *Biophys. J. 80*, 360-370.

101. Dong, W. J., Xing, J., Chandra, M., Solaro, J., and Cheung, H. C. (2000) Structural mapping of single cysteine mutants of cardiac troponin I, *Proteins 41*, 438-447.

102. Dong, W. J., Robinson, J. M., Stagg, S., Xing, J., and Cheung, H. C. (2003) Ca2+-induced conformational transition in the inhibitory and regulatory regions of cardiac troponin I, *J. Biol. Chem. 278*, 8686-8692.

103. Patton, C., Thompson, S., and Epel, D. (2004) Some precautions in using chelators to buffer metals in biological solutions, *Cell Calcium 35*, 427-431.

104. George, S. E., Su, Z., Fan, D., Wang, S., and Johnson, J. D. (1996) The Fourth EF-Hand of Calmodulin and Its Helix−Loop−Helix Components: Impact on Calcium Binding and Enzyme Activation†, *Biochemistry 35*, 8307-8313.

105. Beck, D. A. C., McCully, M.E., Alonso, D. O. V., and Daggett, V. (2000-2012) in lucem molecular mechanics (*ilmm*).

106. Levitt, M., Hirshberg, M., Sharon, R. & Daggett, V. (1995) Potential-energy function and parameters for simulations of the molecular-dynamics of proteins and nucleic-acids in solution, *Comput. Phys. Commun. 91*, 215-231.

107. Levitt, M., Hirshberg, M., Sharon, R., Laidig, K. E., and Daggett, V. (1997) Calibration and testing of a water model for simulation of the molecular dynamics of proteins and nucleic acids in solution, *J. Phys. Chem. B 101*, 5051-5061.

108. Kell, G. S. (1967) Precise Representation of Volume Properties of Water at 1 Atmosphere, *J. Chem. Eng. Data 12*, 66-69.

109. Lee, B., and Richards, F. M. (1971) The interpretation of protein structures: estimation of static accessibility, *J Mol Biol 55*, 379-400.

110. Wilkinson, J. M., and Grand, R. J. (1975) The amino acid sequence of troponin I from rabbit skeletal muscle, *Biochem J 149*, 493-496.

111. He, T. C., Zhou, S., da Costa, L. T., Yu, J., Kinzler, K. W., and Vogelstein, B. (1998) A simplified system for generating recombinant adenoviruses, *Proc Natl Acad Sci U S A 95*, 2509-2514.

112. Santana, L. F., Kranias, E. G., and Lederer, W. J. (1997) Calcium sparks and excitation-contraction coupling in phospholamban-deficient mouse ventricular myocytes, *J Physiol 503 (Pt 1)*, 21-29.

113. Coutu, P., and Metzger, J. M. (2002) Optimal range for parvalbumin as relaxing agent in adult cardiac myocytes: gene transfer and mathematical modeling, *Biophys J 82*, 2565-2579.

114. Herron, T. J., Devaney, E., Mundada, L., Arden, E., Day, S., Guerrero-Serna, G., Turner, I., Westfall, M., and Metzger, J. M. (2010) Ca2+-independent positive molecular inotropy for failing rabbit and human cardiac muscle by alpha-myosin motor gene transfer, *FASEB J 24*, 415-424.

115. Gagne, S. M., Tsuda, S., Li, M. X., Smillie, L. B., and Sykes, B. D. (1995) Structures of the Troponin-C Regulatory Domains in the Apo and Calcium-Saturated States, *Nat. Struct. Biol. 2*, 784-789.

116. Putkey, J. A., Sweeney, H. L., and Campbell, S. T. (1989) Site-Directed Mutation of the Trigger Calcium-Binding Sites in Cardiac Troponin-C, *J. Biol. Chem. 264*, 12370-12378.

117. Baryshnikova, O. K., Robertson, I. M., Mercier, P., and Sykes, B. D. (2008) The dilated cardiomyopathy G159D mutation in cardiac troponin C weakens the anchoring interaction with troponin I, *Biochemistry 47*, 10950-10960.

118. Ramakrishnan, S., and Hitchcock-DeGregori, S. E. (1996) Structural and functional significance of aspartic acid 89 of the troponin C central helix in Ca2+ signaling, *Biochemistry 35*, 15515-15521.

119. Rarick, H. M., Tu, X. H., Solaro, R. J., and Martin, A. F. (1997) The C terminus of cardiac troponin I is essential for full inhibitory activity and Ca2+ sensitivity of rat myofibrils, *J. Biol. Chem. 272*, 26887-26892.

120. Hoffmann, B., Schmidt-Traub, H., Perrot, A., Osterziel, K. J., and Gessner, R. (2001) First mutation in cardiac troponin C, L29Q, in a patient with hypertrophic cardiomyopathy, *Hum. Mutat. 17*, 524.

121. Tardiff, J. C. (2011) Thin filament mutations: developing an integrative approach to a complex disorder, *Circ Res 108*, 765-782.

122. Gether, U., Lin, S., Ghanouni, P., Ballesteros, J. A., Weinstein, H., and Kobilka, B. K. (1997) Agonists induce conformational changes in transmembrane domains III and VI of the beta2 adrenoceptor, *EMBO J 16*, 6737-6747.

123. Gether, U., Lin, S., and Kobilka, B. K. (1995) Fluorescent labeling of purified beta 2 adrenergic receptor. Evidence for ligand-specific conformational changes, *J Biol Chem 270*, 28268-28275.

124. Dong, W. J., and Cheung, H. C. (1996) Calcium-induced conformational change in cardiac troponin C studied by fluorescence probes attached to Cys-84, *Biochim Biophys Acta 1295*, 139-146.

125. Robertson, I. M., Boyko, R. F., and Sykes, B. D. (2011) Visualizing the principal component of (1)H,(15)N-HSQC NMR spectral changes that reflect protein structural or functional properties: application to troponin C, *J. Biomol. NMR 51*, 115-122.

126. Lewit-Bentley, A., and Rety, S. (2000) EF-hand calcium-binding proteins, *Curr Opin Struct Biol 10*, 637-643.

127. Marsden, B. J., Shaw, G. S., and Sykes, B. D. (1990) Calcium binding proteins. Elucidating the contributions to calcium affinity from an analysis of species variants and peptide fragments, *Biochem Cell Biol 68*, 587-601.

128. Sopkova-de Oliveira Santos, J., Oling, F. K., Rety, S., Brisson, A., Smith, J. C., and Lewit-Bentley, A. (2000) S100 protein-annexin interactions: a model of the (Anx2-p11)(2) heterotetramer complex, *Biochim Biophys Acta 1498*, 181-191.

129. Hofmann, A., Escherich, A., Lewit-Bentley, A., Benz, J., Raguenes-Nicol, C., Russo-Marie, F., Gerke, V., Moroder, L., and Huber, R. (1998) Interactions of benzodiazepine derivatives with annexins, *J Biol Chem 273*, 2885-2894.

130. Perron, B., Lewit-Bentley, A., Geny, B., and Russo-Marie, F. (1997) Can enzymatic activity, or otherwise, be inferred from structural studies of annexin III?, *J Biol Chem 272*, 11321-11326.

131. Lewit-Bentley, A., Bentley, G. A., Favier, B., L'Hermite, G., and Renouard, M. (1994) The interaction of metal ions with annexin V: a crystallographic study, *FEBS Lett 345*, 38-42.

132. Elkins, K. M., Gatzeva-Topalova, P. Z., and Nelson, D. J. (2001) Molecular dynamics study of Ca(2+) binding loop variants of parvalbumin with modifications at the "gateway" position, *Protein Eng 14*, 115-126.

133. Li, M. X., Wang, X., Spyracopoulos, L., and Sykes, B. D. (2001) Structure of the n-domain of cardiac troponin C in complex with bepridil and cardiac troponin-I147-163., *Biophysical Journal 80*, 88a-88a.

134. McKay, R. T., Saltibus, L. F., Li, M. X., and Sykes, B. D. (2000) Energetics of the induced structural change in a Ca2+ regulatory protein: Ca2+ and troponin I peptide binding to the E41A mutant of the N-domain of skeletal troponin C, *Biochemistry 39*, 12731-12738.

135. Paakkonen, K., Sorsa, T., Drakenberg, T., Pollesello, P., Tilgmann, C., Permi, P., Heikkinen, S., Kilpelainen, I., and Annila, A. (2000) Conformations of the regulatory domain of cardiac troponin C examined by residual dipolar couplings, *Eur. J. Biochem. 267*, 6665-6672.

136. Sorsa, T., Pollesello, P., and Solaro, R. J. (2004) The contractile apparatus as a target for drugs against heart failure: Interaction of levosimendan, a calcium sensitiser, with cardiac troponin c, *Mol. Cell. Biochem. 266*, 87-107.

137. Maytum, R., Lehrer, S. S., and Geeves, M. A. (1999) Cooperativity and switching within the three-state model of muscle regulation, *Biochemistry 38*, 1102-1110.

138. Guinto, P. J., Haim, T. E., Dowell-Martino, C. C., Sibinga, N., and Tardiff, J. C. (2009) Temporal and mutation-specific alterations in Ca2+ homeostasis differentially determine the progression of cTnT-related cardiomyopathies in murine models, *Am J Physiol Heart Circ Physiol 297*, H614-626.

139. He, H., Javadpour, M. M., Latif, F., Tardiff, J. C., and Ingwall, J. S. (2007) R-92L and R-92W mutations in cardiac troponin T lead to distinct energetic phenotypes in intact mouse hearts, *Biophys J 93*, 1834-1844.

140. Robinson, P., Mirza, M., Knott, A., Abdulrazzak, H., Willott, R., Marston, S., Watkins, H., and Redwood, C. (2002) Alterations in thin filament regulation induced by a human cardiac troponin T mutant that causes dilated cardiomyopathy are distinct from those induced by troponin T mutants that cause hypertrophic cardiomyopathy, *J Biol Chem 277*, 40710-40716.

141. Mirza, M., Marston, S., Willott, R., Ashley, C., Mogensen, J., McKenna, W., Robinson, P., Redwood, C., and Watkins, H. (2005) Dilated cardiomyopathy mutations in three thin filament regulatory proteins result in a common functional phenotype, *J Biol Chem 280*, 28498-28506.

142. Mogensen, J., Murphy, R. T., Shaw, T., Bahl, A., Redwood, C., Watkins, H., Burke, M., Elliott, P. M., and McKenna, W. J. (2004) Severe disease expression of cardiac troponin C and T mutations in patients with idiopathic dilated cardiomyopathy, *J Am Coll Cardiol 44*, 2033-2040.

143. Kekenes-Huskey, P. M., Lindert, S., and McCammon, J. A. (2012) Molecular Basis of Calcium-Sensitizing and Desensitizing Mutations of the Human Cardiac Troponin C Regulatory Domain: A Multi-Scale Simulation Study, *PLoS Comput Biol 8*, e1002777.

144. Wang, D., Robertson, I. M., Li, M. X., McCully, M. E., Crane, M. L., Luo, Z., Tu, A.-Y., Daggett, V., Sykes, B. D., and Regnier, M. (2012) Structural and

Functional Consequences of the Cardiac Troponin C L48Q Ca2+-Sensitizing Mutation, *Biochemistry 51*, 4473-4487.

145. Sopkova, J., Renouard, M., and Lewit-Bentley, A. (1993) The crystal structure of a new high-calcium form of annexin V, *J Mol Biol 234*, 816-825.

146. Dong, W. J., Xing, J., Ouyang, Y., An, J., and Cheung, H. C. (2008) Structural kinetics of cardiac troponin C mutants linked to familial hypertrophic and dilated cardiomyopathy in troponin complexes, *J Biol Chem 283*, 3424-3432.

147. McCully, M. E., Beck, D. A., and Daggett, V. (2008) Microscopic reversibility of protein folding in molecular dynamics simulations of the engrailed homeodomain, *Biochemistry 47*, 7079-7089.

148. Solaro, R. J. (2008) Multiplex kinase signaling modifies cardiac function at the level of sarcomeric proteins, *J Biol Chem 283*, 26829-26833.

149. Metzger, J. M., and Westfall, M. V. (2004) Covalent and noncovalent modification of thin filament action: the essential role of troponin in cardiac muscle regulation, *Circ Res 94*, 146-158.

150. Solaro, R. J., and Rarick, H. M. (1998) Troponin and tropomyosin: proteins that switch on and tune in the activity of cardiac myofilaments, *Circ Res 83*, 471-480.

151. Rarick, H. M., Tang, H. P., Guo, X. D., Martin, A. F., and Solaro, R. J. (1999) Interactions at the NH2-terminal interface of cardiac troponin I modulate myofilament activation, *J Mol Cell Cardiol 31*, 363-375.

152. van der Velden, J., Papp, Z., Zaremba, R., Boontje, N. M., de Jong, J. W., Owen, V. J., Burton, P. B., Goldmann, P., Jaquet, K., and Stienen, G. J. (2003) Increased Ca2+-sensitivity of the contractile apparatus in end-stage human heart failure results from altered phosphorylation of contractile proteins, *Cardiovasc Res 57*, 37-47.

153. Gaponenko, V., Abusamhadneh, E., Abbott, M. B., Finley, N., Gasmi-Seabrook, G., Solaro, R. J., Rance, M., and Rosevear, P. R. (1999) Effects of troponin I phosphorylation on conformational exchange in the regulatory domain of cardiac troponin C, *J Biol Chem 274*, 16681-16684.

154. Finley, N., Abbott, M. B., Abusamhadneh, E., Gaponenko, V., Dong, W., Gasmi-Seabrook, G., Howarth, J. W., Rance, M., Solaro, R. J., Cheung, H. C., and

Rosevear, P. R. (1999) NMR analysis of cardiac troponin C-troponin I complexes: effects of phosphorylation, *FEBS Lett 453*, 107-112.

155. Ward, D. G., Cornes, M. P., and Trayer, I. P. (2002) Structural consequences of cardiac troponin I phosphorylation, *J Biol Chem 277*, 41795-41801.

156. Deng, Y., Schmidtmann, A., Redlich, A., Westerdorf, B., Jaquet, K., and Thieleczek, R. (2001) Effects of phosphorylation and mutation R145G on human cardiac troponin I function, *Biochemistry 40*, 14593-14602.

157. Pinto, J. R., Siegfried, J. D., Parvatiyar, M. S., Li, D., Norton, N., Jones, M. A., Liang, J., Potter, J. D., and Hershberger, R. E. (2011) Functional characterization of TNNC1 rare variants identified in dilated cardiomyopathy, *J Biol Chem 286*, 34404-34412.

158. Schmidtmann, A., Lindow, C., Villard, S., Heuser, A., Mugge, A., Gessner, R., Granier, C., and Jaquet, K. (2005) Cardiac troponin C-L29Q, related to hypertrophic cardiomyopathy, hinders the transduction of the protein kinase A dependent phosphorylation signal from cardiac troponin I to C, *FEBS J 272*, 6087-6097.

159. Dong, W. J., Chandra, M., Xing, J., She, M., Solaro, R. J., and Cheung, H. C. (1997) Phosphorylation-induced distance change in a cardiac muscle troponin I mutant, *Biochemistry 36*, 6754-6761.

160. Chandra, M., Dong, W. J., Pan, B. S., Cheung, H. C., and Solaro, R. J. (1997) Effects of protein kinase A phosphorylation on signaling between cardiac troponin I and the N-terminal domain of cardiac troponin C, *Biochemistry 36*, 13305-13311.

161. Westfall, M. V., Turner, I., Albayya, F. P., and Metzger, J. M. (2001) Troponin I chimera analysis of the cardiac myofilament tension response to protein kinase A, *Am J Physiol Cell Physiol 280*, C324-332.

162. Kobayashi, T., and Solaro, R. J. (2005) Calcium, thin filaments, and the integrative biology of cardiac contractility, *Annu Rev Physiol 67*, 39-67.

163. Noland, T. A., Jr., Guo, X., Raynor, R. L., Jideama, N. M., Averyhart-Fullard, V., Solaro, R. J., and Kuo, J. F. (1995) Cardiac troponin I mutants. Phosphorylation

by protein kinases C and A and regulation of Ca(2+)-stimulated MgATPase of reconstituted actomyosin S-1, *J Biol Chem 270*, 25445-25454.

164. Dohet, C., al-Hillawi, E., Trayer, I. P., and Ruegg, J. C. (1995) Reconstitution of skinned cardiac fibres with human recombinant cardiac troponin-I mutants and troponin-C, *FEBS Lett 377*, 131-134.

165. Preston, L. C., Ashley, C. C., and Redwood, C. S. (2007) DCM troponin C mutant Gly159Asp blunts the response to troponin phosphorylation, *Biochem Biophys Res Commun 360*, 27-32.

166. Baryshnikova, O. K., Li, M. X., and Sykes, B. D. (2008) Modulation of cardiac troponin C function by the cardiac-specific N-terminus of troponin I: influence of PKA phosphorylation and involvement in cardiomyopathies, *J Mol Biol 375*, 735-751.

167. Nishimura, S., Nagai, S., Sata, M., Katoh, M., Yamashita, H., Saeki, Y., Nagai, R., and Sugiura, S. (2006) Expression of green fluorescent protein impairs the force-generating ability of isolated rat ventricular cardiomyocytes., *Mol Cell Biochem 286*, 59-85.

168. Herron, T. J., Vandenboom, R., Fomicheva, E., Mundada, L., Edwards, T., and Metzger, J. M. (2007) Calcium-independent negative inotropy by beta-myosin heavy chain gene transfer in cardiac myocytes., *Circ Res 100*, 1182-1190.

169. Coutu, P., Bennett, C. N., Favre, E. G., Day, S. M., and Metzger, J. M. (2004) Parvalbumin corrects slowed relaxation in adult cardiac myocytes expressing hypertrophic cardiomyopathy-linked alpha-tropomyosin mutations, *Circ Res 94*, 1235-1241.

170. Janssen, P. M., Stull, L. B., and Marban, E. (2002) Myofilament properties comprise the rate-limiting step for cardiac relaxation at body temperature in the rat, *Am J Physiol Heart Circ Physiol 282*, H499-507.

171. Robbins, J. (2000) Remodeling the cardiac sarcomere using transgenesis, *Annu Rev Physiol 62*, 261-287.

172. Michele, D. E., Albayya, F. P., and Metzger, J. M. (1999) Thin filament protein dynamics in fully differentiated adult cardiac myocytes: toward a model of sarcomere maintenance, *J Cell Biol 145*, 1483-1495.

173. Westfall, M. V., Rust, E. M., and Metzger, J. M. (1997) Slow skeletal troponin I gene transfer, expression, and myofilament incorporation enhances adult cardiac myocyte contractile function., *Proc. Natl. Acad. Sci. USA 94*, 5444-5449.

174. Feng, H. Z., Hossain, M. M., Huang, X. P., and Jin, J. P. (2009) Myofilament incorporation determines the stoichiometry of troponin I in transgenic expression and the rescue of a null mutation., *Arch Biochem Biophys 487*, 36-41.

175. Siri, F. M., Krueger, J., Nordin, C., Ming, Z., and Aronson, R. S. (1991) Depressed intracellular calcium transients and contraction in myocytes from hypertrophied and failing guinea pig hearts, *Am J Physiol 261*, H514-530.

176. Janssen, P. M., and Periasamy, M. (2007) Determinants of frequency-dependent contraction and relaxation of mammalian myocardium, *J Mol Cell Cardiol 43*, 523-531.

177. Marston, S. B. (2011) How do mutations in contractile proteins cause the primary familial cardiomyopathies?, *J Cardiovasc Transl Res 4*, 245-255.

178. Li, Y., Charles, P. Y., Nan, C., Pinto, J. R., Wang, Y., Liang, J., Wu, G., Tian, J., Feng, H. Z., Potter, J. D., Jin, J. P., and Huang, X. (2010) Correcting diastolic dysfunction by Ca2+ desensitizing troponin in a transgenic mouse model of restrictive cardiomyopathy, *J Mol Cell Cardiol 49*, 402-411.

179. Jagatheesan, G., Rajan, S., Petrashevskaya, N., Schwartz, A., Boivin, G., Arteaga, G. M., Solaro, R. J., Liggett, S. B., and Wieczorek, D. F. (2007) Rescue of tropomyosin-induced familial hypertrophic cardiomyopathy mice by transgenesis, *Am J Physiol Heart Circ Physiol 293*, H949-958.

180. Pinto, J. R., Yang, S. W., Hitz, M. P., Parvatiyar, M. S., Jones, M. A., Liang, J., Kokta, V., Talajic, M., Tremblay, N., Jaeggi, M., Andelfinger, G., and Potter, J. D. (2011) Fetal cardiac troponin isoforms rescue the increased Ca2+ sensitivity produced by a novel double deletion in cardiac troponin T linked to restrictive cardiomyopathy: a clinical, genetic, and functional approach, *J Biol Chem 286*, 20901-20912.

181. Liu, B., Lee, R. S., Biesiadecki, B. J., Tikunova, S. B., and Davis, J. P. (2012) Engineered Troponin C Constructs Correct Disease-related Cardiac Myofilament Calcium Sensitivity, *J Biol Chem 287*, 20027-20036.

182. Morrison, K. L., and Weiss, G. A. (2001) Combinatorial alanine-scanning, *Curr Opin Chem Biol 5*, 302-307.

183. Moreira, I. S., Fernandes, P. A., and Ramos, M. J. (2007) Computational alanine scanning mutagenesis--an improved methodological approach, *Journal of Computational Chemistry 28*, 644-654.

Appendix

MD movies made from the simulation trajectories:

1. cNTnC●Ca^{2+}●cTnI$_{147\text{-}163}$ structure simulations WT *vs*. L48Q

2. Apo cNTnC structure simulations WT *vs*. L48Q

3. cNTnC•Ca^{2+} structure simulations WT *vs*. L48Q

4. cNTnC●Ca^{2+}●cTnI$_{147\text{-}163}$ structure simulations WT *vs*. I61Q

Vita

2000-2004……………………………………………………………...….. Tongji University

………………………………………………………B.S Material Sciences and Engineering

2004-2007……………………………………………………………...….. Tongji University

………………………………………………………M.S Polymer Science and Engineering

2004-2012.. .... ………. ………... Graduate Reseach Assistant

…………………………………………………………………..University of Washington

Publications

Wang D., Robertson I.M., Li M.X., McCully M.E., Crane M.L., Luo Z., Tu A.Y., Daggett V., Sykes B.D., Regnier M. Structural and functional consequences of the cardiac troponin C L48Q Ca^{2+}-sensitizing mutation. *Biochemistry,* 51 (22) : 4473–4487, 2012.

Abstracts:

1. **Wang D**, Korte FS, McMichael J, Luo ZX, Tu A, McCully ME, Daggett V and Regnier M. Mutations that Alter cTnC Ca^{2+} Binding Affect Interactions with cTnI and Cardiomyocyte Contraction. *Biophysical Journal,* 100(3): 360a, 2011. Invited for platform presentation.
2. **Wang D**, Korte FS, McMichael J, McCully ME, Luo ZX, Tu A, Daggett V and Regnier M. Effects of Cardiac TnC Variants on cTnC-cTnI Interaction;Solution and Molecular Dynamics Simulation Studies. *Biophysical Journal* , 98(3): 149a-150a, 2010
3. Korte FS, **Wang D**, Dai J, Buckley K, Murry CE, Daggett V, and M Regnier. Mutations that alter cTnC Ca^{2+} binding affect interactions with cTnI and cardiomyocytes Ca^{2+} handling. *European Muscle Conference*. Padua, Italy. 2010.
4. Korte FS, **Wang D**, Martyn DA, and M Regnier. Sarcomere length dependence of the force-pCa relationship in cardiac muscle is determined by properties of individual regulatory units. *Biophysical Journal*, 96(3): 223a-224a, 2009. Invited for platform presentation.
5. **Wang D**, Korte FS, Luo C, Tu A-Y, and M Regnier. Effects of Cardiac Troponin C Mutants on TnC-TnI interaction and its modulation by PKA phosphorylation. *Biophysical Journal*, 96(3):501a, 2009.